



Polytechnic University of Marche  
Ph.D. School in Engineering Sciences  
Curriculum in Environmental, Building Engineering and Architecture

---

**Exploiting Artificial Intelligence to build realistic numerical models:  
A Digital Twin application in Structural Health Monitoring**

Ph.D. Dissertation of:  
Georgios – Panagiotis Salachoris

Advisor: Prof. Stefano Lenzi

Co – Advisor: Prof. Francesco Clementi

Curriculum supervisor:  
Prof. Francesco Fatone

XXXIV Cycle





Università Politecnica delle Marche  
Scuola di Dottorato di Ricerca in Scienze dell'Ingegneria  
Curriculum in Ingegneria Civile, Ambientale, Edile e Architettura

---

**Sfruttare l'intelligenza Artificiale per costruire modelli numerici realistici:**

**Un'applicazione Digital Twin nello Structural Health Monitoring**

Ph.D. Dissertation of:  
Georgios Panagiotis Salaohoris

Advisor: Prof. Stefano Lenzi

Co – Advisor: Prof. Francesco Clementi

Curriculum supervisor:  
Prof. Francesco Fatone

XXXIV Ciclo



## Acknowledgements

First and foremost, I want to thank my father, my mother and my sister for believing in me and encouraging me to pursue this course. There are no words to express my gratitude for their constant support and unconditional love throughout these years and in my life in general.

I am very grateful to my advisor Prof. Stefano Lenci for giving me the opportunity to undertake and complete my Ph.D. program in the Polytechnic University of Marche as well as sharing knowledge, providing support, teachings, advice, suggestions and motivation. Our conversations were always a source of inspiration. Besides my advisor, I would heartily like to thank my co-advisor Prof. Francesco Clementi for providing all the necessary tools for this research work. The energy, understanding, fruitful discussions and support shown permitted me to complete this Thesis successfully. I would like to particularly thank my friend Gianluca Standoli for his constant support, understanding and encouragement throughout this long journey. I am grateful to all my research colleagues for our spirited discussions, encouragement and support these last few years.

Thank you!

## **Abstract**

Structural Health Monitoring has received wide recognition and development the last years. Advancements have been made in many of the fields, like sensing technologies, applications and data processing. Due to the increasing need for preservation of Cultural Heritage buildings that are affected by the multi hazardous environment and specifically earthquakes, the automatization of Structural Health Monitoring techniques has become an important research subject. The preservation of Cultural Heritage requires the combination of in situ investigations and accurate analytical models in order to understand and correctly interpret the empirical evidence in order to to successfully apply advanced structural analyses and assess the state of Heritage Buildings.

The Thesis focuses on the computational methods, correlation techniques and model updating with a nature-inspired metaheuristic algorithm indicating their advantages and drawbacks. The application of all the components comes under the form of a case study where the dynamic behavior of the Civic Tower of Ostra is thoroughly investigated by means of a detailed numerical model and calibrated against the experimental modal features. The pairing is based on the automatic procedure of calibration by a metaheuristic population-based genetic algorithm and use of machine learning. This step allows to successfully estimate the uncertainties of the unknown material parameters, considering both an isotropic and an orthotropic behavioral model for masonry. The results enable to validate the methodology and establish baseline information of the condition of the structure along with performance standards that will serve to control the structural integrity over time.



## Abstract

Structural Health Monitoring ha ricevuto un ampio riconoscimento e sviluppo negli ultimi anni. Sono stati fatti progressi in molti campi, come le tecnologie di rilevamento, le applicazioni e l'elaborazione dei dati. A causa della crescente necessità di preservare gli edifici del patrimonio culturale che sono interessati dall'ambiente multi-pericoloso e in particolare dai terremoti, l'automazione delle tecniche di monitoraggio della salute strutturale è diventata un importante argomento di ricerca. La conservazione del patrimonio culturale richiede la combinazione di indagini in situ e modelli analitici accurati al fine di comprendere e interpretare correttamente l'evidenza empirica al fine di applicare con successo analisi strutturali avanzate e valutare lo stato degli edifici del patrimonio.

La Tesi si concentra sui metodi computazionali, sulle tecniche di correlazione e sull'aggiornamento dei modelli con un algoritmo metaeuristico ispirato alla natura indicandone vantaggi e svantaggi. L'applicazione di tutti i componenti si presenta sotto forma di un caso studio in cui il comportamento dinamico della Torre Civica di Ostra viene approfondito mediante un modello numerico dettagliato e calibrato rispetto alle caratteristiche modali sperimentali. L'applicazione si basa sulla procedura automatica di calibrazione mediante un algoritmo genetico metaeuristico basato sulla popolazione e sull'uso dell'apprendimento automatico. Questo passaggio consente di stimare con successo le incertezze dei parametri sconosciuti del materiale, considerando sia un modello comportamentale isotropo che ortotropo per la muratura. I risultati consentono di convalidare la metodologia e stabilire informazioni di base sulle condizioni della struttura insieme a standard di prestazione che serviranno a controllare l'integrità strutturale nel tempo.



# Contents

<b>Introduction</b> .....	1
<b>Motivation</b> .....	1
<b>Literature Review</b> .....	2
<b>Thesis Aim and Structure</b> .....	4
<b>Chapter 1: Model updating methods and correlation techniques</b> .....	6
<b>1.1 Introduction</b> .....	6
<b>1.2 Analytical Modelling – Finite Element Analysis</b> .....	6
<b>1.3 Experimental Modelling</b> .....	7
<b>1.4 Connection of FE Analysis and Experimental Testing</b> .....	7
<b>1.4.1 Direct Methods</b> .....	9
<b>1.4.2 Iterative Methods</b> .....	10
<b>1.5 Correlation techniques</b> .....	12
<b>Chapter 2: Optimization Algorithms</b> .....	15
<b>2.1 Introduction</b> .....	15
<b>2.2 Heuristic and Metaheuristic definitions</b> .....	15
<b>2.2.1 Population-based metaheuristic algorithms</b> .....	16
<b>Chapter 3: Metamodel, validation and Sensitivity analysis</b> .....	23
<b>3.1 Introduction</b> .....	23
<b>3.2 Design of experiments</b> .....	24
<b>3.3 Role of Metamodels</b> .....	24
<b>3.3.1 Theoretical background</b> .....	25
<b>3.3.3 Validation techniques</b> .....	26
<b>3.4 Sobol’s sensitivity analysis</b> .....	28
<b>3.4.1 Theoretical background</b> .....	28
<b>Chapter 4: Case study: Civic Tower of Ostra</b> .....	30
<b>4.1 Introduction to the case study</b> .....	30
<b>4.2 Geometrical and material survey</b> .....	32
<b>4.3 Ambient Vibration Testing</b> .....	34
<b>4.4 Field testing procedure</b> .....	35
<b>4.5 Operational Modal Analysis</b> .....	37
<b>4.5.1 Data processing</b> .....	37
<b>4.5.2 Theoretical Background on the SSI-based methods</b> .....	37

4.5.3 Modal results .....	39
4.6 Numerical modelling and updating via Genetic Algorithm.....	43
4.6.1 Preliminary FE model.....	44
4.6.2 GA-based model updating.....	47
4.7 Calibration process .....	49
4.7.1 Twelve-group discretization approach.....	49
4.7.1 Model updating results .....	52
Chapter 5: Concluding remarks .....	58
<b>APPENDIX A – Evaluation of the influence of material parameters in automatic calibration .....</b>	<b>62</b>
<b>A.1. Genetic algorithm workflow .....</b>	<b>62</b>
<b>A.2 Metamodel.....</b>	<b>64</b>
<b>A.2.1 Parameters definition .....</b>	<b>64</b>
<b>A.2.2 Validation .....</b>	<b>65</b>
<b>A.2.2.1 Analytical validation results.....</b>	<b>65</b>
<b>A.2.2.2 Test – Train split validation results .....</b>	<b>68</b>
<b>A.2.2.3 K-fold validation results .....</b>	<b>71</b>
<b>A.3. Sensitivity analyses for isotropic material approach.....</b>	<b>74</b>
<b>A.4. Sensitivity analyses for orthotropic material approach .....</b>	<b>80</b>
<b>A.5. Convergence criteria .....</b>	<b>86</b>
<b>A.6 Example of an iterative “Trial and Error” calibration for the NM18 .....</b>	<b>94</b>
<b>A.6.1 Iterative approach without consideration of Sobol’s Indexes .....</b>	<b>94</b>
<b>A.6.2 Iterative approach considering 1% of Sobol’s Indexes .....</b>	<b>95</b>
<b>A.6.3 Iterative approach considering 10% of Sobol’s Indexes .....</b>	<b>95</b>
<b>References .....</b>	<b>98</b>

## List of figures

Figure 1: Model updating methods flowchart.....	9
Figure 2: Generic Genetic Algorithm flowchart.....	19
Figure 3: Representation of Population, Chromosome, Gene definitions of the genetic algorithm. .....	19
Figure 4: Example of crossover pairing, before and after.....	21
Figure 5: Example of mutation of a gene, before and after.....	21
Figure 6: Example of pseudocode of a Genetic Algorithm.....	22
Figure 7: K-fold validation of a dataset, with k = 10.....	27
Figure 8: Train/test schema of a dataset.....	28
Figure 9: Ostra Civic Tower localization.....	30
Figure 10: San Francesco Church and the tower before bombardments (a) and a view of the central square to the present days (b).....	31
Figure 11: Geometrical Survey of the investigated tower: Front views (top) and CAD sections (bottom).....	33
Figure 12: Excerptps from the photographic survey of the tower:(1) Trapdoor accessing the upper level and connecting iron ladder;(2) close-up of the 4th level brickwork;(3) concrete slab of the 3rd floor with ladder opening;(4) particular of the reinforcement intervention with tie rods;(5) close-up of the 2 <sup>nd</sup> level internal brickwork;(6) external brickwork of the 1 <sup>st</sup> level ;(7) basement brickwork;(8) spiral staircase at the entrance level.....	34
Figure 13: Instrumentation used for the ambient vibration tests.....	35
Figure 14: Sensor layouts and corresponding acceleration timeseries for the 2018 and 2019 dynamic testing campaigns(Blue,Green, Red colours indicate signals in x,y,z directions respectively).....	36
Figure 15: Complexity plots of the identified experimental modes for EM 2018 (a) and EM 2019 (b).....	40
Figure 16: Mode shapes of 2018 and 2019 EM's identified with the SSI method (in blue) and cross-comparison with the respective mode shapes identified with EFDD method (in red).....	41
Figure 17: Comparison between mode shapes of EM 2018 (in blue) and cooresponding ones EM 2019 (in red).....	42
Figure 18: FE modelling of the Civil Tower of Ostra: (a) Axonometric view, (b) Bottom view at foundation level.....	44
Figure 19: Frequencies values and mode shapes resulting from modal analysis operated on the preliminary FE model.....	46
Figure 20: Workflow for the projection of the experimental data onto the NM for the genetic algorithm updating,with measured nodes highlighted.....	48
Figure 21: GA-based model updating flowchart of the case study.....	49
Figure 22: Updating variables for the twelve-groud discretization of the FE model. Each material group is named as "X" followed by a subscript composed by a number (00 to 12) which stands for the group and a letter ("M" for masonry, "C" for concrete and "F" for the filling material).....	50
Figure 23: Numerical Mode Shapes after calibration using isotropic material modelling.....	55
Figure 24: Numerical mode shapes after calibration using orthotropic material modelling.....	56

Figure A. 1: Analytical model validation for isotropic model: curve fitting of frequencies test samples.....	65
Figure A. 2: Analytical model validation for isotropic model: curve fitting of mode shapes test samples.....	66
Figure A. 3: Analytical model validation for Orthotropic model: curve fitting of frequencies test samples.....	66
Figure A. 4: Analytical model validation for Orthotropic model: curve fitting of mode shapes test samples.....	67
Figure A. 5: Train/Test split validation for Isotropic model: curve fitting of frequencies test samples.....	68
Figure A. 6: Train/Test validation for Orthotropic model: curve fitting of mode shapes test samples.....	69
Figure A. 7: Train/Test validation for Orthotropic model: curve fitting of frequencies test samples.....	69
Figure A. 8: Train/Test split validation for Orthotropic model: curve fitting of mode shapes test samples.....	70
Figure A. 9: K-fold validation for Isotropic model: curve fitting of frequencies test samples.....	71
Figure A. 10: K-fold validation for Isotropic model: curve fitting of mode shapes test samples.....	72
Figure A. 11: K-fold validation for Orthotropic model: curve fitting of frequencies test samples.....	72
Figure A. 12: K-fold validation for Orthotropic model: curve fitting of mode shapes test samples.....	73
Figure A. 13: Sobol sensitivity analysis over first order indices for Kriging method. Thresholds of Sobol Indices (SI) respectively highlighted in black ( $SI = \pm 1\%$ ), red ( $SI = \pm 5\%$ ) and green ( $SI = \pm 10\%$ ).....	75
Figure A. 14: Sobol sensitivity analysis over total order indices for Kriging method. Thresholds of Sobol Indices (SI) respectively highlighted in black ( $SI = \pm 1\%$ ), red ( $SI = \pm 5\%$ ) and green ( $SI = \pm 10\%$ ).....	76
Figure A. 15: Variation of NM19 material parameters in comparison to NM18 (in blue) and NM19_0 (in orange) considering all parameters in the calibration process.....	78
Figure A. 16: Variation of NM19 material parameters with respect to NM18 considering a reduced number of variables based on different thresholds of SI.....	79
Figure A. 17: Sobol sensitivity analysis over first order indices for Kriging method. Thresholds of Sobol Indices (SI) respectively highlighted in black ( $SI = \pm 1\%$ ), red ( $SI = \pm 5\%$ ) and green ( $SI = \pm 10\%$ ).....	81
Figure A. 18: Sobol sensitivity analysis over total order indices for Kriging method. Thresholds of Sobol Indices (SI) respectively highlighted in black ( $SI = \pm 1\%$ ), red ( $SI = \pm 5\%$ ) and green ( $SI = \pm 10\%$ ).....	82
Figure A. 19: Variation of NM19 material parameters in comparison to NM18 (in blue) and NM19_0 (in orange), considering all parameters in the calibration process.....	84
Figure A. 20: Variation of NM19 material parameters with respect to NM18 considering a reduced number of variables based on different thresholds of SI.....	85
Figure A. 21: Influence of number of iterations on the convergence rate of NM2018 with isotropic material approach: calibration considering (a) all material parameters and (b) reduced number of parameters (based on thresholds fixed for SI).....	87
Figure A. 22: Influence of number of iterations on the convergence rate of NM2019_0 with isotropic material approach: calibration considering (a) all material parameters and (b) reduced number of parameters (based on thresholds fixed for SI).....	88

Figure A. 23: Comparison of convergence rate variations in the updating process of NM2019 isotropic model starting from NM2018 and using 2000 iterations: GA-based approach (green) versus Sobol method for different thresholds (blue, orange and yellow). .....	89
Figure A. 24: Influence of number of iterations on the convergence rate of NM2018 with orthotropic material approach: calibration considering (a) all material parameters and (b) reduced number of parameters (based on thresholds fixed for SI).....	90
Figure A. 25: Influence of number of iterations on the convergence rate of NM2019_0 with orthotropic material approach: calibration considering (a) all material parameters and (b) reduced number of parameters (based on thresholds fixed for SI).....	91
Figure A. 26: Comparison of convergence rate variations in the updating process of NM2019 orthotropic model starting from NM2018 and using 2000 iterations: GA-based approach (green) versus Sobol method for different thresholds (blue, orange and yellow). .....	92

## List of Tables

Table 1: Global Modal parameters identified for EM 2018 and EM 2019 .....	39
Table 2: MAC between mode shapes identified with SSI and EFDD methods. (a)EM 2018 and (b)EM 2019.....	41
Table 3:Percentage variation between modal frequencies damping ratios of EM 2018 and EM 2019. ....	42
Table 4: MAC between EM's mode shapes identified with the SSI method .....	43
Table 5: Elastic properties of the initial FE model. ....	45
Table 6: Preliminary results (NM0) and differences with the experimental frequency values (EM). ....	45
Table 7: MAC between numerical and experimental mode shapes: (a) NM0-EM 2018 and (b) NM0-EM 2019. ....	46
Table 8: Lower and Upper bounds for isotropic elastic properties (E is for the Elastic Young's, $\nu$ is the Poisson's ratio and $\gamma$ is the mass density).....	51
Table 9: Lower and Upper bounds for orthotropic elastic properties (G is the shear modulus while the subscripts L,N,T indicate the Longitudinal, Normal and Tangential components respectively. (*) Concrete stayed as isotropic material.....	51
Table 10: Optimal values for the material parameters of the isotropic FE models after calibration and successive updating.....	52
Table 11: Optimal values for the material parameters of the orthotropic FE model after calibration against 2018 EM modal data. (*) Concrete stayed as isotropic material. ....	53
Table 12:Optimal values for the material parameters of the orthotropic FE model after calibration against 2019 EM modal data. (*) Concrete stayed as isotropic material. ....	53
Table 13: Comparison between 2018 experimental (EM) and numerical (NM) frequencies for different material modelling approaches and different updating parameters.....	54
Table 14:Comparison between 2019 experimental (EM) and numerical (NM) frequencies for different material modelling approaches and different updating parameters.....	54
Table 15: CrossMAC between EM's and calibrated NM's considering isotropic and orthotropic materials:(a) NM 2018 with isotropic material,(b) NM 2019 with isotropic material, (c) NM2018 with orthotropic material, (d) NM2019 with orthotropic material. ....	57
Table A. 1: Initial parameters normal probabilistic distribution .....	64
Table A. 2: Analytical validation of frequencies .....	67
Table A. 3:Analytical validation of mode shapes .....	68
Table A. 4: Train/Test split validation of frequencies. ....	70
Table A. 5: Train/Test validation of mode shapes. ....	70
Table A. 6: K-fold validation of frequencies.....	73
Table A. 7: K-fold validation of mode shapes. ....	73
Table A. 8: Material parameters considered for calibration of NM19 after Sobol sensitivity analysis, using isotropic approach.....	77
Table A. 9: Variation of calibrated frequencies of NM19 in relation to the number of parameters subdued to updating process. ....	80
Table A. 10: Material parameters considered for calibration of NM19 after Sobol sensitivity analysis, using orthotropic approach. ....	83

Table A. 11: Variation of calibrated frequencies of NM19 in relation to the number of parameters subdued to updating process. ....	86
Table A. 12: Variation of frequencies of calibrated NM2018 with isotropic approach in relation to different number of iterations. ....	92
Table A. 13: Variation of frequencies of calibrated NM2019_0 with isotropic approach in relation to different number of iterations. ....	93
Table A. 14: Variation of frequencies of calibrated NM2018 with orthotropic approach in relation to different number of iterations. ....	93
Table A. 15: Variation of frequencies of calibrated NM2019_0 with orthotropic approach in relation to different number of iterations. ....	93

## Introduction

### Motivation

In the last decades, the world has been under the constant threat of natural disasters (volcanic eruptions, tornadoes, tsunamis, earthquakes) that caused a great amount of deaths and were reason for severe impacts that affected the social and economic development of the countries impacted. In many ways this implies that each country needs to have certain levels of preparedness in order to appropriately respond to the needs for reconstruction works, costs and humanitarian aid, created by these disasters which are often unsustainable. Each country has its own different territories, cities and villages which come with diverse elements of risks for Heritage buildings, infrastructures, etc. These risks are related to the multi-hazard environment and to different factors such as aging effects, excessive loads, accidents, etc., that provoke damage.

Masonry constructions are considered one of the most vulnerable structures. The vulnerability is due to several factors like the builder's expertise, the quality of the materials utilized for the construction and place of origin. In areas with high seismic activity, these structures represent an important part of the stock. In recent decades, there is an increasing interest for the study, conservation and restoration of heritage buildings because they benefit the social and economic activity.

Italy has been affected by numerous and diverse seismic sequences over the years and some of the most recent events (Friuli (1976), Irpinia (1980), Umbria – Marche (1996/97), Molise (2002), L'Acquila (2009), Emilia – Romagna (2012), Central Italy (2016/17) ) determined how restoration and preservation plans should be carried out. Restoration, maintenance and conservation plans for historical monuments and heritage structures are often under the jurisdiction of public administrations which are called to work with limited budgets. Therefore, the study and development of tools capable of studying the effects of seismic sequences and how they affect the historical structures is of great interest. To this date, Structural Health Monitoring (SHM) systems are a reliable choice to track and assess structural behavior. They can provide near real-time information for assessing the integrity and reliability of structures, allowing also for the quantification of changes in the inherent characteristics. They can also serve as early warnings for identifying faults not visible to the human eye. Furthermore, the SHM systems are divided in different methods including vibration-based methods which are based on the monitoring of structural vibrations under operational conditions with no external excitation sources. These systems are used to provide valuable information to improve the protection and conservation of heritage structures by means of diagnostic data. This procedure enables a condition-based approach with increasing economic potential. This approach is enriched with the use of machine learning and numerical methods to develop accurate analytical Finite Element models and facilitate the implementation of damage assessment studies.



## Literature Review

Many authors have defined, explained, study and research the concept of Structural Health Monitoring (SHM) and its applications. In general, SHM is defined as the process of implementation of a damage detection strategy for aerospace, civil and mechanical systems that aims at the automated assessment of the structural performance and its evolution over time using data acquired by sensory means ([1], [2]). In simpler terms, SHM in essence is a coagulation of different systems, disciplines and processes for observing, tracking and sampling data over a period of time to assess the quality of structural systems under the continuous accumulation due to aging effects and propagation of already existed damage in the systems configuration or new injuries of the structural state, results of operational and environmental conditions ([3]). Different reviews on the subject of SHM concerning the detection, location and characterization of damage within changes in the vibration response and approaches made through computational modelling and machine learning applications can be found in ([4]–[6]). Damage identification methods require large amounts of data and analysis techniques in order to create categories that describe each phenomenon. These techniques are followed by applications that take in consideration changes in sensitive features, with those being mainly the modal frequencies, mode shapes and damping. The change that is introduced into a system considering its material or geometric properties and considerably affects its current or future state, is defined as damage. ([7], [8]). To correctly define the concept of damage a comparison must be made between two states of the system, an initial one that is considered the “healthy” state or undamaged and a following state. The definition of the “healthy” state comes after careful evaluation and investigation of the changes that the structure has historically undergone, construction techniques used, investigation of the materials and mapping of damaged components([9], [10]).

The condition of a systems state can be described by categorizing each action taken for identifying the damage with a level. In the first level it is needed to determine whether damage or not is present in the investigated system. The second level it is called to detect the different locations of damage. The third level calls for the quantification, extension definition and recognition of the damage and the fourth level calls for a possible prediction of the service life of the structure. Damage quantification, localization and life service prediction remain subjects that deal with many difficulties. This happens due to the vast number of different variables that directly affect the subject. The prognosis of a systems state comes not only from vibration based systems but is complemented by environmental and operational conditions ([11]), testing, calibrating procedures, machine learning and modeling resulting in estimates of possible conditions and remaining life-cycle.

In the SHM field different techniques and approaches are present and can be described under different categories. A first category that approaches each problem globally, a second category that approaches the problem in a more specified manner locally and a third category that unites the former two by means of automated data-driven, modelling procedures and machine learning presenting so a more complete

solution. In the first group, vibration, image, displacement-based techniques are present along with those that go through geographical information system applications and are considered suitable solutions for the investigation of the complete system. These result in information gained for the global response of the system or compounds of different systems. The local group describes, in-situ inspection and investigation procedures of a structure or concentrates the efforts on different components of a structure and design experimental campaigns for material properties identification ([3], [12]–[16]). The third category is a unification between the global and local approaches that together with smart computational techniques searches for automated solutions that describe physics based problems and results not only in a categorical response of a state but also its quantification and visualization ([2], [17]–[22]).

Among the different strategies for SHM, some receive an increasing interest such as Ambient Vibration Testing (AVT), Long Term Vibration Monitoring, Data-driven methods. These strategies are based upon the continuous acquisition of the dynamic responses under operational conditions of a structure, application of statistical tools aimed at creating a flow of data for the identification of dynamic features ([23]–[27]), recognizing and removing environmental noises from the acquired responses and give sense to notable changes between states of the systems. Studies are made also in the recognition of anomalies in time-series design features by utilizing machine learning techniques ([28]–[30]). The dynamic features that are recognized and estimated with the help of automated procedures are increasingly used in vibration-based systems to assess structural performance and create early warning applications ([31]). In order to study the reduction of the increasing economic burden that comes with an SHM system, different studies and research concentrate to define the optimal framework of sensory hardware to apply on a structure. The frameworks properties look for the number, spatial location and type of sensor to utilize in order to maximize the information gained per unit cost utilizing evolutionary algorithms for the optimization procedure between cost and utility ([32]–[34]).

Structural Health Monitoring systems and especially ones that are based upon vibration studies offer reliably the identification of the dynamic characteristics through Operational Modal Analysis techniques and tracking of modal parameters ([35], [36]). Statistical tools are continuously being developed in order to study the variance in the data that is associated with the vibrational response, environmental conditions and detection of anomalies in structural behavior, mainly corresponding to variations of the natural frequencies and respective mode shapes. Such techniques are based on multivariate analysis ([37]), Principal Component Analysis (PCA) ([38], [39]). Recent advancements find also use of direct optimization procedures and data-driven models for damage detection that take account of environmental conditions and study their influence on structural behavior. Such methods are the Bayesian data driven model and Gaussian data driven model ([40]–[42]). These approaches open also the way for complete numerical solutions based on the Digital Twin framework. The framework aims at supporting different engineering domains into a unified set, it mainly articulates computational models, sensors, learning, real-time analysis, diagnosis and possible prognosis. Contrary to a Building Information Modelling approach, which involves the generation, manipulation and management of physical and functional characteristics, a Digital Twin refers to a complete digital replica of physical assets, systems and processes

that can be used for various purposes ([22], [26], [43]–[45]). In order to create a passage between the identification procedures and the computational simulations, model updating studies are made that study the effectiveness of different optimization procedures. The optimization studies follow different methods, such as gradient-based methods (quasi-Newton, augmented Lagrangian), response surface methods and nature inspired algorithms ([46]–[48]).

While the planning of an SHM system can potentially offer an accurate estimation of the structural systems state and predict potential problems, there are also limitations and aspects to take into consideration regarding their application Cultural Heritage structures. Some problems are, the selection of hardware solutions, number of sensors and are of physical nature. Some are of computational nature like feature extraction based on sensitivity studies, Finite Element modelling and updating or come by as decisions of the correct selection, training and validation procedure of a machine learning model.

## Thesis Aim and Structure

Considerable progress and breakthroughs have been made in the different fields of SHM. These fields include computational, statistical, data analysis and management alongside with new sensing technologies.

Within this context, the present research work introduces and describes the different methods and techniques used for a model updating procedure. The definition of the design parameters for the study is made in function of their sensitivity and how much they affect the results. The study of a nature inspired algorithms is presented with focus on population-based genetic algorithm, along with the influences the properties of the algorithm have on the desired result. The desired result is provided as a minimization of the complex problem between the identified natural frequencies and the numerical response of the finite element model and its modal shapes.

- Chapter 1: The first chapter introduces the model updating problem. It discusses on the workflow that is usually followed and updating methods that can be applied to solve the problem. Lastly, it introduces and discusses some of the well-known correlation techniques.
- Chapter 2: The second chapter introduces in general fashion some existing categories of computational intelligence, their place in Structural Health Monitoring and applications to model updating procedures. The focus is mainly on the characteristic class of population-based optimization algorithms giving details on the genetic algorithm and its operators.
- Chapter 3: The third chapter's main objective is Sobol's sensitivity analysis. In order to arrive at that objective an introduction is made on the metamodels and their purpose. The chapter presents different concepts such as the design of experiments, the role of the metamodels and validation techniques. Finally, a discussion is made on the theoretical backgrounds for both metamodels and sensitivity analysis.

- Chapter 4: The fourth chapter presents the results of the combining concepts of the previous chapters with the case study of the Civic Tower of Ostra. It explains the Civic Towers historical background and presents the field work carried out. It discusses the application of different identification techniques for two Ambient Vibration Tests. It then proceeds to introduce the complete workflow of the model updating procedure with the population-based genetic algorithm. It also analyses how the stochastic nature of the nature-inspired algorithm functions under different considerations one of which is by sensitivity analysis.
- Chapter 5: The conclusions of the present Thesis are summarized.

An Appendix with useful information about the work carried out during the study is reported at the end of this dissertation.

## Chapter 1: Model updating methods and correlation techniques

### 1.1 Introduction

The increasing demand for performance and new construction techniques have brought engineers to require robust testing and analysis tools. For example, to observe the changes in resistance and performance of a masonry structure, different analysis and confrontations must be made between an initial model and subsequent ones. The changes in the structural capacity provokes changes in the vibrational responses and thus the structural problem can also be considered as a vibration problem([36]).

In order to provide solutions to vibration problems in a structure, the dynamic behavior of the structure needs to be studied, understood and an accurate dynamic model needs to be developed. The analyses of the dynamic behavior with such a model optimize costing and testing efforts. For example, a decadence in the vibrational response of the structure could imply that there is a damage. An appropriate model makes it possible to evaluate changes in the structural design and plan solutions for retrofitting works. There are two ways of achieving the development of a suitable dynamic model of a structure, firstly with an analytical prediction and secondly by experimental measurement.

### 1.2 Analytical Modelling – Finite Element Analysis

If the structure is defined by a simple geometrical shape and the physical properties have a uniform definition throughout, then a simple partial differential equation of motion can be used to describe its dynamic properties. There are well known approaches for simple problems such as those of beams, shafts, shells and plates. For other more complicated approaches, these analytical solutions provide limited results because the necessary approximations required to apply are restrictive in order to accurately describe the dynamic properties.

The need for a method for modelling complex structures with non-homogeneous mapping of physical properties has led to the development of Finite Element Analysis (FEA). To this day, due to the advancements in numerical methods the FEA analysis is the most utilized technique in structural dynamic problems.

The fundamental principle of the finite element method is to recognize and divide the complex structure into smaller elements such as beams, shells, plates. The matrixes of mass and stiffness are defined and assembled considering the connectivity and boundary conditions that are applied. Once the model has been built, the equations of motion can be solved by using diverse variations of algorithms to obtain the dynamic behavior of the structure.

The FEA model can be subsequently used in order to perform different types of analysis. Some consider only a linear approach to arrive in conclusions, while others consider the non-linear part of the physical problem, stress analysis, lifetime prediction, etc. It becomes possible to evaluate the dynamic properties of a new or existing structure so

that inadequacies in its design can be spotted and changes applied to prevent incidents that could lead to higher reparation costs.

FE models need to be applied thoughtfully, because inaccurate or misleading modelling can lead to erroneous responses. Further considerations must be made on the modelling process due to simplifications of the geometry detail and the uncertainty of the physical properties especially when those are evaluated under a non-destructive testing (NDT) approach, ([49]–[51]).

### 1.3 Experimental Modelling

In addition to the analytical approach described in the previous section, another step needs to be made to develop a dynamic model of a structure. The experimental model is created by performing Ambient Vibration Tests (AVT) or Long - Term Monitoring (LTM), utilizing data analysis techniques and statistical tools on the measurements.

In a traditional approach, excitations and responses of the structure are measured to define the modal properties. The extraction of the modal properties without the measurement of an input force comes with a decrease in a projects cost and analysis time. This experimental approach is called output-only modal analysis and is a technique in which there is no need to measure the input excitations but just the responses. Contrarily to the traditional approach where a laboratory scale model needs to be constructed and tested, the output-only modal analysis can be performed on the site of the structure. This means that the use of the structure is not interrupted at any time and the analysis is performed under normal operating conditions (also known as Operational Modal Analysis (OMA)) with installation of sensors at key points. Finite Model Updating (FMU) is performed considering the data received from output-only modal analysis and arrives at a point where the Finite Element (FE) model can accurately represent the measured dynamic behavior.

### 1.4 Connection of FE Analysis and Experimental Testing

As a first step of the approach, the analytical model is used to predict the behavior of the structure considering its physical parameters as uncertainties. The next step comes from the OMA testing where the dynamic properties of the structure are directly measured. This creates a two-way validation where the experimental model validates the accuracy of the analytical model. This means that the FEA model's geometrical and physical inaccuracies are low, although this perfect condition is rarely seen to be the case. The problem that emerges then is that two different sets of dynamic properties describe the same structure. While neither can be said to be perfect, both have features that can be confronted to adjust the dynamic response of the structure.

Different limitations and assumptions are present in both approaches, the FE model and the experimental model are described by different characteristics and provide different advantages and disadvantages. Generally, the FE models' dynamic characteristics appear

to be more detailed and cover a wider range of frequencies if required. However, simplifications to the geometry and uncertainties of the physical properties of the elements create a situation where the FE model can provide inaccurate or incorrect results. At this point the experimental data or identified dynamic properties are the “correct” responses that define a closer representation of the structure, because they are obtained directly from the measurements of the structure rather than a simulation. Due to the usually limited number of sensors, because of economic factors, the information obtained is contained within a specific range rather than a complete searched space as can be provided by the FEA model. The principle of correlating these two approaches is to create the best possible outcome while overcoming the limitations that negatively affect the approach. Assuming that the experimental modal data has a higher degree of confidence, modal updating schemes have been developed with purpose of improving or correcting the FE model by utilizing the experimental test results as a base.

The initial step into model updating has always been accomplished by “trial and error” approaches which are dependent on engineering judgment and intuition. Although this approach works well in simple cases, the increasing complexity of a FEA model reveals the limitations of the “trial and error” method. Hence, more systematic approaches have become necessary to overcome this increasing difficulty. Generally, it is accepted that model updating methods are divided into two categories, the direct methods and the iterative methods. The direct methods mainly use the modal properties and are computationally efficient to implement. Consequently, they reproduce measured data in an exact manner although they don’t consider the physical properties of the model which causes them to provide unreliable results. On the other hand, Iterative methods are applied as solutions to minimization problems which utilize an objective function, that is generally provided as a non-linear function of selected modal features. The analysis is carried out by either confronting eigen-data (eigenvalues, eigenmodes) or frequency response function (FRF) data. These iterative methods can be applied, with certain constraints, to a wider search space for features updating and can overcome the limitations of the direct methods.

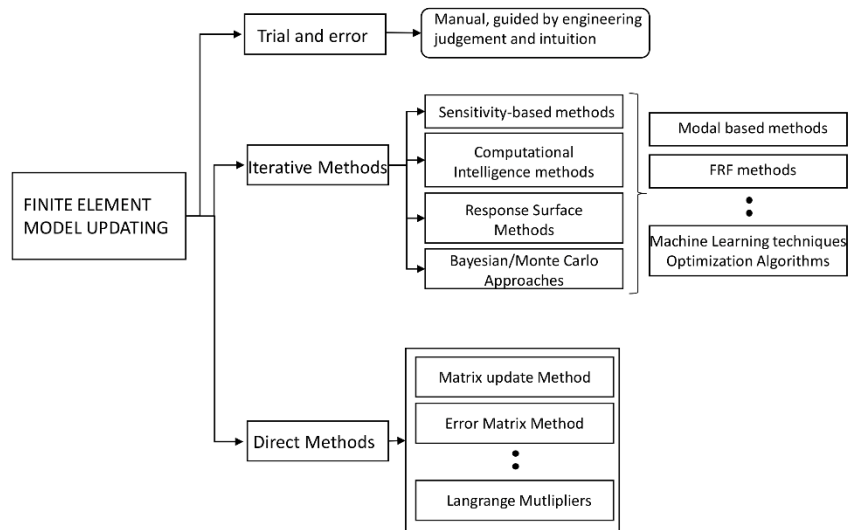


Figure 1: Model updating methods flowchart

### 1.4.1 Direct Methods

The direct methods generally use modal characteristics to recondition the analytical model. These approaches are presented as accurate and computationally efficient methods as they don't require any design parameters and iterations to execute the update. Several techniques were developed like the Lagrange Multipliers method which was introduced by Baruch ([52]), to force modal orthogonality constraints. Proceeding by the assumption that the mass matrix is fixed, the eigenvectors were selected for the updating by minimizing the weighted Euclidean norm of the differences between the analytical and experimental eigenvectors subjected to orthogonality constraints. The updated quantities are then used to update the stiffness matrix. Another method, called the Matrix-update method was proposed by Berman([53]), where the mass matrix was updated considering measured modal displacements and adopted in its process also the Lagrange Multipliers approach previously mentioned. The mass and stiffness matrices were thought as symmetric due to the consideration of an additional constraint. An analytical model improvement was later proposed ([54]) that combined the mass and stiffness matrices correction procedures. An orthogonality sensitivity-based method was studied by Guo ([55]) for model correction. In this method, the mass and stiffness matrices can be improved simultaneously with no changes in the size of the matrices or the configuration of the model.

Although diverse direct methods for model updating exist in the literature, their high complexities often mentioned, exclude them from being used for damage detection purposes.

Advantages of the techniques that apply direct methods are:

- High degree of convergence and accurate results;
- The model reflects the measured quantities in an exact manner;



- They do not take in consideration physical parameters.

The disadvantages are:

- Need for highly accurate measurement data;
- High sensitivity to noise;
- Equality between the sizes of measured and calculated responses;
- Unrealistic representation along the FEA model elements due to loss of symmetry to the model's matrices.

## 1.4.2 Iterative Methods

Iterative methods can be represented by different categories. These methods do not apply changes directly to the structures matrixes but perform the recondition in a step by step basis. The important part of these methods is the ability to assign different parameters and change them according to the problem. There are several different parameters to consider, like the number of physical parameters of a model, the feature parameters of the optimization algorithm, their sensitivity etc. The categories can be subdivided as:

- Sensitivity-based approach

Sensitivity-based approaches are used for their capability to calibrate a model by considering the influence of the design variables have on the results. In other words, it defines the study of how different sources of uncertainty, of a model or system, found in its inputs can contribute to the overall uncertainty of the results of the model.

- Response surface approach

Is a statistical approach that considers a correlation between sets of predetermined design variables and their corresponding responses viewed as polynomial functions. With this approach an optimization problem is considered in order to find the least variation between the FEA model and the measured data. It is a computationally efficient method that provides solutions even for complex problems.

- Bayesian and Monte Carlo approach

A Model Updating technique influenced by the Bayes theorem and considers a set of data with a probability distribution which reflects that of a model. The solution to these methods come with the application of a Monte Carlo algorithm to apply randomness and can end up with accurate results while avoiding overfitting of the model. The design variable estimation come with accurate results from the point of view of physics-based problems. Although obtaining accurate results for these approaches reveals to be problematic because of issues such as the high computational costs that derive from the solution of complex integrals or the definition for the solutions intervals that are required to be known in advance.

- Computational Intelligence approach

Computational intelligence approaches are considered for model updating because of their ability to handle different applications. The model updating is presented as an optimization problem in which parameters that physically represent the structure are selected and updated to achieve the required matching between the FE model and the experimental data. One factor that influences the parameters update comes from the uncertainty quantification. Main techniques of computational intelligence include machine learning and evolutionary algorithms.

Machine Learning (ML) studies computer algorithms that improve through experience by use of data. It is part of the wider part of Artificial Intelligence. The algorithms of machine learning essentially take sample data and train on it to make predictions and recognize patterns on new unseen data. The training samples can come either from a probabilistic design of experiments that is considered representative of the domain or from real data that has undergone analysis to understand and where needed cleaning operations are performed.

Evolutionary algorithms describe part of computational intelligence techniques that provide efficient mathematical approaches and can solve complex optimization problems like problems of high non-linearity, multimodal interactions, etc. The approach to model updating and damage detection with these algorithms enhances the ability to detect changes. Furthermore, the approach to model updating provides more accurate solutions and helps to overcome problems related to many local optima, by trying to find the global optimum.

In summary, the advantages of iterative methods are:

- High parametrization of the algorithms making them provide solution to case specific problems;
- Physical parameters are considered (Bounds);
- Variety of algorithms and solutions are present, proprietary or open source;
- Application of machine learning to automate procedures and gain knowledge;
- Estimation, quantification and sensitivity of uncertainty of the design variables in respect to the results;

The disadvantages are:

- High computational costs for calculations or training and test of ML models
- Background to a wide variety of disciplines is required (Statistical, Structural, Economical Programming)

## 1.5 Correlation techniques

Having set a basis for model updating in the Finite Element environment with the mentioned methods in the earlier section, it is needed to enter in a more detailed manner to the correlation techniques that are usually utilized in the model updating environment.

Correlation can be thought of as an initial indicator of the quality of an analytical model. Considering experimental data as the more accurate measurement it is used as basis to qualify the finite element model. Having defined tolerances and if within these tolerances the difference between the experimental and analytical model is contained then it is judged to be enough and no further updating is required. In contrast, if the differences are larger, the updating schemes continue considering the overall agreement between them.

Measured data sets are often considered incomplete as they are taken at selected locations and directions. The approach used in order to surpass this problem is to either reduce the analytical models degrees of freedom (DOFs) to the size of the experimental one or project the degrees of freedom of the experimental one to the analytical model, considering also the unknown, unmeasured locations of the FE model.

- Natural Frequency correlation

One of the most common correlation indicators and simplest, is to correlate two modal models with a direct comparison between the natural frequencies. For example, if a plot of experimental values is confronted against the analytical ones and has little to no differences, then the datasets are perfectly correlated.

The percentage difference between the experimental and numerical frequencies can be defined as:

$$\Delta f = \frac{|f_{exp} - f_{num}|}{f_{exp}} \times 100 \quad \text{Eq. 1}$$

and the complete frequency correlation indicator may be used as:

$$\Delta f = \sqrt{\sum_{i=1}^n \left( \frac{f_{exp}^i - f_{num}^i}{f_{exp}^i} \right)^2} \quad \text{Eq. 2}$$

While use of this correlation indicator is followed by high degree of accuracy, it needs also other indicators to act as constrains. This is because even if there is agreement between natural frequencies there is often disagreement between the resulting mode shapes of a structure.

- Mode Shape correlation

Mode shapes present themselves as a factor of comparison. Plotting experimental and analytical mode shapes against each other should result in corresponding designs. An indicator was thought of by Allemang and Brown ([56]), called the modal scale factor (MSF) and provides means of normalizing all the estimates of the same vector. Considering that diverse simplifications are made to the FE model and so the mass distributions between the real structure and the model may be different, the mode shapes should be scaled accordingly. When the two distinct vectors are scaled in a similar manner, then elements of the vector can be appropriately adjusted to provide a better estimate or indicate the type of erroneous vector by superimposing on the modal vector.

$$MSF(\Phi_\alpha, \Phi_\chi) = \frac{\{\Phi_\alpha\}^T \{\Phi_\chi\}^*}{\{\Phi_\alpha\}^T \{\Phi_\alpha\}^*} \quad Eq. 3$$

- Modal Assurance Criterion (MAC)

The pairing between modes in updating procedures based on modal data is one of the most crucial tasks. The matching of modes can be a challenging task especially when structures of high modal densities are considered. The Modal Assurance Criterion (MAC) is often used for pairing and comparison between mode shapes. A matrix of coefficients is computed with the following:

$$MAC_{i,j} = \frac{(\{\Phi_a\}_i^T \{\Phi_x\}_j^*)^2}{\{\Phi_a\}_i^T \{\Phi_x\}_i^* \{\Phi_x\}_j^T \{\Phi_x\}_j^*} \quad Eq. 4$$

Values of MAC close to unity suggest that the compared mode shapes are closely correlated.

- Coordinate Modal Assurance Criterion (COMAC)

Parting from the initial MAC concept proposes a way that the correlation is now directed to the degrees of freedom of the structure and not only to the mode shapes. Having first constructed the mode pairs, it calculates the correlation at each interested coordinate point over all the correlated mode shapes.

$$COMAC = \sum_{i=1}^n \left( \frac{|(\Phi_a)_{ir} (\Phi_x)_{ir}^*|^2}{(\Phi_a)_{ir}^2 (\Phi_x)_{ir}^2} \right) \quad Eq. 5$$

Again, to have an acceptable correlation between the coordinate space, the COMAC values should be near the unity.

- Frequency Response Function correlation (FRF)

The Frequency response correlation function is used to compare mainly experimental and analytical transfer functions. Usually only a visual inspection of the plots is needed to determine the degree of correlation. An error indicator may be also computed using the Euclidean norm of response function vectors at discrete frequencies:

$$\epsilon_{\text{Hij}} = \frac{\|(H_a)_{ij} - (H_x)_{ij}\|}{\|(H_a)_{ij}\|} \quad \text{Eq. 6}$$

Considering also an application of the MAC technique, on the concept of frequency shifting, ([57]) proposed to measure the close differences between measured and analytical FRF by the following criterion:

$$FDAC(f_A, f_X, j) = \frac{(\{H_A(f_A)\}_j^T \{H_X(f_X)\})^2}{(\{H_A(f_A)\}_j^T \{H_A(f_A)\}_j) (\{H_X(f_X)\}_j^T \{H_X(f_X)\}_j)} \quad \text{Eq. 7}$$

The frequency response domain criterion (FDAC) is the equivalent of the Modal Assurance Criterion but in the FRF domain. The same ranges of values also apply. A value close to unity means a perfect correlation while values close to zero mean that there some to no correlation at all.

Direct methods approach the model updating problem in ways that are advantageous due to the high accuracy that is provided. The lack of consideration of physical parameters of the model makes them less appealing. Contrary, the iterative methods appear to contribute with a wider variety of solutions in SHM. The definition physical parameters and control of the search space makes them more appealing for damage localization and quantification purposes. These approaches can result computationally more expensive, require background in more than one discipline in order to be correctly utilized and to be able to interpret the results. The automatization of model pairing along with the information that can be gained studying and quantifying uncertainties of design parameters and models offers a different point of view on existing and potential problems. A key point of the process of model updating comes with the selection of the appropriate optimization algorithm that will perform the necessary steps to achieve the least possible difference between the experimental and numerical models.

## Chapter 2: Optimization Algorithms

### 2.1 Introduction

A way to recognize what optimization is, comes by defining a problem in which finding the values of input parameters that are closely related to an objective function and results in a function evaluation. The minimization or maximization of the function's evaluation, as what is considered the best possible outcome, is defined by the nature of the problem and the solution one tries to accomplish.

In Structural Health Monitoring (SHM) and specifically in Finite Element Model Updating (FEMU), the nature of the problem is usually one of minimization of an objective function. The objective function can be composed by one or more terms made by correlation indexes. The correlation indexes are populated by the dynamic properties of the experimental and numerical models. An important part of the updating procedure comes with the selection of the algorithm by which the optimization is going to be resolved.

Many classic algorithms appear to be deterministic in nature. These deterministic-natured optimization algorithms use gradient information to direct the optimization process to a solution. By that they take the name of gradient-based algorithms. For example, the Newton – Raphson algorithm is gradient-based due to the use of the function's derivatives. This means that the algorithm requires the derivative which in some cases is not easily obtainable or can be expensive to calculate. If there are discontinuities in the objective function, then these algorithms do not perform as is desired and so non-gradient approaches are preferred, ([58]). Another option between the deterministic gradient or non-gradient based approaches is offered by the classes of heuristic and metaheuristic algorithms.

### 2.2 Heuristic and Metaheuristic definitions

The stochastic algorithms are mainly divided in two categories: Those that are heuristic and the metaheuristic. The word heuristic is derived from a Greek work that means “to discover” and describes a method that comes from experience and helps go through different things. Much like the process of elimination, process of searching or the process of “trial and error”. The heuristic optimization comes as the name suggests by “trial and error”. This approach produces acceptable solutions to complex problems in a considerate time. The complexity of the problem provokes certain degrees of difficulty, because not all possible solutions can be searched in a reasonable amount of time. The aim is to find a good solution in an acceptable timeframe. Thus, another problem is generated, that of the quality of the solution as there is no guarantee that the best solution can be found for the given problem or if it does, it doesn't mean that is unique and no other solution exists ([59]).

Therefore, a further development of the heuristic algorithms presents itself under the name of metaheuristic algorithms. The term is a combination of the Greek prefix “meta”, which means “beyond” and “heuristic”, “to search”. The performance of this category is better than simple heuristics. Notable characteristics of the metaheuristic algorithms are found in the definitions of diversification and intensification. By diversification it is meant to generate diverse solutions by looking at the entire search space for the optimal solution. Intensification means to focus entirely on the search of the optimal solution in a local region by exploiting the information gained by the current solution found in the vicinity of the searched region. This method in combination with diversification applies also a random factor in the exploration of the search space. This applied randomness ensures two things; first, the solution will not be trapped in a local optimum and second, it will converge to optimality. Metaheuristic algorithms can be categorized further in two ways, namely: Single-solution based and population-based. One of the most popular metaheuristic categories are the population-based algorithms that include genetic algorithms (GA), particle swarm optimization (PSO), firefly algorithm (FA), which all use multiple agents or particles.

In literature the definition of heuristics does not find an agreeable difference. Some use the heuristics and metaheuristics as synonymous meanings. The ongoing trends tend to name all the stochastic algorithms that have properties of randomization and local search as metaheuristics. In the present work this convention is also applied.

### 2.2.1 Population-based metaheuristic algorithms

In this section some of the well-known population-based metaheuristic algorithms are going to be presented, along with their focus of application in Structural Health Monitoring, theoretical background, advantages and drawbacks, with focus on the population-based genetic algorithm.

- Firefly Algorithm

The Firefly Algorithm was initially introduced by Yang at Cambridge University in 2007, ([60]). It is a bio-inspired metaheuristic algorithm applied to optimization problems. The algorithm is inspired by the behavior fireflies have in the night. This means that there are certain rules the algorithm follows to achieve this behavior and by construction there are three rules that are followed. The first rule is that all the fireflies are unisex, which means that the fireflies can be attracted to each brighter one. The second rule determines the brightness each firefly has by the objective function and the third rule states that the attractiveness is directly proportional to the brightness but decreases with distance. A firefly will be attracted to a brighter one although if no brighter one exists it will move randomly.

Taking this algorithm from a physics point of view it is needed to set some definitions. The lights intensity is defined as inverse proportional to the square of the distance  $r$ , from the source. If the light encounters a medium with a certain absorption coefficient  $\lambda$ , then the intensity  $I$  varies with the distance  $r$ , as:

$$I(r) = I_0 e^{-\lambda r} \quad \text{Eq. 8}$$

With  $I_0$  the lights intensity at the source point.

By combining the definitions, we have:

$$I(r) = I_0 e^{-\lambda r^2} \quad \text{Eq. 9}$$

The attractiveness similarly as:

$$A(r) = A_0 e^{-\lambda r^2} \quad \text{Eq. 10}$$

Where  $A_0$  is the attractiveness value at  $r = 0$ .

If the location of a firefly is at  $x' = (x'_1, x'_2, \dots, x'_n)$  and is brighter than the firefly located at  $x = (x_1, x_2, \dots, x_n)$ , the firefly located at the  $x_{th}$  position will move towards the one at the  $x'_{th}$  position. The updated location of the firefly of the  $x_{th}$  position will be done as:

$$x = x + A_0 e^{-\lambda r^2} (x' - x) + a\varepsilon \quad \text{Eq. 11}$$

The last term,  $a\varepsilon$  defines the randomization with  $a$ , the randomization parameter which varies between  $[0,1]$  and  $\varepsilon$ , the vector of random numbers. The term  $(x' - x)$  of the Eq. 11, is due to the attraction between the fireflies or  $x$  towards  $x'$ .

The workflow that this algorithm follows is to initially generate a set of random solutions  $\{x_1, x_2, \dots, x_k\}$ . Then for each solution compute the intensity  $\{I_1, I_2, \dots, I_k\}$ . At this point each firefly will move towards the brighter ones or randomly depending on the existence of brightness and update the solution. These steps will continue unless a stop criterion or tolerance is fulfilled.

Different applications of the firefly algorithm can be found as the works of González ([61]), where the implementation was used to determine damage conditions. It evaluated the dynamic response of a test system and compared it against a database constructed by different damage scenarios to determine the damages magnitude and location. Other applications of the firefly algorithm concentrate their interest on optimal sensor placement (OSP) and damage detection, ([62], [63]).



- Particle swarm optimization (PSO):

This nature population based stochastic technique was developed by Eberhart and Kennedy in 1995 ([64]) and was initially to confront continuous problems of optimization. The systems procedure initializes by setting up randomly generated potential solutions and then performs a search for the optimum one by swarms that follow the best particle.

Set for N-dimensional search space,  $m^{\text{th}}$  particles are generated as part of a population  $\{X_1, X_2, \dots, X_m\} \subset R^n$  and the  $i^{\text{th}}$  particle position is defined as  $X_i = (x_{i1}, x_{i2}, \dots, x_{iD})^T$ . The velocity a particle acquires is represented by another vector  $V_i = (v_{i1}, v_{i2}, \dots, v_{iD})^T$ . The best position visited previously by the particle  $X_i$  is then denoted as  $P_i = (p_{i1}, p_{i2}, \dots, p_{iD})^T$ , while the best position amongst all the particles of the population is represented by  $P_g = (p_{g1}, p_{g2}, \dots, p_{gD})^T$ .

Each particle adjusts its position dynamically according to the command of following the current optimal particle and updates the speed according to:

$$v_{id}^{i+1} = \omega v_{id}^t + c_1 r_1 (p_{id}^t - x_{id}^t) + c_2 r_2 (p_{gd}^t - x_{id}^t) \quad \text{Eq. 12}$$

$$x_{id}^t = x_{id}^t + v_{id}^t \quad \text{Eq. 13}$$

Where:

- $t$ , stands for the iteration time;
- $d$ , represents the particles dimension;
- $i$ , represents the particles number;
- $m, r_1, r_2$  are randomly generated coefficients between 0 and 1;
- $\omega$ , represents the inertia weight;
- $c_1, c_2$  are learning factors that adjust on each iteration's length.

Many times, in literature it was noted the importance of the inertia weight  $\omega$ , but in its place  $\omega^t$  is used and is defined as:

$$\omega^t = \omega_{max} - \frac{\omega_{max} - \omega_{min}}{t_{max}} \times t \quad \text{Eq. 14}$$

With this strategy, the inertia weight decreases during the execution of the algorithm. The accepted values found in literature for  $\omega_{max}$  and  $\omega_{min}$  are set to [0.9,0.4].

Implementations of this algorithm can be found in several sectors of structural health monitoring for optimal sensor placement and damage detection using different variations and hybrid forms of the algorithm, ([47], [65]–[67]).

- Genetic Algorithm

During the year 1950, the problem of artificial intelligence was studied, and Alan Turing proposed ([68]) a method so a machine could “learn” to simulate the learning process that happens in a child’s brain. This was later used by Barricelli in 1954 ([69]) by guiding the first successful experiment regarding artificial evolution. However it was not until 1975 that the Genetic Algorithm (GA) was applied to function optimization by John Holland, ([70]). The genetic algorithm was inspired by Charles Darwin’s theory of natural selection and itself under the heading of the larger class of evolutionary algorithms (EA). It emerges as an important tool that aims at efficient solutions for problems with wide range of solutions and complex search spaces by relying on biological inspired operators that take the names of mutation, crossover and selection.

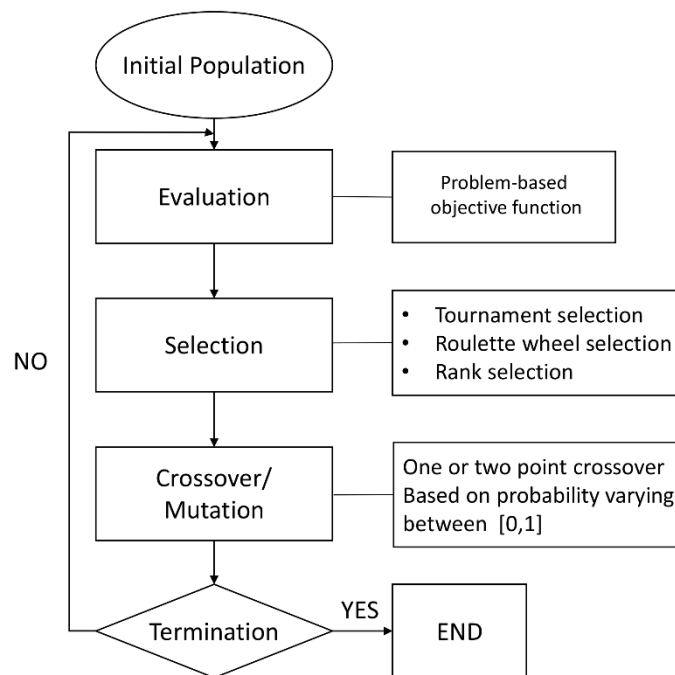


Figure 2: Generic Genetic Algorithm flowchart.

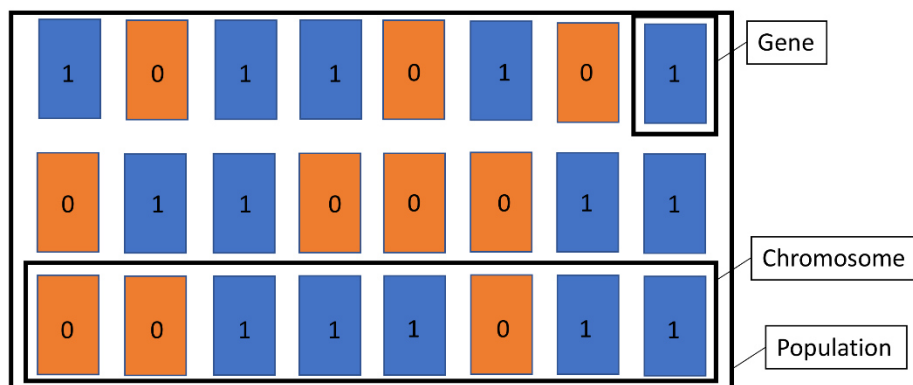


Figure 3: Representation of Population, Chromosome, Gene definitions of the genetic algorithm.

The process of the genetic algorithm usually starts by the definition of randomly generated solutions allowing so the possibility to find a solution in the entire search space. It is a process of iteration and each population of the iteration is called a generation. The size of the population depends on the nature of the problem and contains several possible solutions. There are occasions on which solutions may be in “seeded” areas where optimums are likely to be found.

In each generation, the performance of every individual is measured by an objective function. The objective function may vary according to the problem and usually in the context of structural health monitoring is compiled by different correlation techniques like those found in Chapter 1. The solutions with higher performance are then selected in a stochastic manner from the generated population and the ones with higher performance values are affected by the processes of mutation and recombination to form the next generation. The selection can include previous solutions in the next generation if a certain threshold of performance is reached. Then the new generation of candidate solutions is used in the upcoming iteration of the algorithm.

An important part of the genetic algorithm as mentioned earlier are the genetic operators and the role they have in the algorithms function. To be able to give comprehensive discussion, solutions and examples are going to be represented by binary strings, another form of encoding for the genetic algorithm. The interactions between these operators makes the behavior of the algorithm complex. However, individually the role each has is straightforward, ([71]–[74]). The Selection operator determines which individuals are chosen for the purpose of crossover and mutation as well as the number of children every individual reproduces. Its main purpose is to guarantee that the individuals whose performance is better, will be chosen to be parents. To this end there are several different strategies that can be used such as the Tournament Selection, Roulette Wheel Selection or Rank Selection.

- Tournament Selection is the most common technique used for the selection operator because of its efficiency and implementation. In this procedure, several individuals are selected randomly. Then a competition is held amongst the individuals to determine the one with highest performance to be used in the new generation. Diversity is a key point of the tournament selection and it is upheld due to the equal chance to be chosen given to the individuals even if that reduces the convergence speed.
- Roulette Wheel Selection also called fitness-proportionate uses values of fitness to choose which are the parents. The best performer amongst the individuals stands a higher chance to be selected.
- Rank Selection is done as the name suggests by assigning a rank. The fitness value here is used to rank the individuals of the population. The ones with best rank are used at the next generation.

The Crossover operator work is to select random point of the individual and exchange parts between the parents. Then a new offspring is produced based on the point chosen with the exchanged parts of the parents. The application of this tactic ensures that no duplications between the parents are going to be made and the new population generated has the desirable parts or qualities of the parents. It is defined as a probability

that ranges between  $[0,1]$ , where 0 means that all offspring are made by crossover and 1 means that the old generation of individuals is copied as is to the new generation.

Different strategies can be implemented for this operator as well like the one-point crossover, two-point crossover or uniform crossover.

- One-point crossover works when a crossover point of the individual is selected and are used between the parents to create two offspring.
- Two-point crossover defines two points to be selected on the individual. It then exchanges these two points for the generation of two offspring.
- Uniform crossover doesn't divide the chromosome into segments but treats each gene separately. Essentially uses a 50-50 chance for each chromosome to decide whether or not it will be considered in the offspring.

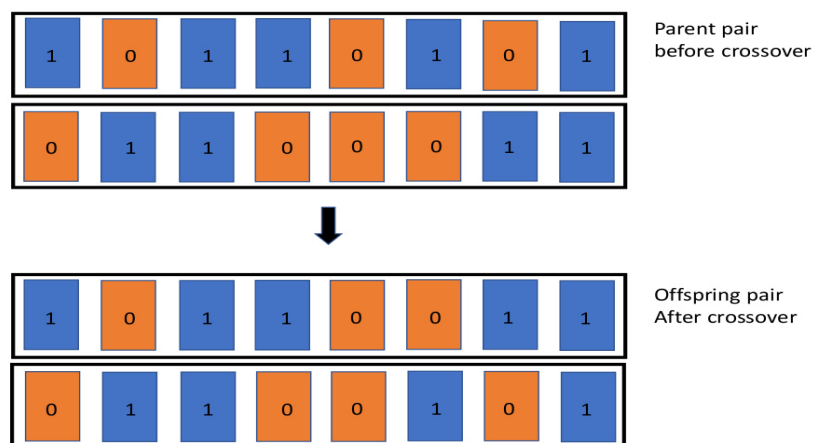


Figure 4: Example of crossover pairing, before and after

Mutation operator takes its place once the crossover is finished. This operator applies stochastic changes to one or more parents to create new offspring. The rate of mutation is defined as a probability in the range  $[0,1]$ . Higher the probability of the mutation operator, wider the search space becomes but the convergence also becomes more difficult, in contrary with low mutation probability the search space is narrowed down and the convergence becomes easier to obtain. The operator can be thought of as an adaptive search to the global optimum.

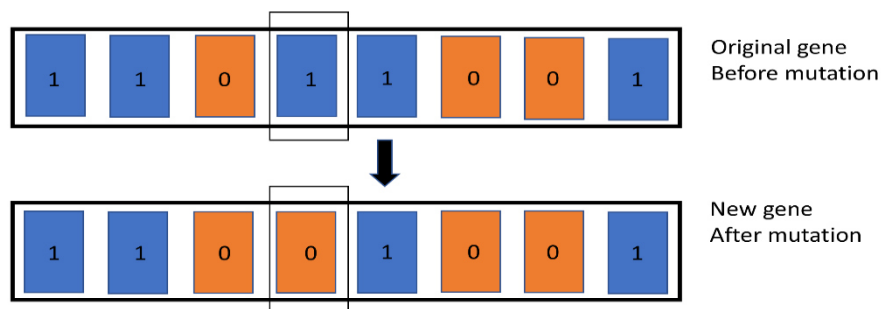


Figure 5: Example of mutation of a gene, before and after.

- Let  $P = \{X_1, X_2, \dots, X_n\}$  be the population
- GA procedure:
  - Begin:
  - Initialize  $P(t)$
  - While not terminate
    - Begin
      - » Evaluate fitness of population members  $P(t)$
      - » Select members of  $P(t)$  based on fitness
      - » Produce offspring of pairs using genetic operators
      - » Replace individuals of  $P(t)$  based on fitness with these offspring
    - End
  - End

*Figure 6: Example of pseudocode of a Genetic Algorithm*

Each of these algorithms comes with each own advantages and drawbacks. A common advantage between these algorithms is the easy implementation and efficiency they present to updating problems. Although the approach to efficiency is closely related with the complexity of the problem. Drawbacks are concentrated in the ability of each algorithm to surpass local optimums and the convergence rate. The firefly algorithm, is slow in convergence and has low exploration capability, making it difficult at times to achieve optimal solutions ([75]). The particle swarm optimization algorithm, suffers from the same drawbacks, ([76]). Unlike the genetic algorithm, the firefly and particle swarm optimization algorithms do not change the population in each generation but they iteratively update the positions and velocities of their members. They have no “notion” of the “survival of the fittest” or other operators although they keep the interaction and influence between their members. Having these notions on the genetic algorithm, signifies that the search space does not remain static, it explores different regions avoiding local optima searching for the global optimal solution.

## Chapter 3: Metamodel, validation and Sensitivity analysis

### 3.1 Introduction

In the field of computer experiments, sensitivity analysis is made to explore the relationship between the inputs and outputs of data. To proceed with a model updating procedure it is needed to select different parameters, called also design variables, as candidates to produce the required results. Design variables are presented as entities that can generally change the properties of a model, with those being either geometrical or physical, within specified tolerances ([77]). There are two points of view on how many parameters should be considered; the first is to allow all the possible parameters to participate in the updating process, and the second is to select a subset of them based on their physical meaning or by engineering experience. In this way the problem of parameter selection is introduced.

In earlier years, the selection of the parameters was done by engineering experience but being empirical and due to the increasing complexity models have it is thought as evaluation for the design variables. Among different methods, direct methods were applied in the work of design variables selection. In the work of Ahmadian et al. ([78]), a matrix decomposition method was used to update the eigenvalues and eigenvectors of individual elements and. But as it was discussed in Chapter 1, the use of such direct methods often leads to a good reproduction of the data with high accuracy but loses in terms of physical meaning. Of course, the need for physical meaning depends on the nature of the problem.

There are numerous studies and research on local sensitivity methods, ([79], [80]). Methods that select a subset of parameters or groups and minimize a function for updating purposes ([81], [82]). There is a distinction to be made regarding this diversity of the methods: One category methods acts locally, varying one parameter at a time, with others being fixed; a second category acts globally quantifying the influence of the candidate parameters on the whole range of application to determine the impact on the output and a third category is composed by the screening methods that cover the input space and determine in a qualitative manner the most influential inputs with some simulations. The problem with the methods of local sensitivity is the approach they have with by defining local gradient on the response of the analytical model, meaning that the applicability of the methods is concentrated to the close space of the initial parameters estimate. Also, these methods cannot measure the uncertainty in the model because they are able to recognize only the part of the parameters that are sensitive and take no account of test data. Global sensitivity methods offer advantages not found in the local method, such method is the variance-based sensitivity analysis or Sobol's sensitivity analysis. To properly calculate the indexes of a global sensitivity method there are several iterations must be made. Due to the high computational cost of this method cannot be applied directly to a finite element model, so an alternative is needed. The alternative comes in the form of a metamodel. The metamodels purpose is to reduce the

computationally high strain that the analysis needs be evaluated. To do so it is important to define the domain of application. This definition comes usually with a design of experiment (DOE).

### 3.2 Design of experiments

A Design of experiments defines a strategy in which the substitutive model for multi-subject purposes (metamodel), like calculating the Sobol's indexes from sensitivity analysis, is designed. The strategy involves the generation of sample points by factorial or probabilistic approaches:

- Factorial Design of experiments

A factorial design of experiments consists of two or more factors (or design variables) and each of these factors has its values defined discretely by levels. In that way the effect of the level of a factor can be studied against other factor levels. This approach also provides an estimation of the experimental error due to its replicability, especially when the system is simple. Depending on the number of factors and levels, it becomes difficult to maintain the replicability and sense of magnitude on the response.

- Probabilistic Design of experiments

Contrary to the factorial design, where the design variables are factors discretized by levels, the probabilistic design sees the variables as probability distributions. This approach facilitates the use of probability theory and allows knowledge of uncertainty to be applied more effectively. Even if this approach come with a high computational cost and knowledge of probability, the understanding of the wider range of applied uncertainty defines solutions that otherwise could not be seen.

There are certain requirements in summary that a design of experiments is to fulfill to ensure the accuracy and obtain a good model. These requirements concern the appropriate number of design variables, the domain or distribution that better represents them. The number of experiments also defines a fundamental parameter because too small of a sample can lead in underfitting and too many experiments can lead to overfitting, alas to no or wrong conclusions and affect the quality of the metamodel.

### 3.3 Role of Metamodels

The estimation of sensitivity indices usually comes with an elevated number of evaluations to be done due to the crude discrete integration methods that are applied. In the model updating field in order to reduce the computational strain, metamodels are build. Metamodels, also referred as "surrogate models" or "response surfaces" are part of "low computational weight" models to study physical systems, in which specifically set model inputs are related to determined model outputs ([83]–[85]). Possible implementations of metamodels come from the large field of computer experiments,

with a popular one being the Gaussian process model but also polynomials, Polynomial Chaos Expansion, splines or Neural Networks. As the metamodel approximates the experiment, the error that derives from the process must be considered and the accuracy of the model needs to be carefully examined.

### 3.3.1 Theoretical background

The Gaussian process model, also called Kriging has its origins in Geostatistics, ([86]) and it is considered a standard tool in computer experiments for different reasons. It interpolates the data and aims at creating a predictor that can be denoted as  $\hat{G}$  and is assumed to be a realization of the normal process  $Y: \Omega \times R^d \rightarrow R$ , defined by:

$$Y(\omega, x) = f(x) + F(\omega, x) \quad \text{Eq. 15}$$

Where:

- $f(x)$  defines the trend;
- $F(x, \omega)$  is a zero – mean Gaussian process with a covariance function  $C: R^d \times R^d \rightarrow R$  dependent on the vector of parameters  $x \in R$ , for some given event  $\omega \in \Omega$ :

$$E[F(x), F(y)] = C_{\theta}(x, y). \quad \text{Eq. 16}$$

The trend is taken equal to the generalized linear model:

$$f(x) = f(x)^t \beta \quad \text{Eq. 17}$$

The method approximates the model F by the means of the Y given that:

$$Y(\omega, x^{(i)}) = y^{(i)}, \quad \forall i = 1, \dots, n \quad \text{Eq. 18}$$

It follows that the metamodel can be written as:

$$\check{G} = E[Y(\omega, x) | Y(\omega, x^{(i)}) = y^{(i)}, \quad \forall i = 1, \dots, n] \quad \text{Eq. 19}$$

and defined as:



$$\check{G} = (f(x))^t \check{\beta} + (C_\theta(x))^t C_\theta^{-1} (y - F \check{\beta}) \quad \text{Eq. 20}$$

with  $\check{\beta}$  being the least squares estimator for  $\beta$  :

$$\check{\beta} = (F^t C_\theta^{-1} F)^{-1} F^t C_\theta^{-1} y \quad \text{Eq. 21}$$

Having the functions defined, the Kriging predictor is constructed by selection of  $\beta$  parameters and  $\theta$  correlation parameters. Given the high coefficient of determination ( $R^2$ ) obtained from different stages of validation (see sub-Section A.2.2), this model was ultimately employed as reference for the calculation of the Sobol Indices.

### 3.3.3 Validation techniques

As it was briefly stated in the introduction, a metamodel approximates the experiment, the error that derives from the process must be considered and the accuracy of the model must be examined. In this regard there are several validation techniques that can be applied. Validation techniques are used to get the error of the constructed model which can be considered as close to the true error found in the population. Among the most popular techniques, the k-fold validation and the train and test techniques are those with higher applications [87], [88].

- The k-fold validation

The K-fold cross validation technique relies on the division of the dataset (called X) into K mutually exclusive sub-samples ( $X_n$  with  $n = 1, 2, \dots, m$ ). A sub-sample is set aside for the response surface to be built on the remaining sub-samples. The approximation error is then estimated utilizing the sub-sample that was left aside and is defined as:

$$R_i = \frac{1}{|X_i|} \sum_{X \in N} |h(X) - h^N(X_i)|^2 \quad \text{Eq. 22}$$

in which the quantity  $|h(X) - h^N(X_i)|^2$  is the predicted residual, namely the difference between the evaluation and the prediction at point  $X_i$  of the sub-sample. The approximation errors are estimated using each sub-sample as validation, whereas the

remaining sub-samples are used for training. At the end of the process, the K-fold cross validation error estimate is obtained as the average:

$$R_{K-Fold} = \frac{1}{K} \sum_{i=1}^K R_i \quad \text{Eq. 23}$$

The k value must be chosen according to the data. A poorly chosen value may create misinterpretations on the quality of the model. Common tactics on the decision of the k value are divided between a representative tactic, where the value of k is chosen in order for the remaining sample to be large enough to represent statistically the broader dataset, the  $k = n$  tactic, where k is equal to the size of the dataset and in such way gives the opportunity to each test sample to be used and the  $k = 10$  tactic, where the number of folds is fixed to 10. The value of 10 was found in various experimentations as the value that results in the model's skill estimate with low bias and modest variance [89].

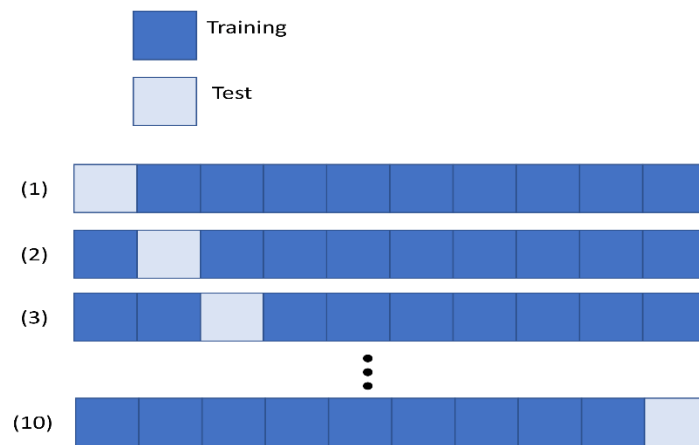


Figure 7: K-fold validation of a dataset, with  $k = 10$ .

- Train/test validation

The procedure for the train/test validations, considers taking a dataset and dividing it into two subsets. The first subset is used to train the model and the second subset is used to test the model. The difficulty of this validation comes in terms of size for the data that needs to be appropriately large. This means that it is specific to each different problem. The initial dataset must be a suitable representation of the domain with enough records to cover the majority of the cases along with the cases that present uncommon variations. Conversely, the procedure is not appropriate when the dataset is small because there will be not enough data for the training and the test to effectively evaluate the model's performance.



Figure 8: Train/test schema of a dataset.

### 3.4 Sobol's sensitivity analysis

Sobol's method is based on the decomposition of the model's output variance into additions of variances of the input in increasing dimensionality. This type of sensitivity analysis determines the contribution each input holds and their interaction to the overall output variance of the model. The decomposition of the output's variance employs the same principle as the analysis of variance in a factorial design. The first mention of the decomposition is found by Hoeffding [90] and was used to obtain independent random variables for the purpose of studying properties of U-statistics. In later years the it the decomposition was found to be unique and Sobol in 1993 repurposed it under the context of sensitivity analysis,([91], [92]).

#### 3.4.1 Theoretical background

Let  $Y = f(X)$ , where  $X = (X_1, X_2, \dots, X_d)'$  a vector of independent variables whose distribution  $\mu = \mu_1 \otimes \dots \otimes \mu_d$  and  $f: \Delta \rightarrow R$  with  $f(X) \in L^2(\mu)$  denoting the space of square-integrable functions with respect to measure  $\mu$ .

The function can be decomposed into additive terms as:

$$f(X) = f_0 + \sum_{i=1}^d f_s(X_i) + \sum_{i<j} f_{i,j}(X_i, X_j) + \dots + f_{1,\dots,d}(X_1, \dots, X_d) \quad \text{Eq. 24}$$

The terms  $f_i(X_i)$  represent first-order effects, second-order interactions and combinations of input variables. The uniqueness of the decomposition comes from  $f_I(X_I), I \subset \{1, \dots, d\}$  have zero mean.

$$E(f_I(X_I)) = 0, I \subseteq \{1, \dots, d\} \quad \text{Eq. 25}$$

And the conditional expectations fulfill the non -simplification conditions:

$$E(f_I(X_I) | X_j) = 0, J \subset I \subseteq \{1, \dots, d\} \quad \text{Eq. 26}$$

From the Eq. 25 and Eq. 26, it follows that the terms have zero correlation:

$$E(f_I(X_I)f_{I'}(X_{I'})) = 0, I \neq I' \quad \text{Eq. 27}$$

The decomposition can be obtained by recursive integration. By computing the variance of Eq. 24 we have:

$$D = \text{Var}(f(X)) \quad \text{Eq. 28}$$

Where each term quantifies the impact the input parameters have on the response.

These variances are known as unscaled Sobol Indices ([92]). The first order Sobol Index is used as a quantifying measure of the influence of first-order effects. When the term  $I$ , contains more than one input parameters, the Sobol Index quantifies the pure interaction influence or the parameters contained in  $I$ . Dividing the index by the overall variance  $D$ , gives the scales Sobol Index:

$$SI = \frac{\text{Var}(f_I(X_I))}{D} = \frac{D_I}{D} \quad \text{Eq. 29}$$

With this division, the index is normalized to fall in the range between 0 and 1 making it easier to assess. An extension of this index comes from Homma and Saltelli ([93]), called the total sensitivity index. It describes the influence the parameters have including all interactions of any order that contains at least one of them. In this way, the influence amongst all orders is measured which makes it a valuable tool for the screening of input parameters. It is defined as the sum of all partial variances that contain at least one of the parameters:

$$D_I^T = \sum_{J \cap I \neq \emptyset} D_J \quad \text{Eq. 30}$$

The application of the methods described can be found in the APPENDIX A – Evaluation of the influence of material parameters in automatic calibration of the case study, showing metrics and considerations made for the metamodel and sensitivity analysis of the Case Study.

## Chapter 4: Case study: Civic Tower of Ostra

### 4.1 Introduction to the case study

Masonry towers are one of the most widespread structural typologies among the various Italian Cultural Heritage (CH) buildings. One peculiar characteristic of this category of buildings is their evident slenderness. This aspect, together with the numerous uncertainties associated to masonry structures, such as irregularities and imperfections, complexity of the internal structure, local variability of the materials, as well as the effects of past damages and repairs, make this category of structures particularly vulnerable to seismic actions. Located about 40 km away from Ancona, Ostra is one of the typical villages of the Marche region, in Central Italy. Lying on a hill, overlooking the river Misa Valley, it is said that Ostra was founded by the exiles of the Roman Empire and its original name, till 1881, was Montalboddo. Destroyed during Goths invasion, the village was rebuilt, and during the Middle Age, it was surrounded by a protective wall, 1200 meters long, interspersed with square section towers, nine of those still existing today.

Nowadays, the centre of the city life is represented by the central Piazza dei Martiri, located in the upper part of the historic centre, where the most important buildings, such as Palazzo Comunale, San Francesco Church, La Vittoria Theatre, are found. Among them, the most emblematic building of the city stands: Ostra Civic Tower (Figure 9). Built in the XVI century, this tower is also known as “Clock Tower” because of the ancient clock gears still present today, even if no longer in operation.

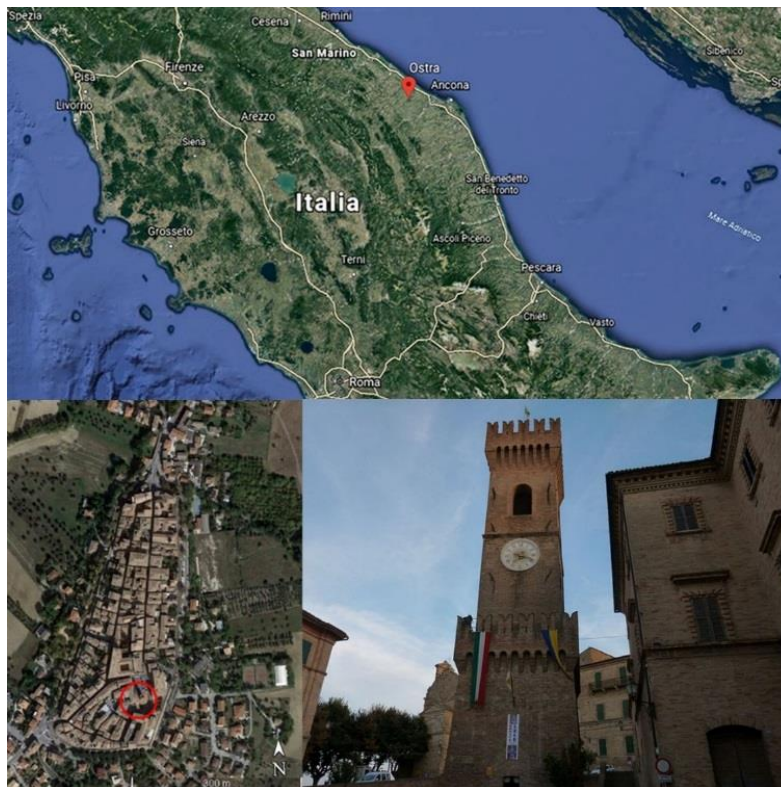


Figure 9: Ostra Civic Tower localization.

According to historical sources [94], [95], the belfry tower was originally connected to San Giovanni Church (Figure 10a). The two buildings had autonomous origins: the church was mentioned for the first time in archival documents in 1454, while the tower was built in 1552 at the behest of the magistracy. The bell, hosted today by the third order of floors, dates to 1631.



*Figure 10: San Francesco Church and the tower before bombardments (a) and a view of the central square to the present days (b)*

With its architecture and double staircase, the church closed the fourth side of the square, making it an elegant “living room”. The interior of the structure treasured various artworks, including many altarpieces such as that of Andrea Sacchi (1599/1661) depicting San Bonaventura da Bagnoregio and San Tommaso d'Aquino (today stored at the Superintendence of Urbino). Though, following the aerial bombardments occurred in 1944 during the II World War, only the church façade and the civic tower survived.

Because of the precarious conditions of the structures, it was decided to intervene by demolishing the rests of the façade and strengthening the tower. Façade demolition led to the uncovering of the foundations of the tower walls and of the external staircase of the building, making them prone to degradation phenomena due to atmospheric agents and pollutants. Therefore, foundation works were promptly carried out along with the recovery of the base walls. Parts of the external walls and battlements damaged by the bursts of artillery bullets were also restored.

After the works, a new architectural arrangement of the square became indispensable. Some projects envisaged creating a decent background, in harmony with the palaces that frame the town square, and erecting a building that could replace the beautiful (demolished) façade and which could form, together with the civic tower, a single majestic and harmonious architectural complex (Figure 10b).

## 4.2 Geometrical and material survey

With an overall height of 30 meters (before the interventions executed in 1950, when the foundations were partially uncovered and the top part was added, the original height was 25 meters), the Civic Tower of Ostra is a historical masonry structure featuring four main parts: the basement, the central body, the bell cell and the top roof (Figure 11). In what concerns the parts belonging to the original tower, the bell cell is unchanged, while the central body is partially reconstructed, as the changes of the masonry texture reveal.

The basement consists of a truncated pyramid, whose lower base measures approximately 7.30 x 7.50 m<sup>2</sup>, while the upper base is about 5.30 x 5.60 m<sup>2</sup>. This part develops up to a height of 9.55 meters, culminating in an embattled balcony. Hereon, the parallelepipedal central body starts, keeping the same shape for additional 9.50 meters. Then, the cross section of the tower slightly reduces at the level of the bell cell and remains unchanged till the embattled enlargement of the upper part.

The tower results composed of five floors: the first three are connected through spiral staircases starting from the ground level, while the last two orders of floors are reachable using an iron ladder. The clock mechanism is located on the second floor, whereas the bell cell occupies the third level, whose perimetral walls are pierced by single-light arched windows, one per side. The entrance is located on the main façade (north-east oriented), which overlooks Piazza dei Martiri.

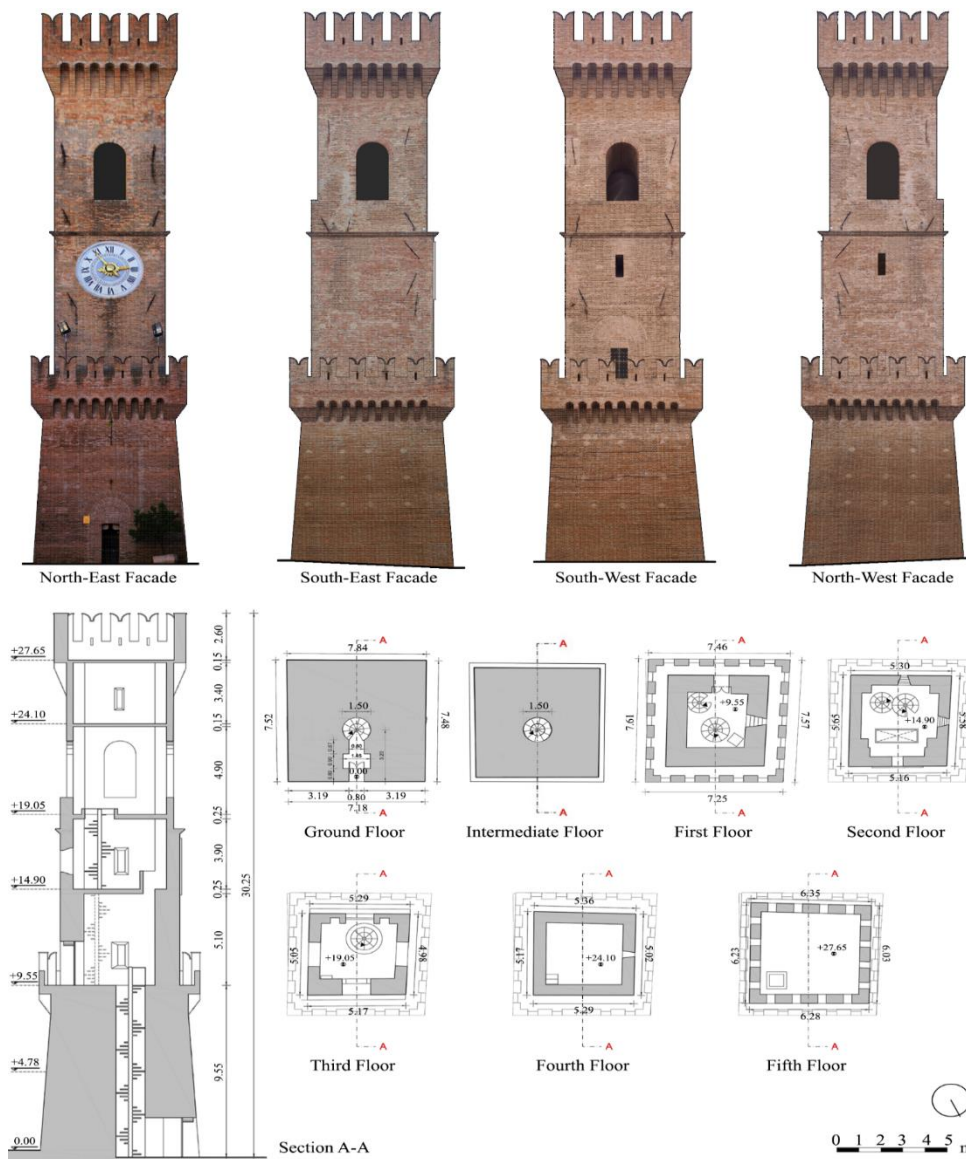


Figure 11: Geometrical Survey of the investigated tower: Front views (top) and CAD sections (bottom)

The survey allowed to distinguish different construction features and materials across the tower (Figure 12). Particularly, the bearing walls, whose thickness ranges from 1.1 meters in the lower part (first floor) to 0.6 meters in the upper part (last floor), resulted built with solid brick masonry and thin mortar joints. As for the basement walls, their remarkable thickness let infer the presence of an inner rubble core between brick outer layers, though no investigation could be performed to confirm the hypotheses about their internal morphology. The structural interventions undergone by the tower include the reinforced concrete slabs constituting the floors, whose thickness varies from 0.11 meters to 0.27 meters, the concrete columns built to reinforce the corners at the third level, and the iron tie-rods installed after the 1997 seismic events of Umbria-Marche region aimed at restraining possible out-of-plane mechanisms. No worrying cracks nor other structural damages were detected during the visual inspection.





Figure 12: Excerpts from the photographic survey of the tower: (1) Trapdoor accessing the upper level and connecting iron ladder; (2) close-up of the 4th level brickwork; (3) concrete slab of the 3rd floor with ladder opening; (4) particular of the reinforcement intervention with tie rods; (5) close-up of the 2<sup>nd</sup> level internal brickwork; (6) external brickwork of the 1<sup>st</sup> level; (7) basement brickwork; (8) spiral staircase at the entrance level.

### 4.3 Ambient Vibration Testing

Given its non-destructive nature, Ambient Vibration Testing (AVT) has become a common in situ investigation technique for the estimation of dynamic parameters associated with the global behavior of historical structures. This tool results extremely useful to collect reliable experimental data and increase the level of knowledge of the structure whenever its historical value may pose limitations to the application of other diagnostic techniques for the system's characterization. By deploying a set of sensors at selected locations and capturing the vibration response of the structure to random ambient excitations (traffic, wind, human walking, micro-tremors), the dynamic features of the system, namely natural frequencies ( $f$ ), damping ratios ( $\xi$ ) and mode shapes ( $\varphi$ ), can be extracted and used to better interpret the actual behaviour of age-old constructions, which are often highly complex and mechanically diverse.

In the last years, numerous works showed the potentiality of vibration monitoring through accelerometric sensors in the study of behavior of historical buildings, both for short-term [96], [97] and long-term applications [98]. Indeed, besides the economic benefits associated with the possibility of using freely available environmental excitations, AVT allows to perform rapid screenings of the structural fitness under real operational and boundary conditions. Moreover, the processing of the acquired vibration data enables the construction of an Experimental Model (EM) of the structure, which provides

the dynamic parameters that the Numerical Model (NM) has to match to realistically reproduce the structural response [99].

#### 4.4 Field testing procedure

In order to characterize the dynamic behavior of the Civic Tower of Ostra, two field dynamic campaigns in operational conditions were conducted in June 2018 and in February 2019. The sensor network was composed of four triaxial piezoelectric accelerometers, with an integrated MEMs tiltmeter system for correction of errors due to inclination, characterized by a maximum measurement range of 8g, a sensitivity of 1000 mV/g and a bandwidth range from 0.8 to 100 Hz. The digitization process was automated through an A/D converter with 24bits of resolution, 120 dB of dynamic range and provided with anti-aliasing filter. The synchronization between sensors was ensured by a 4-channel Sync Hub connecting the accelerometers to the PC for data storage (Figure 13).



Figure 13: Instrumentation used for the ambient vibration tests.

In both campaigns, three setups were used to measure the response of the tower in 8 selected points evenly deployed on the opposite corners of four levels (Figure 14). Each setup consisted of four accelerometers: two were fixed on the top floor and kept as reference sensors, while the remaining two were moved downward in each acquisition so as to record the vibration processes of the tower along the three directions of the 8 identified points, allowing to catch all the meaningful modal displacements of the structure, including torsional components. It is noted that the sensor layouts for the signal acquisition were established in accordance with the results of a preliminary numerical modal analysis coupled with an Optimal Sensor Placement (OPT) procedure [100], [101], with the intent of identifying the best position for the accelerometers to

maximize the quality of the AVT information despite the limited number of available sensors.

To comply with Rodriguez's indications [21], the total duration of the acquisition was set longer than 2000 times the estimated fundamental period of the structure: indeed, every registration lasted around 40 minutes, thereby assuring the elimination of the possible influence of non-stochastic excitations. Moreover, to guarantee a high frequency resolution for the spectral density estimation, a sampling frequency of 1024 Hz was adopted, resulting in 2,457,600 datapoints per time series.

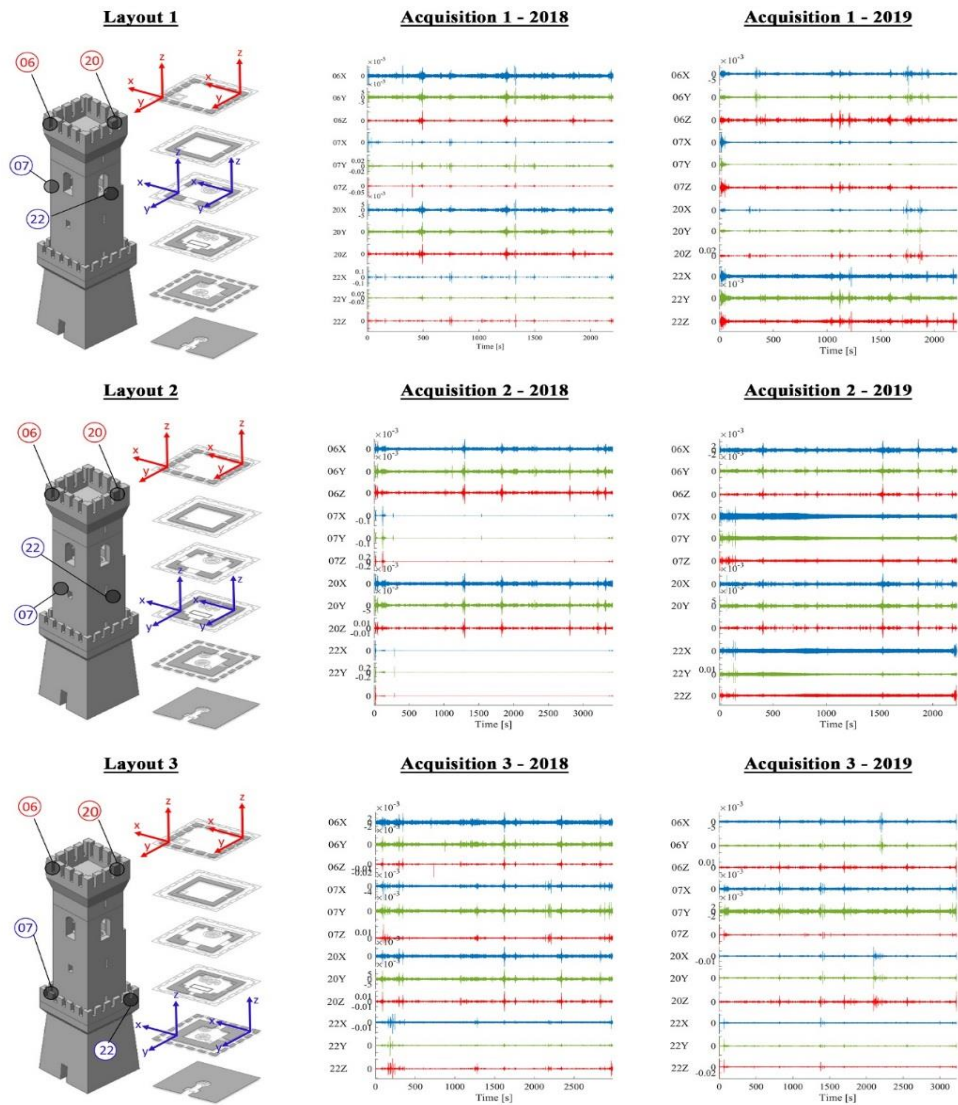


Figure 14: Sensor layouts and corresponding acceleration timeseries for the 2018 and 2019 dynamic testing campaigns (Blue, Green, Red colours indicate signals in x,y,z directions respectively).

## 4.5 Operational Modal Analysis

### 4.5.1 Data processing

The extraction of the dynamic features of the tower (i.e. natural frequencies  $f$ , damping ratios  $\xi$  and mode shapes ( $\phi$ )) was performed through the application of Operational Modal Analysis (OMA) techniques, using the acceleration time series acquired in operating conditions through the afore-mentioned contact sensor network. Many are the output-only dynamic identification approaches available in the literature that can be adopted for this purpose, both in the time and in the frequency domain [102]–[105]. Yet, regardless of the strategy, a pre-processing stage is needed before further data elaboration in order to remove residual noise and possible trends from the vibration signals, filter undesired frequency components, minimize leakage errors and eventually down-sample the time series to reduce the subsequent data processing time.

As for the present work, the pre-processing operation was executed through a Matlab© script, applying a 10<sup>th</sup> order Butterworth low-pass filter to the raw signals. Then, the cleaned data were down sampled, passing from a spectral resolution of 1024 Hz to 100 Hz. As observed in analogous structures, the frequency content of interest for the tower fell in the range 0-10 Hz, thus data were further decimated with a factor of 8, reducing the analyzed range to 0-12.5 Hz. Finally, the pre-processed signals were analyzed through the Stochastic Subspace Identification (SSI) method available in the commercial software ARTeMIS [106].

### 4.5.2 Theoretical Background on the SSI-based methods

The SSI method can be considered as one of the principal approaches for the extraction of modal parameters from output-only vibration data. The large attention lately received by SSI methods is likely due to the fact that these techniques are apt to accurately identify closely spaced modes and especially suited to be automated [107]. For the sake of completeness, only a brief description of this modal identification procedure is provided hereafter; for further details [108].

SSI can be implemented in two classic forms: covariance driven (SSI-cov) and data driven (SSI-data). Working in the time domain, the SSI method starts from the construction of a State Space model, where the second order equation of motion is converted into a system composed of two linear equations, called respectively “state equation” Eq. 31 and “observation equation” Eq. 32, which in the case of ambient vibration testing (unknown input) read:

$$\mathbf{x}_{k+1} = \mathbf{A}\mathbf{x}_k + \mathbf{w}_k \quad \text{Eq. 31}$$

$$\mathbf{y}_k = \mathbf{C}\mathbf{x}_k + \mathbf{v}_k \quad \text{Eq. 32}$$

where:

- $k$  is the generic time instant;
- $\mathbf{x} \in \mathcal{R}^{nx1}$  is the discrete-time state vector;
- $\mathbf{y} \in \mathcal{R}^{lx1}$  is the vector containing the  $l$  output measurements;
- $\mathbf{A} \in \mathcal{R}^{nxn}$  is the system matrix that describes all the dynamic information of the system;
- $\mathbf{C} \in \mathcal{R}^{lxn}$  is the corresponding output matrix;
- $\mathbf{w} \in \mathcal{R}^{nx1}$  is a white noise vector process representing disturbances and modelling inaccuracies;
- $\mathbf{v} \in \mathcal{R}^{lx1}$  is another white noise vector process representing the measurement noise due to sensor inaccuracy.

These equations represent the discrete-time state space form of the dynamics of a linear-time-invariant system under unknown excitation. Particularly, Eq. 31 models the dynamic behavior of the physical system, whereas Eq. 32 controls which part of the dynamic system can be observed in the output of the model. The core of the process aims at identifying the system dynamic matrix  $\mathbf{A}$  by fitting the state-space model to the experimental data. In case of SSI-cov method, the modal estimates are obtained from the Singular Value Decomposition (SVD) of the block Toeplitz matrix, a matrix gathering the covariances of the measured output time series; while in case of SSI-data, the modal identification is performed starting from the SVD of the block Hankel matrix, a matrix containing past and future output measurements.

Like all parametric system identification techniques, a user-defined integer is required to process the data, i.e. the maximum model order. In principle, the model order must be twice the number of the modes that are needed to describe the dynamic response of the system. Notwithstanding, to identify weakly excited modes, it is often necessary to consider larger model orders which can lead in turn to the appearance of many spurious modes associated to the noise content of the measurements. To overcome this issue, different SSI analyses with a range of candidate model orders can be carried out trying to identify the model order that better fits the experimental data and leads to the best stabilization diagram. The latter is an order-frequency plot in which the estimated physical (structural) and computational (spurious) modes are represented as poles and discriminated based on the fulfilment of user-specified requirements (e.g. maximum allowed deviation between successive models in terms of modal frequencies, damping ratios and MAC values). If the model order is high enough, a repeated trend of stable poles will appear in the SSI output diagram, allowing the estimation of the structural modes characterizing the system.

### 4.5.3 Modal results

In both dynamic testing campaigns, five vibration modes were identified in the frequency range 0-10 Hz: two close-spaced translational modes ( $\varphi_1$ ) and ( $\varphi_2$ ) in  $x$  and  $y$  directions, respectively, featuring in-phase modal components; one torsion mode ( $\varphi_3$ ); and two dominant double bending modes ( $\varphi_4$ ), ( $\varphi_5$ ) in the  $xz$  and  $yz$  planes, respectively. As expected, the first two vibration modes exhibit relatively high frequency values compared to those featured by typical historical masonry towers. This outcome is imputable to the low aspect ratio ( $\lambda = 4$ ) characterizing the tower object of study as well as to the increased stiffness resulted from the past restoration works.

The estimated natural frequencies and damping ratios, used for the following calibration process, are reported in Table 1 for both campaigns, together with the Mode Complexity Factor (MCF) associated to each mode. This value is a scalar that lies in the range 0%-100% and quantifies the degree of complexity of a mode shape, namely how much the modal vector differs from a real-valued one [109], [110]. Real-valued mode shapes feature complexities close to 0 (MCF = 0%), while mode shapes with predominant imaginary components exhibit complexity values close to 1 (MCF = 100%). The dispersion of the real and imaginary parts of each mode is further analyzed by plotting their components in a two-dimensional polar coordinate system, namely through the complexity plots, as illustrated in Figure 15. It is observed that in the first dynamic testing campaign, the first three mode shapes, as well as the last one, are close to monophasic vectors (components are aligned along the horizontal direction) and only the fourth mode has a higher complexity, whereas in the second dynamic testing campaign the modal components of both the third and fourth modal vectors present greater complexities. This slight difference between the MCF values of the two campaigns is probably associated to the different level of ambient excitations present during the AVTs which might have affected the signal-to-noise ratio introducing some inaccuracy in the modal estimates. However, it is worth mentioning that the actual mode shapes of a physical system are never exactly monophasic vectors, thus some degree of complexity is always expected in the experimental modes.

Table 1: Global Modal parameters identified for EM 2018 and EM 2019

Mode	<u>2018</u>			<u>2019</u>		
	$f$ [Hz]	$\xi$ [%]	MCF [%]	$f$ [Hz]	$\xi$ [%]	MCF [%]
$\varphi_1$	2.082	0.817	3.929	2.092	0.762	3.320
$\varphi_2$	2.156	0.893	0.178	2.165	0.787	0.370
$\varphi_3$	6.293	0.578	2.765	6.302	0.666	11.241
$\varphi_4$	6.442	2.423	12.471	6.449	3.397	19.642
$\varphi_5$	6.941	2.463	2.053	6.872	2.739	4.851

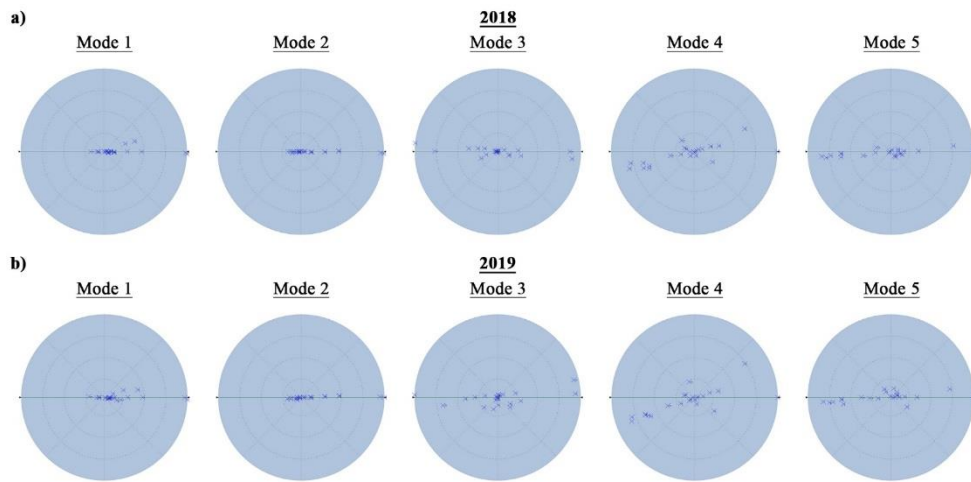


Figure 15: Complexity plots of the identified experimental modes for EM 2018 (a) and EM 2019 (b).

To drive the accurate selection of the structural modes, a cross-validation was performed by comparing the modes identified with the SSI modal estimator against the ones extracted through another OMA technique operating in the frequency domain, namely the Enhanced Frequency Domain Decomposition (EFDD) [111]. The close pairwise correspondence of the five vibration modes estimated in each campaign is visually highlighted in Figure 16, where the mode shapes from the two modal estimators are superimposed, and also confirmed by the values of the Modal Assurance Criterion (MAC) reported both in Figure 16 and in Table 2. As well-known in the literature, the MAC is a statistical indicator used to measure the degree of similarity between mode shape vectors [112]: the closer the values are to 1 (MAC = 100%), the higher the correlation between modes and vice versa.

2018				
Mode 1	Mode 2	Mode 3	Mode 4	Mode 5
$f_{SSI} = 2.082$ Hz $f_{EFDD} = 2.082$ Hz	$f_{SSI} = 2.156$ Hz $f_{EFDD} = 2.155$ Hz	$f_{SSI} = 6.293$ Hz $f_{EFDD} = 6.305$ Hz	$f_{SSI} = 6.442$ Hz $f_{EFDD} = 6.459$ Hz	$f_{SSI} = 6.941$ Hz $f_{EFDD} = 6.950$ Hz
Translational X	Translational Y	Torsional	Bending X	Bending Y
MAC <sub>SSI-EFDD</sub> = 100%	MAC <sub>SSI-EFDD</sub> = 99.8%	MAC <sub>SSI-EFDD</sub> = 86.7%	MAC <sub>SSI-EFDD</sub> = 92.4%	MAC <sub>SSI-EFDD</sub> = 98.0%
2019				
Mode 1	Mode 2	Mode 3	Mode 4	Mode 5
$f_{SSI} = 2.092$ Hz $f_{EFDD} = 2.090$ Hz	$f_{SSI} = 2.165$ Hz $f_{EFDD} = 2.165$ Hz	$f_{SSI} = 6.302$ Hz $f_{EFDD} = 6.301$ Hz	$f_{SSI} = 6.449$ Hz $f_{EFDD} = 6.443$ Hz	$f_{SSI} = 6.872$ Hz $f_{EFDD} = 6.893$ Hz
Translational X	Translational Y	Torsional	Bending X	Bending Y
MAC <sub>SSI-EFDD</sub> = 99.9%	MAC <sub>SSI-EFDD</sub> = 99.7%	MAC <sub>SSI-EFDD</sub> = 81.2%	MAC <sub>SSI-EFDD</sub> = 89.1%	MAC <sub>SSI-EFDD</sub> = 94.3%

Figure 16: Mode shapes of 2018 and 2019 EM's identified with the SSI method (in blue) and cross-comparison with the respective mode shapes identified with EFDD method (in red).

Table 2: MAC between mode shapes identified with SSI and EFDD methods. (a)EM 2018 and (b)EM 2019.

		a)					b)						
CrossMAC	2018	SSI					CrossMAC	2019	SSI				
		2.082 Hz	2.156 Hz	6.293 Hz	6.442 Hz	6.941 Hz			2.092 Hz	2.165 Hz	6.302 Hz	6.449 Hz	6.872 Hz
EFDD	2.082 Hz	1.000	0.000	0.000	0.032	0.002	EFDD	2.090 Hz	0.999	0.001	0.001	0.034	0.003
	2.155 Hz	0.002	0.998	0.001	0.000	0.024		2.165 Hz	0.003	0.997	0.002	0.000	0.027
	6.305 Hz	0.003	0.002	0.867	0.028	0.001		6.301 Hz	0.004	0.002	0.812	0.006	0.003
	6.459 Hz	0.036	0.000	0.039	0.924	0.021		6.443 Hz	0.034	0.001	0.061	0.891	0.020
	6.950 Hz	0.001	0.026	0.002	0.010	0.980		6.893 Hz	0.002	0.028	0.002	0.008	0.943



Analysing in depth the global modal parameters estimated in 2018 and 2019, no significant change is found in terms of frequency values ( $f$ ) as the percentage variations recorded between corresponding modes are less than or equal to 1.0%(Table 2), meaning that the global dynamic behaviour of the tower remained unchanged in the period elapsed between the two campaigns. As concerns modal damping ( $\xi$ ), relatively high percentage variations are found when comparing the damping ratios of corresponding modes between 2018 and 2019, with a maximum difference greater than 20% for the 4<sup>th</sup> mode (Table 3). Unlike frequencies, damping values are much more prone to be affected by measurement uncertainties and random error sources. Still, all the estimated values are consistently under 5% in each campaign, allowing to infer that, in the present case, the observed scatter is not associated with incipient damage mechanisms, but it is related to the intrinsic complex nature of this modal parameter.

Table 3: Percentage variation between modal frequencies damping ratios of EM 2018 and EM 2019.

Mode	$f_{EM18}$ [Hz]	$\xi_{EM18}$ [%]	$f_{EM19}$ [Hz]	$\xi_{EM19}$ [%]	$\Delta f$ [%]	$\Delta \xi$ [%]
$\varphi_1$	2.082	0.817	2.092	0.762	0.478	-7.218
$\varphi_2$	2.156	0.893	2.165	0.787	0.416	-13.469
$\varphi_3$	6.293	0.578	6.302	0.666	0.143	13.213
$\varphi_4$	6.442	2.423	6.449	3.397	0.109	28.672
$\varphi_5$	6.941	2.463	6.872	2.739	-1.004	10.077

In what concerns the experimental mode shapes estimated from 2018 and 2019 AVT data (Figure 17), their configuration is consistent over time and clearly points out the typical behavior of a monolithic cantilever beam with rigid constraint at the base. The principal components of displacement result well-defined for each mode and a nearly perfect correlation is found between corresponding mode pairs. The cross-validation process operated through the MAC matrix (Table 4) also proves the modes to be consistent, well-decoupled and accurately identified from both field campaigns.

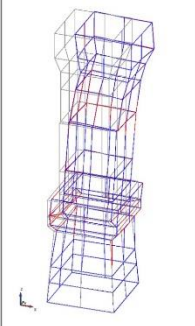
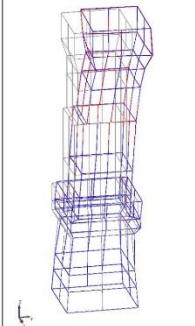
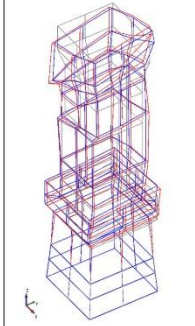
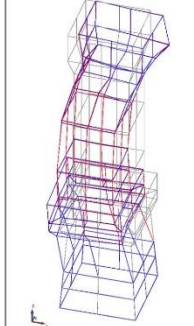
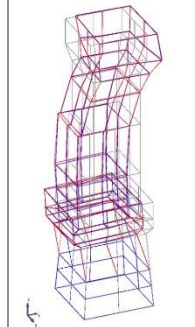
Mode 1	Mode 2	Mode 3	Mode 4	Mode 5
$f_{SSI2018} = 2.082$ Hz $f_{SSI2019} = 2.092$ Hz	$f_{SSI2018} = 2.156$ Hz $f_{SSI2019} = 2.165$ Hz	$f_{SSI2018} = 6.293$ Hz $f_{SSI2019} = 6.302$ Hz	$f_{SSI2018} = 6.442$ Hz $f_{SSI2019} = 6.449$ Hz	$f_{SSI2018} = 6.941$ Hz $f_{SSI2019} = 6.872$ Hz
				
Translational X MAC = 99.2%	Translational Y MAC = 99.5%	Torsional MAC = 98.1%	Bending X MAC = 99.0%	Bending Y MAC = 97.1%

Figure 17: Comparison between mode shapes of EM 2018 (in blue) and corresponding ones EM 2019 (in red).

Table 4: MAC between EM's mode shapes identified with the SSI method

CrossMAC 2018-2019		EM19				
		2.092 Hz	2.165 Hz	6.302 Hz	6.449 Hz	6.872 Hz
EM18	2.082 Hz	0.992	0.000	0.001	0.037	0.001
	2.156 Hz	0.003	0.995	0.004	0.001	0.026
	6.293 Hz	0.002	0.000	0.981	0.077	0.018
	6.442 Hz	0.030	0.000	0.110	0.990	0.010
	6.941 Hz	0.005	0.025	0.009	0.002	0.971

## 4.6 Numerical modelling and updating via Genetic Algorithm

The uniqueness and complexity of heritage structures make the understanding of their actual behaviour a true challenge. By updating FE models with OMA information, one can reproduce as closely as possible the measured response of the structure and carry out a reliable condition assessment. The process consists in updating the system matrices of the FE model (mass, stiffness and possibly damping matrices) till the difference between experimental and numerical modal data is minimized. If the FE model is not adequately representative of the reality, structural assessment cannot be performed.

As was already stated in Chapter 1, despite the degree of maturity of existing modal-based updating techniques for the calibration of realistic numerical models, experience has shown that the updating process is not trivial especially when trying to upgrade these procedures for damage localization purposes [14], [113]. [14], [114]. First and foremost, the FE model for updating requires a level of detail sufficient enough to represent both geometric and structural forms. Moreover, the number of parameters to update should be selected in order to guarantee a well-conditioned problem, independent of the contingent state of the structure and easily replicable in nearly real-time to evaluate possible global and local changes with respect to the reference modal data. The determination of reasonable initial values for the updating parameters, together with the definition of their lower and upper bounds, also plays an important role to guarantee the convergence of the iterative process and the physical significance of the final updated parameters.

Rooted in these considerations, a modal-based updating procedure relying on Genetic Algorithms (GA) is hereafter presented and employed to calibrate a realistic FE model of the masonry tower under investigation and establish baseline information for future comparative analyses at global and local level.

### 4.6.1 Preliminary FE model

An initial 3D FE model (NM<sub>0</sub>) of the tower was built using MidasFea© in order to preliminarily assess the meaningful dynamic characteristics of the structure. The peculiar geometry of the tower, which is one of the parameters that mostly affects its global dynamic response, required a very high degree of detail in the modelling process of the different elements and construction features like openings, wall thickness, geometrical irregularities, etc. Particular attention was given to the reproduction of the rubble-filled masonry of the basement of the tower as well as to the concrete floors of the higher levels which were considered as rigid diaphragms in their plane. As concerns secondary elements, like stairs, deformable wooden floors, clock mechanism and bells, they were not explicitly modelled, but their influence was accounted for as added masses.

Once the geometry of the tower was defined (Figure 18), all the solids composing the model were discretized as 4-node tetrahedral elements, whose mesh size was set equal to 0.3 m, resulting into a model with 21,726 nodes, 78.926 volume elements and 67.806 DOFs. Considering the tower as a cantilever beam, rigid constraints were applied at the base.

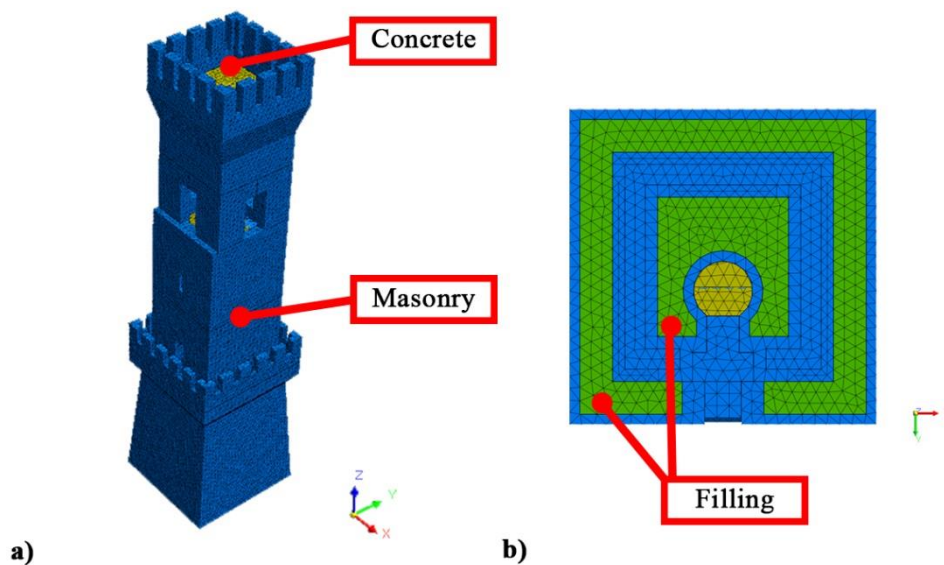


Figure 18: FE modelling of the Civil Tower of Ostra: (a) Axonometric view, (b) Bottom view at foundation level.

At first, a three-group material discretization was applied, modelling each material as homogeneous and isotropic, with Young's modulus ( $E$ ), Poisson's ratio ( $\nu$ ) and mass density ( $\gamma$ ) chosen according to the Italian Technical Standards for Structures [115]. The initial values assumed for the afore-mentioned elastic parameters are reported in Table 5. It is noticed that in the definition of the elastic modulus of the concrete, a 30% reduction was considered, because of the uncertainties linked to aging effects, while for the rubble

masonry properties the values suggested in the Italian code for irregular masonry were assigned.

Table 5: Elastic properties of the initial FE model.

<b>Material</b>	<b>E</b> <b>[MPa]</b>	<b><math>\nu</math></b> <b>[-]</b>	<b><math>\gamma</math></b> <b>[kN/m<sup>3</sup>]</b>
Masonry	1800	0.20	18
Concrete	18000	0.20	25
Filling	1100	0.20	18

A preliminary modal analysis, implemented through the Lanczos method [116]–[119], was carried on the initial FE model to evaluate the dynamic properties of the tower and quantify the residuals between numerical and experimental modal parameters. The results from this first step are reported in Table 6, where the remarkable differences between actual experimental frequencies (EM) and calculated numerical frequencies (NM<sub>0</sub>) of the not yet calibrated model are highlighted.

Table 6: Preliminary results (NM<sub>0</sub>) and differences with the experimental frequency values (EM).

<b>Mode</b>	<b><math>f_{NM0}</math></b> <b>[Hz]</b>	<b><math>T_{NM0}</math></b> <b>[s]</b>	<b>Eff. Mass</b> <b>Direction</b> <b>X [%]</b>	<b>Eff. Mass</b> <b>Direction</b> <b>Y [%]</b>	<b><math>f_{EM18}</math></b> <b>[Hz]</b>	<b><math>f_{EM19}</math></b> <b>[Hz]</b>	<b><math> \Delta f_{EM18-}</math></b> <b>NM<sub>0</sub> </b> <b>[%]</b>	<b><math> \Delta f_{EM19-}</math></b> <b>NM<sub>0</sub> </b> <b>[%]</b>
$\varphi_1$	1.509	0.663	35.80	0.00	2.082	2.092	27.52	27.87
$\varphi_2$	1.536	0.651	0.00	35.72	2.156	2.165	28.76	29.05
$\varphi_3$	5.012	0.200	0.02	0.00	6.293	6.302	20.36	20.47
$\varphi_4$	5.821	0.172	21.21	0.00	6.442	6.449	9.64	9.74
$\varphi_5$	5.883	0.170	0.00	29.38	6.941	6.872	15.24	14.39

With respect to the mode shapes (Figure 19), their main displacement components present a good visual correlation with their experimental counterpart, being the first two modes translational in the  $x$  and  $y$  direction, respectively, the third mode a torsional one, and the last two being dominant bending modes in the  $xz$  and  $yz$  planes.

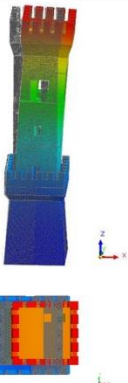

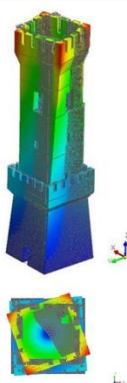
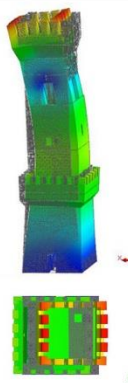
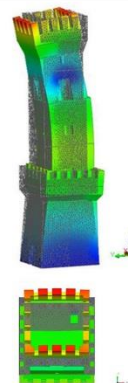
Mode 1 $f = 1.509$ Hz	Mode 2 $f = 1.536$ Hz	Mode 3 $f = 5.012$ Hz	Mode 4 $f = 5.821$ Hz	Mode 5 $f = 5.883$ Hz
				
Translational X	Translational Y	Torsional	Bending X	Bending Y
MAC <sub>NM0-EM18</sub> = 77.6% MAC <sub>NM0-EM19</sub> = 82.5%	MAC <sub>NM0-EM18</sub> = 81.5% MAC <sub>NM0-EM19</sub> = 67.2%	MAC <sub>NM0-EM18</sub> = 22.1% MAC <sub>NM0-EM19</sub> = 2.6%	MAC <sub>NM0-EM18</sub> = 52.2% MAC <sub>NM0-EM19</sub> = 47.6%	MAC <sub>NM0-EM18</sub> = 1.1% MAC <sub>NM0-EM19</sub> = 44.7%

Figure 19: Frequencies values and mode shapes resulting from modal analysis operated on the preliminary FE model.

On the other hand, the comparison of the degree of consistency between numerical and experimental modal vectors in terms of MAC values (Table 7) shows a fair correlation only for the first two fundamental modes of the tower, while higher modes feature quite a poor (4<sup>th</sup> and 5<sup>th</sup> modes) or no (3<sup>rd</sup> mode) correlation either using 2018 or 2019 modal data as comparative metric.

Table 7: MAC between numerical and experimental mode shapes: (a) NM0-EM 2018 and (b) NM0-EM 2019.

CrossMAC		EM18					CrossMAC		EM19				
		2.082 Hz	2.156 Hz	6.293 Hz	6.442 Hz	6.941 Hz			2.092 Hz	2.165 Hz	6.302 Hz	6.449 Hz	6.872 Hz
NMO	1.509 Hz	0.776	0.023	0.016	0.038	0.003	NMO	1.509 Hz	0.825	0.025	0.000	0.066	0.005
	1.536 Hz	0.002	0.815	0.002	0.002	0.040		1.536 Hz	0.001	0.672	0.007	0.003	0.026
	5.012 Hz	0.004	0.006	0.221	0.000	0.003		5.012 Hz	0.050	0.038	0.026	0.029	0.029
	5.821 Hz	0.010	0.000	0.054	0.522	0.011		5.821 Hz	0.005	0.003	0.031	0.476	0.020
	5.883 Hz	0.042	0.007	0.091	0.019	0.650		5.883 Hz	0.005	0.025	0.124	0.000	0.447

## 4.6.2 GA-based model updating

As mentioned in previous chapters, iterative model updating procedures aim at calibrating an FE model through the solution of an inverse problem based on modal analysis, where corrections are applied to local physical and/or mechanical parameters of the FE model by setting an objective function and searching for the optimum solution till the difference between experimental and numerical modal data is minimized. To overcome the limitations inherently associated to manual or approximate updating processes, a genetic algorithm (GA) implemented in Code\_Aster© software environment [120] was used in this work to calibrate the FE model of Ostra Civic Tower.

The genetic algorithms are inspired by Darwin's theory and are based on the process of natural selection. These algorithms are considered robust tools for solving optimization problems and explore diverse regions of interest by running the same problem on different conditions and allowing to locate with high probability the global optimum without getting trapped into local minima [116], [119], [121], [122]. They are part of a stochastic method that "mimics" the evolution through combinations of random mutations and natural selection in order to find optimal numerical values of functions. A better understanding of the methodology can be achieved through the description of the updating process scheme as it was implemented.

NM and EM were initially imported and read by Code\_Aster© ([123]), where a condensed experimental model (CEM) containing the frequency and mode shape data belonging to the five estimated modes was created. Then, CEM data were projected onto the NM (Figure 20) in order to upscale the EM DOFs. This operation enabled the possibility to visualize and interact with the data onto a 3D model while also creating the dependencies for the displacement calculations between the existing nodes of the NM with respect to the data of the EM.

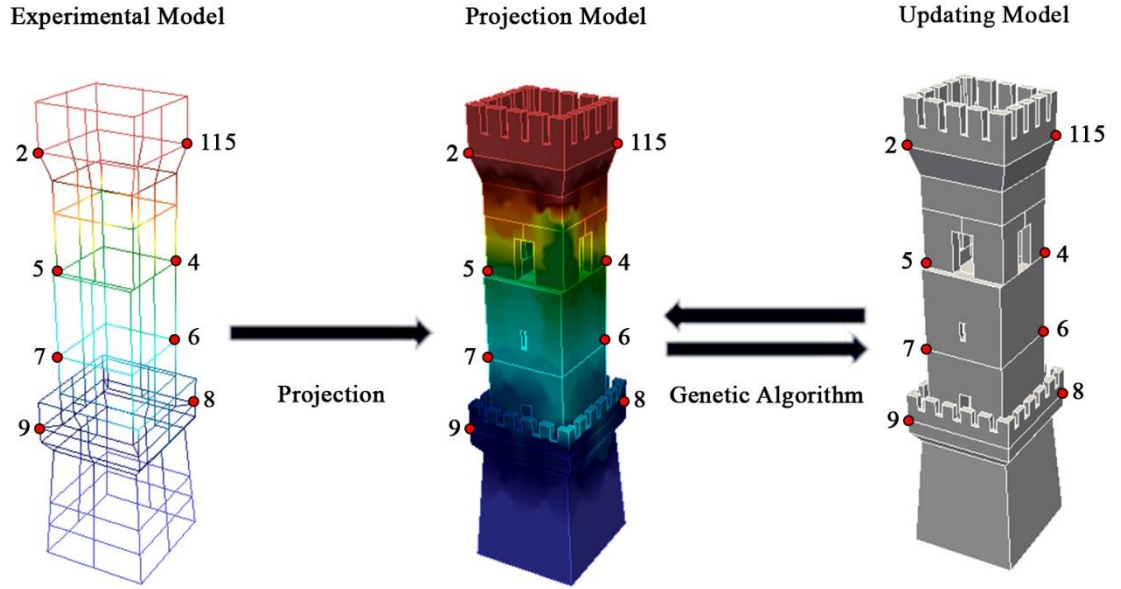


Figure 20: Workflow for the projection of the experimental data onto the NM for the genetic algorithm updating, with measured nodes highlighted.

Once the projection was done, a preliminary modal analysis was performed, generating the initial population for the values of the unknown material properties to be considered in the calibration process. Upper and lower bounds of physical significance were also set for each updating parameter based on values retrieved from the literature and belonging to analogous structures. Any value within the bounds was a candidate solution.

For each iteration, the fulfilment of convergence criteria established beforehand was progressively checked using a very strict two-term objective function that accounted for both frequencies and mode shapes residuals between EM and NM models, as reported below:

$$\Delta f + \Delta_{crossMAC} = \sqrt{\sum_{i=1}^n \left( \frac{f_{exp}^i - f_{num}^i}{f_{exp}^i} \right)^2} + \sqrt{\sum_{i=1}^n (1 - MAC^i)^2} \quad Eq. 33$$

$$\leq 0.05$$

The model updating process was set to stop either when the residual tolerance of two consecutive steps reached  $1e^{-4}$  or after 2000 evaluations (Figure 21), hence ensuring the stability of the iterative solution.

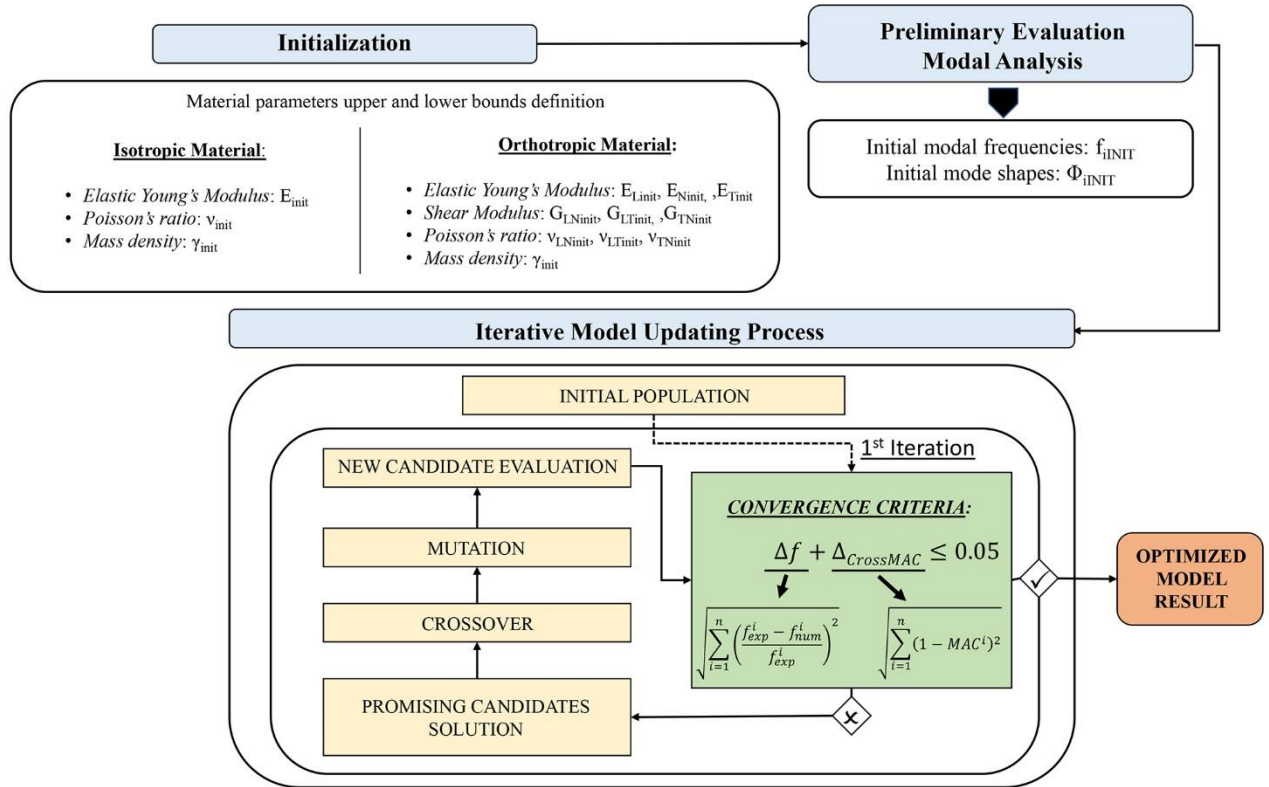


Figure 21: GA-based model updating flowchart of the case study.

## 4.7 Calibration process

### 4.7.1 Twelve-group discretization approach

To account for the visible variability of the masonry properties across the tower and better tune the model dynamic response, the number of updating parameters was increased by further discretizing the preliminary FE model into twelve parts, or solid groups (Figure 22). The GA-based updating process was then repeated by employing as reference modal data the frequencies and MAC values of the five vibration modes estimated from both the 2018 and 2019 AVT measurements, and iteratively varying the elastic parameters assigned to each of the twelve parts till the residuals between numerical and experimental modal data were minimized. The final number of updating parameters thus greatly exceeded the initial number considered in the preliminary assessment.



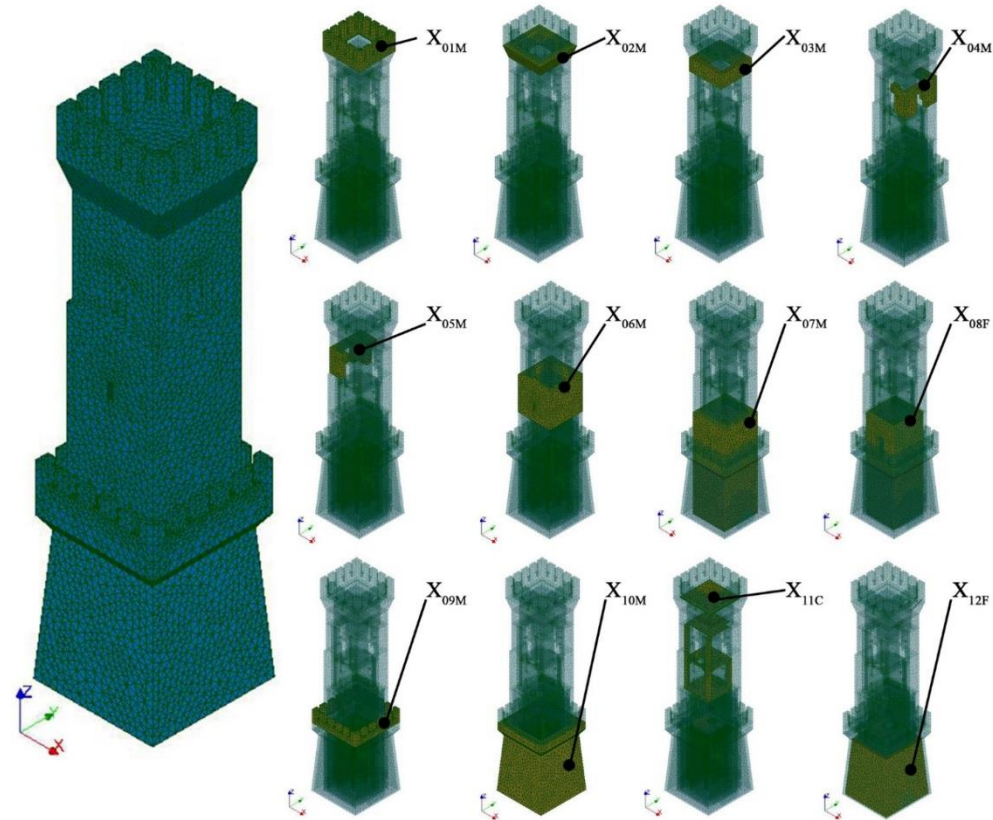


Figure 22: Updating variables for the twelve-group discretization of the FE model. Each material group is named as "X" followed by a subscript composed by a number (00 to 12) which stands for the group and a letter ("M" for masonry, "C" for concrete and "F" for the filling material).

The elastic properties of the twelve parts were attributed considering two different behavioural models for the materials: in the first stage all materials were modelled as homogeneous and isotropic, requesting the solution of a thirty-six parameters convergence problem ( $3 \times 12 = 36$ ), whereas in the second stage the masonry material was modelled as orthotropic due to its complex and non-homogeneous internal structure, leading to the calibration of one hundred-thirteen updating parameters (masonry:  $10 \times 11 = 110$ ; concrete:  $3 \times 1 = 3$ ). It is remarked how the complexity and high dimensionality of the optimization problem could not be tackled via a manual updating procedure but required a sophisticated algorithm capable of dealing with large and multi-dimensional problems.

Reasonable variation ranges for the material parameters were assigned to each part in accordance with the values provided by the Italian Technical Standards for Structures [115]. [124] as well as with the values retrieved from the literature for analogous materials and in light of the outcome of the condition survey. The established upper and lower bounds [125]–[129] are summarized in Table 8 and Table 9 for the isotropic and orthotropic cases, respectively. The initial population of updating variables used in the GA-based updating process was randomly selected within these bounds.

Table 8: Lower and Upper bounds for isotropic elastic properties ( $E$  is for the Elastic Young's,  $\nu$  is the Poisson's ratio and  $\gamma$  is the mass density).

Material	$E$	$\nu$	$\gamma$
	[MPa] <i>Min - Max</i>	[-] <i>Min - Max</i>	[kN/m <sup>3</sup> ] <i>Min - Max</i>
Masonry	600 - 3300	0.01 – 0.45	15 - 20
Filling	600 - 2400	0.01 - 0.45	15 - 20
Concrete	27000 - 32000	0.01 – 0.45	23 - 26

Table 9: Lower and Upper bounds for orthotropic elastic properties ( $G$  is the shear modulus while the subscripts  $L,N,T$  indicate the Longitudinal, Normal and Tangential components respectively. (\*) Concrete stayed as isotropic material.

Material	$E_L$	$E_N$	$E_T$	$G_{LN}$	$G_{LT}$	$G_{TN}$	$\nu_{LN}$	$\nu_{LT}$	$\nu_{TN}$	$\gamma$
	[MPa] <i>Min- Max</i>	[MPa] <i>Min- Max</i>	[MPa] <i>Min- Max</i>	[MPa] <i>Min- Max</i>	[MPa] <i>Min- Max</i>	[MPa] <i>Min- Max</i>	[-] <i>Min- Max</i>	[-] <i>Min- Max</i>	[-] <i>Min- Max</i>	[kN/m <sup>3</sup> ] <i>Min- Max</i>
Masonry	600- 3300	600- 3300	600- 3300	230- 1400	230- 1400	230- 1400	0.01- 0.45	0.01- 0.45	0.01- 0.45	15-20
Filling	600- 2400	600- 2400	600- 2400	230- 1400	230- 1400	230- 1400	0.01- 0.45	0.01- 0.45	0.01- 0.45	15-20
*Concrete	27000-32000			(automatically calculated)			0.01-0.45			23-26

The main scope of this GA-based model updating procedure, run first considering 36 variables (isotropic material) and then accounting for 113 unknowns (orthotropic material), was to produce a refined baseline model closely representative of the initial experimental target and that could be speedily updated with new data to serve as a future digital twin of the physical structure for predicting its performance against different scenarios. Hence the need of collecting data from two distinct AVT campaigns. In the second updating phase against 2019 experimental data, an in-depth sensitivity analysis [130], [131], whose results are illustrated and widely discussed in APPENDIX A – Evaluation of the influence of material parameters in automatic calibration, was also conducted to evaluate the influence of every single material parameter on the outcome of the updating process. In light of the results, although reducing the number of unknowns is common practice in the literature [132], it was decided to continue calibrating the model through the proposed GA-based procedure and keep all the aforementioned parameters as updating variables, given the greater computational efficiency of the proposed method and considering this the only solution for a future extent of this study to the damage localization field.

### 4.7.1 Model updating results

The optimal mechanical parameters obtained downstream the GA-based updating process of the isotropic FE model of Ostra Civic Tower are reported in Table 10. It is interesting to notice that the final values of the material properties are consistent with the expected ranges and clearly reflect the visible masonry changes resulting from past interventions and restoration works. Particularly, the Young's moduli of the masonry tend to decrease from the basement (reinforced during the 1950s restoration works) to the central body (which was only partially reconstructed) and increase again towards the upper part of the tower (added later), reading values consistent with those reported in the Italian code [115].

*Table 10: Optimal values for the material parameters of the isotropic FE models after calibration and successive updating.*

Updating parameter	<u>2018 NM</u>			<u>2019 NM</u>		
	E [MPa]	$\nu$ [-]	$\gamma$ [kN/m <sup>3</sup> ]	E [MPa]	$\nu$ [-]	$\gamma$ [kN/m <sup>3</sup> ]
X <sub>01M</sub>	2036	0.18	15	2092	0.17	15
X <sub>02M</sub>	2112	0.22	15	1960	0.24	15
X <sub>03M</sub>	1278	0.21	15	1074	0.22	15
X <sub>04M</sub>	1325	0.20	16	1220	0.20	16
X <sub>05M</sub>	1267	0.23	15	1113	0.28	15
X <sub>06M</sub>	2471	0.18	20	3133	0.17	20
X <sub>07M</sub>	3289	0.19	20	3288	0.19	20
X <sub>08F</sub>	2396	0.18	20	2399	0.18	20
X <sub>09M</sub>	2667	0.19	20	2521	0.17	20
X <sub>10M</sub>	3052	0.20	20	3282	0.21	20
X <sub>11C</sub>	27615	0.26	24	27037	0.25	23
X <sub>12F</sub>	1681	0.21	20	1470	0.21	20

Analogous observations can be drawn for the updating parameters calibrated through the GA-based updating process of the orthotropic FE model of the tower, whose results are reported in Table 11 and Table 12. The optimal values obtained for the elastic moduli of the masonry material feature a similar trend of variation as compared to the isotropic FE model, being consistent with the range of values expected from the visual assessment of the masonry quality. Meaningful values are found as far as the material density is concerned, whereas consistent but slightly larger variations are obtained for the Poisson's ratios.

Table 11: Optimal values for the material parameters of the orthotropic FE model after calibration against 2018 EM modal data. (\*) Concrete stayed as isotropic material.

Updating parameter	E <sub>L</sub> [MPa]	E <sub>N</sub> [MPa]	E <sub>T</sub> [MPa]	G <sub>LN</sub> [MPa]	G <sub>LT</sub> [MPa]	G <sub>TN</sub> [MPa]	v <sub>LN</sub> [-]	v <sub>LT</sub> [-]	v <sub>TN</sub> [-]	γ [kN/m <sup>3</sup> ]
X <sub>01M</sub>	2148	2007	1784	1005	894	970	0.20	0.19	0.19	15
X <sub>02M</sub>	2188	2238	2125	679	911	981	0.18	0.20	0.20	15
X <sub>03M</sub>	2449	1877	1726	552	784	663	0.20	0.28	0.19	15
X <sub>04M</sub>	1800	1033	1941	625	939	999	0.21	0.19	0.18	15
X <sub>05M</sub>	1822	1343	2103	627	825	415	0.18	0.18	0.17	15
X <sub>06M</sub>	1607	2091	2439	1258	1168	1077	0.17	0.19	0.16	19
X <sub>07M</sub>	2300	3248	2410	1357	988	1392	0.19	0.19	0.20	20
X <sub>08F</sub>	1974	2387	2283	515	511	712	0.20	0.20	0.18	20
X <sub>09M</sub>	2079	1898	2074	1034	1116	870	0.19	0.17	0.20	20
X <sub>10M</sub>	1700	2978	2322	972	991	991	0.22	0.16	0.21	20
*X <sub>11C</sub>		27345		(automatically calculated)				0.31		24
X <sub>12F</sub>	2007	2212	2118	345	558	748	0.17	0.19	0.20	20

Table 12: Optimal values for the material parameters of the orthotropic FE model after calibration against 2019 EM modal data. (\*) Concrete stayed as isotropic material.

Updating parameter	E <sub>L</sub> [MPa]	E <sub>N</sub> [MPa]	E <sub>T</sub> [MPa]	G <sub>LN</sub> [MPa]	G <sub>LT</sub> [MPa]	G <sub>TN</sub> [MPa]	v <sub>LN</sub> [-]	v <sub>LT</sub> [-]	v <sub>TN</sub> [-]	γ [kN/m <sup>3</sup> ]
X <sub>01M</sub>	2145	2031	1908	946	916	1022	0.21	0.20	0.20	15
X <sub>02M</sub>	2121	2397	1882	636	950	996	0.18	0.20	0.21	15
X <sub>03M</sub>	2294	1909	1761	460	725	614	0.18	0.27	0.19	15
X <sub>04M</sub>	1682	967	1946	564	924	1036	0.22	0.19	0.17	15
X <sub>05M</sub>	1694	1301	2133	528	770	338	0.18	0.17	0.16	15
X <sub>06M</sub>	1615	2092	2230	1374	1122	1221	0.17	0.18	0.16	20
X <sub>07M</sub>	2327	3297	2508	1400	1092	1391	0.19	0.19	0.20	20
X <sub>08F</sub>	1711	2397	2351	563	516	772	0.20	0.21	0.18	20
X <sub>09M</sub>	2048	1956	2143	1038	1116	899	0.20	0.18	0.21	20
X <sub>10M</sub>	1743	3016	2507	1126	1054	1054	0.19	0.16	0.20	20
*X <sub>11C</sub>		27106		(automatically calculated)				0.33		25
X <sub>12F</sub>	2035	2201	2060	330	542	795	0.17	0.20	0.20	20

The frequency results obtained from the modal-based FE model updating of Ostra Civic Tower through GA are exposed in Table 13 and Table 14. For both material modelling approaches, the comparison between EM and NM frequency values is more than satisfactory, being the absolute value of their relative errors always under 4%, with the largest percentage error in correspondence of the 4<sup>th</sup> mode, error that consistently reduces if an orthotropic material is considered for masonry. In general, the orthotropic model allows to better tune the frequencies of the fundamental global modes of the

tower and to closely reproduce the frequencies of higher modes, which are notably more sensitive to localized damage.

Table 13: Comparison between 2018 experimental (EM) and numerical (NM) frequencies for different material modelling approaches and different updating parameters.

Mode	$f_{EM18}$ [Hz]	$f_{NM18}$ [Hz] 36 variables (Isotropic)	$f_{NM}$ [Hz] 113 variables (Orthotropic)	Eff. Mass Direction X [%]	Eff. Mass Direction Y [%]	$ \Delta f_{EM18-NM18} $ [%] (Isotropic)	$ \Delta f_{EM18-NM18} $ [%] (Orthotropic)
$\varphi_1$	2.082	2.070	2.084	34.14	0.01	0.58	0.10
$\varphi_2$	2.156	2.111	2.137	0.01	33.53	2.09	0.88
$\varphi_3$	6.293	6.245	6.284	0.26	0.00	0.76	0.14
$\varphi_4$	6.442	6.693	6.516	29.89	0.11	3.90	1.15
$\varphi_5$	6.941	6.839	6.907	0.12	29.25	1.47	0.49

Table 14: Comparison between 2019 experimental (EM) and numerical (NM) frequencies for different material modelling approaches and different updating parameters.

Mode	$f_{EM19}$ [Hz]	$f_{NM19}$ [Hz] 36 variables (Isotropic)	$f_{NM19}$ [Hz] 113 variables (Orthotropic)	Eff. Mass Direction X [%]	Eff. Mass Direction Y [%]	$ \Delta f_{EM19-NM19} $ [%] (Isotropic)	$ \Delta f_{EM19-NM19} $ [%] (Orthotropic)
$\varphi_1$	2.092	2.079	2.091	33.94	0.00	0.62	0.05
$\varphi_2$	2.165	2.123	2.143	0.00	33.41	1.94	1.02
$\varphi_3$	6.302	6.277	6.229	0.41	0.06	0.40	1.16
$\varphi_4$	6.449	6.645	6.510	29.22	0.03	3.04	0.95
$\varphi_5$	6.872	6.789	6.930	0.02	28.48	1.21	0.84

The numerical mode shapes corresponding to the FE model calibrated with the optimal values of the material parameters are displayed in Figure 23 and Figure 24. Similar considerations can be drawn in this case. Indeed, a very good agreement is visually observed between experimental and numerical mode shape configurations: the 1<sup>st</sup> and 2<sup>nd</sup> mode are in-phase translational modes in x and y directions, respectively, the 3<sup>rd</sup> mode is torsional, while the 4<sup>th</sup> and 5<sup>th</sup> modes result dominant bending modes in the xz and yz planes.

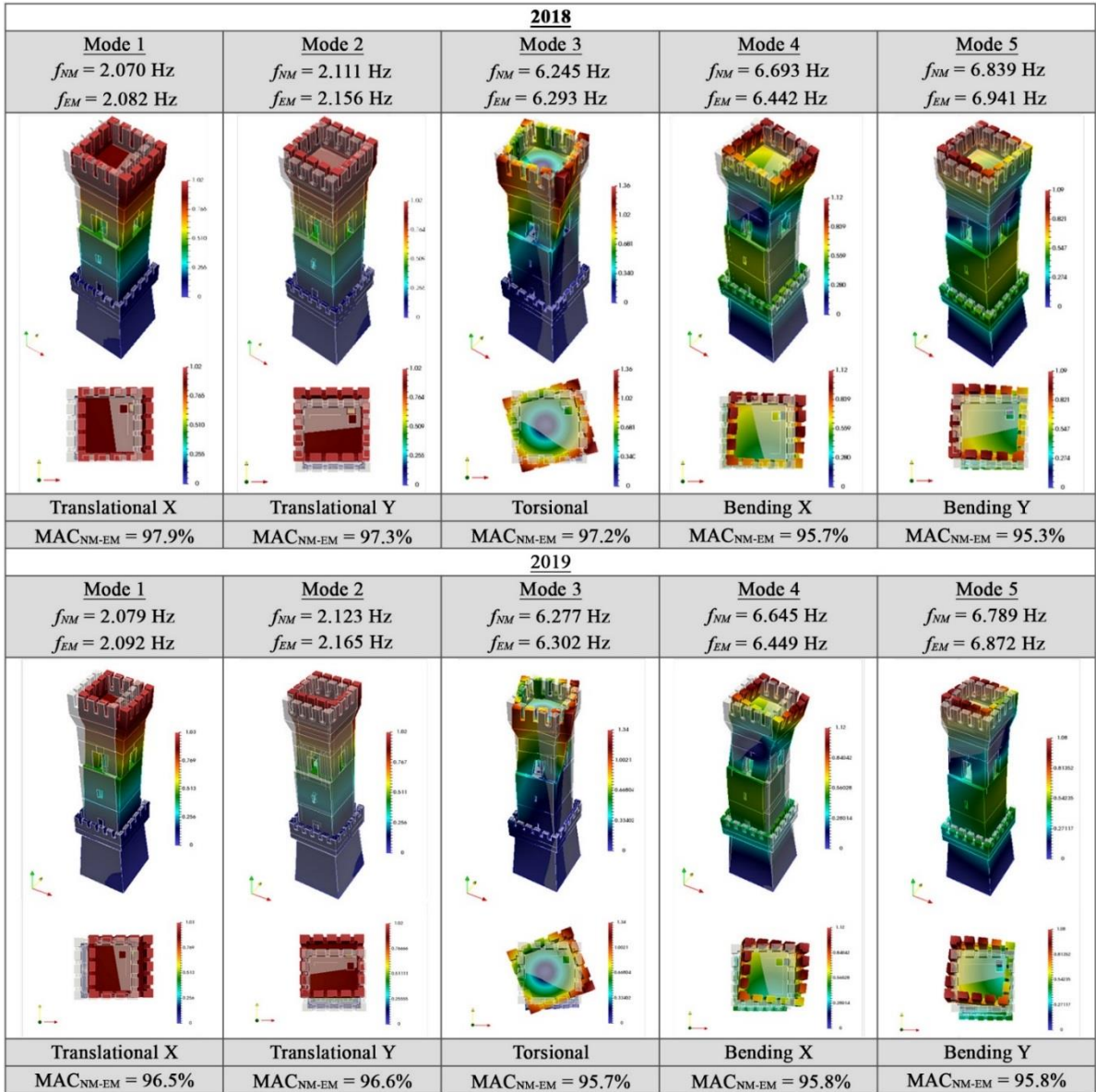


Figure 23: Numerical Mode Shapes after calibration using isotropic material modelling.

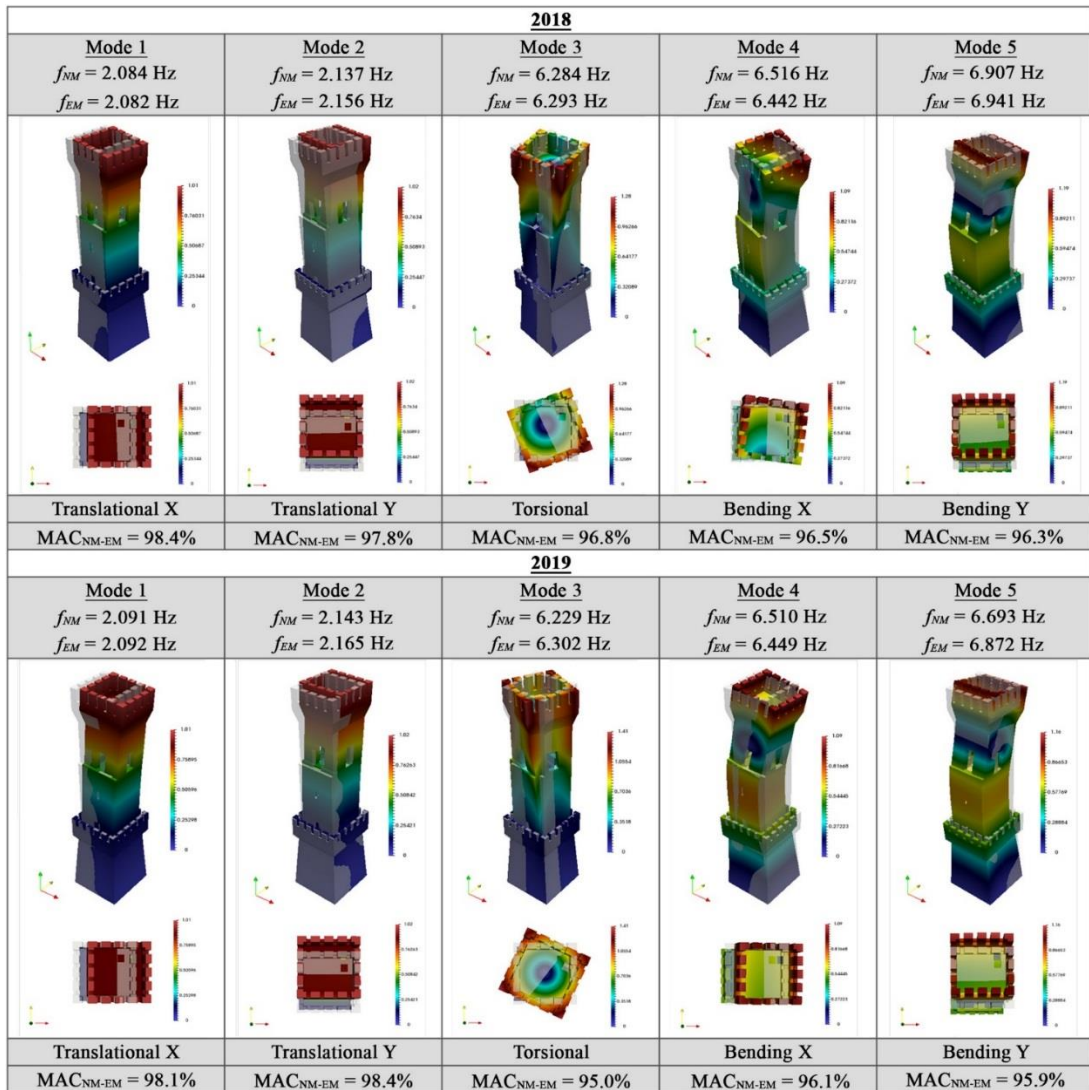


Figure 24: Numerical mode shapes after calibration using orthotropic material modelling.

The direct cross-validation between EM and NM mode shapes through the MAC further proves the good agreement between experimental and numerical counterparts, being all five modes very well correlated (MAC > 95%) and decoupled, as demonstrated by the low values of the out-of-diagonal elements of the Cross-MAC matrix (Table 15). It is worth highlighting the relevance of the achieved results: in fact, the majority of FE model updating techniques applied in the literature typically result into much higher relative errors between experimental and numerical frequencies and, in the rare instances in which a two-term objective function is adopted, into MAC values sensibly lower than 80% for higher order modes.

Table 15: CrossMAC between EM's and calibrated NM's considering isotropic and orthotropic materials:(a) NM 2018 with isotropic material,(b) NM 2019 with isotropic material, (c) NM2018 with orthotropic material, (d) NM2019 with orthotropic material.

		a)					b)						
		EM18					EM19						
CrossMAC		2.082 Hz	2.156 Hz	6.293 Hz	6.442 Hz	6.941 Hz	CrossMAC		2.092 Hz	2.165 Hz	6.302 Hz	6.449 Hz	6.872 Hz
NM18_iso	2.070 Hz	0.976	0.011	0.001	0.018	0.002	NM19_iso	2.079 Hz	0.962	0.016	0.000	0.019	0.000
	2.111 Hz	0.021	0.969	0.000	0.000	0.026		2.123 Hz	0.040	0.963	0.002	0.002	0.027
	6.245 Hz	0.000	0.000	0.972	0.015	0.015		6.277 Hz	0.001	0.000	0.958	0.010	0.024
	6.693 Hz	0.035	0.002	0.011	0.965	0.001		6.645 Hz	0.033	0.001	0.011	0.966	0.002
	6.839 Hz	0.003	0.015	0.005	0.010	0.960		6.789 Hz	0.006	0.017	0.006	0.024	0.960
		c)					d)						
		EM18					EM19						
CrossMAC		2.082 Hz	2.156 Hz	6.293 Hz	6.442 Hz	6.941 Hz	CrossMAC		2.092 Hz	2.165 Hz	6.302 Hz	6.449 Hz	6.872 Hz
NM18_Ortho	2.084 Hz	0.981	0.005	0.001	0.018	0.002	NM19_Ortho	2.091 Hz	0.979	0.004	0.000	0.021	0.001
	2.137 Hz	0.013	0.977	0.000	0.000	0.027		2.143 Hz	0.019	0.981	0.003	0.001	0.028
	6.284 Hz	0.000	0.000	0.959	0.014	0.006		6.229 Hz	0.001	0.000	0.963	0.011	0.013
	6.516 Hz	0.033	0.002	0.013	0.957	0.005		6.510 Hz	0.031	0.001	0.009	0.971	0.020
	6.907 Hz	0.002	0.010	0.001	0.002	0.965		6.693 Hz	0.003	0.011	0.001	0.002	0.968



## Chapter 5: Concluding remarks

The objectives and major contributions of this Thesis concerned the development and exploitation of Artificial Intelligence to build Digital twin models of masonry heritage structures. The methodology aims at the construction of robust models to be used for damage detection, localization and quantification in the field of Structural Health Monitoring. Innovative contributions of this work regard the automatic model updating procedure capable of handling any number of parameters directly on the Finite Element model with the application of a restrictive objective function that aims to minimize considerably the variation between the experimental and numerical data of eigenvalues and eigenvectors.

Chapter 1 has presented the model updating methods and different correlation techniques available. It began with a general introduction of the construction of an experimental model along with its Finite Element twin and posed the question on which method is better to use for model updating having two bases of the same entity. The methods are then presented as direct and iterative ones. The direct methods application show in literature to have accurate results but don't consider physical properties which generates a problem when modelling with the Finite Element methods due to the loss of symmetry of the model's mass and stiffness matrixes. The iterative methods are chosen as the way to go. This class of methods handles different approaches. Each one of the approaches can be utilized as standalone or can be unified with others in order to confront a Structural Health Monitoring problem in its entirety. By analyzing the uncertainty propagation of the properties, the sensitivity each parameter has on the output results and application of Artificial Intelligence to create convenient shortcuts and reduce computational calculus. Along with the iterative methods, this chapter presents different correlation techniques that are applied for model updating. Some correlation techniques deal with frequency confrontation, frequency response functions and modal assurance criterions. Those correlation techniques can be thought of as the filter, the objective function, from which the outputs of the experimental and numerical model are passed and confronted resulting in a minimization problem between them. The objective of a model's update is to minimize an objective function. The terms of an objective function can vary, from one-term, two-terms or more-terms. In the present research work the objective function was constructed as a two-term function, correlating the differences between the experimental and numerical frequencies and mode shapes with a constraint definition of 5%.

Chapter 2 analyses different optimization algorithms and presents advantages and drawbacks of each one. It connects directly with the first chapter because, knowing the method and correlation technique to use, the remaining problem is the algorithm that should be selected for the update. A distinction is made between gradient-based algorithms and nature-based algorithms with major focus on the population based genetic algorithm. Application and theory can be found for the firefly and particle swarm optimization algorithms. The variable that made the genetic algorithm chosen is found in

its genetic operators. These operators during the sequence that is followed, select the best possible candidates of the solution with application of different approaches, try to differentiate the possible best solution by updating parts of the candidates and disturb stochastically variables of the candidates in order to achieve a global optimum solution and not remain in local ones.

The application of model updating techniques directly on a Finite Element model can result, in some cases, in a lengthy operation. The computational strain becomes excessive when the model is subjected to statistical analyses due to the number of different simulations needed for the analyses. A possible solution comes from the construction of metamodels. In Chapter 3 the workflow for the construction of metamodel is presented along with its use to perform sensitivity analyses. The construction of a metamodel is based on samples. The samples are results of the evaluation of a design of experiments. To account for randomness in the samples, a probabilistic design is followed with selected bounds and design for each variable then, a Monte-Carlo approach is applied to generate the space of the samples. The continuation of the workflow was done by applying a Kriging process on the data to correlate the inputs and outputs aiming at the creation of a predictor. The metamodel was then subjected to Sobols sensitivity analysis to find which variables of the model are more sensitive to the outputs (Frequencies and Mode Shapes). This technique aimed at reducing significantly the computational strain otherwise required.

Results of the topics of each chapter that aim at the exploitation of Artificial Intelligence to build realistically Digital Twin models are presented with Chapter 4 and Appendix A with the case study of the Civic Tower of Ostra. The Civic Tower is a Heritage structure situated in the city center of Ostra in Marche region, in the province of Ancona. A preliminary geometrical and material survey were performed that aimed at identifying the main characteristics of the structure. The information gained from these surveys was necessary for the creation of a reliable numerical twin model to be later exploited as reference configuration for more sophisticated linear and non-linear analyses. Two field testing campaigns were carried out to acquire the vibration response of the tower to ambient noise under operational conditions. The acquired data from the AVT procedures, after pre-processing operations, was analyzed using two modal estimators in order to extrapolate, with high degree of fidelity, the dynamic parameters related to the principal modes of the structure, allowing to build a target experimental model for the model updating of the numerical tower. Such a process consists in perturbing the mass and stiffness matrixes that define the system in order to find physically meaningful values for the unknown material properties that could minimize the deviation between the eigenvalues and eigenvectors provided by the OMA. The approach was done through an automatic model updating with genetic algorithm of the OMA eigen-data projected onto the equivalent numerical model. By profiting of a biologically inspired algorithm. The optimization problem was solved by adopting two modelling assumptions for masonry, namely an isotropic and an orthotropic constitutive behavior, where the latter led to a threefold increase in the number of candidate solutions. Different considerations were made for both measurements considering Sobols sensitivity indexes. The sensitivity

analysis was performed through a metamodel constructed using the Kriging approach utilizing 1024 samples and validated through three different techniques. The validation served the purpose of confirming that the metamodel achieves its intended purpose. Constructing the metamodels of both isotropic and orthotropic behavioral models decreases computational strains and makes the calculation of Sensitivity Indexes possible. A future application of the metamodels proposed is to directly update the unknown variables. A possible validation of the update would be a direct confrontation with the Finite Element model taking in consideration the bias error produced by the metamodel. To further elaborate on the model's performance, the sensitivity indexes were categorized based on different percentual variations. This procedure showed the importance of the interactions each component of the discretized numerical model and the isotropic, orthotropic behavioral models has on the results. It also showed how the reduction of the design variables affects the overall quality and accuracy of the models' response. An example of "trial and error" shown in Appendix A, following up on the consideration of how the error estimation is reduced faster, the lower the number of parameters is considered. The "trial and error" approach was performed already knowing the optimal target values from the calibration of NM18. The analysis showed the difficulty to search the entire search space and achieve a high degree of accuracy for the values of the design variables manually, especially when the design variables that describe the comportment of a masonry model are elevated in number. As was already noted, the sensitivity indexes refer to design variables that need to be excluded from the analysis and reduce the computational calculations. While numerically these considerations are reasonable, from a physical point of view such considerations are not entirely correct. In case of an event the whole structure is under stress and does not consider sensitivity obtained from numerical exploitations. This indicates that considerations and application of all the material parameters must be made during a model updating procedure to gain knowledge on the uncertain properties of the material parameters that define the model and aim at the identification, localization and quantification of damage.

The procedure shows that GA-based model updating approaches can be profitably coupled with AVT techniques to simulate the realistic behavior of masonry structures despite the limited information available about the internal morphology of structural elements and the unknown mechanical properties of constituent materials. Although from a theoretical standpoint, due to the metaheuristic nature of the method, it is impossible to ensure that all the local minima – from which the global minimum is recovered – are found during the updating process, the method has been proved effective, robust, and less computationally demanding than conventional global sensitivity analyses. The adopted optimization process also corroborated the hypothesis of using an isotropic model to realistically describe the behavior of large-scale masonry structures, which is quite a common simplification in the literature [133]–[135]. This was possible thanks to one of the main innovative aspects of this work, namely the exploitation of an automatic procedure capable of handling a very large number of unknowns, which enabled to consider as variables all the meaningful parameters describing the orthotropic behavior of the masonry material and to compare the

goodness of the simulated modal response against the one obtained from the isotropic model. Overall, although the orthotropic approach produced slightly better results in terms of final modal residuals, the improvement was not as marked as it could be expected. Due to the complexity of orthotropic modelling when dealing with unconventional historical structures in both linear and non-linear fields, resorting to the isotropic assumption can allow to greatly reduce the computational effort inherent to the calibration process and subsequent analyses, without compromising the accuracy and reliability of the results. Finally, it is worth stressing that, unlike most of current FE model updating techniques, the method herein proposed does not run into difficulties when tackling a great number of parameters and has been demonstrated feasible even when the number of subproblems to solve grows exponentially, confirming its suitability to be employed as preferred tool in Structural Health Monitoring, to optimize the control of the structural integrity at global and local level by creating Digital Twin models

## APPENDIX A – Evaluation of the influence of material parameters in automatic calibration

This appendix details in the first part the workflow of the Genetic Algorithm (GA) model updating procedure employed in the present work along with the validation of the relevant metamodel, and reports in the second part all the results from the sensitivity analyses carried out to evaluate the influence of different unknown parameters on the structure's natural frequencies, namely their impact on the outcome of the modal-based updating process. What emerged from the analyses, particularly when comparing the results with those obtained from a second automatic GA-based calibration using the NM18 as initial baseline model, is summarized below:

- Considering all the unknown parameters in the updating procedure leads to final values of material properties consistent with those obtained by performing the model updating only with a reduced number of parameters;
- The frequencies and mode shapes residuals resulting from the model updated through GA are smaller in comparison to the residuals estimated by updating only the most sensitive parameters of the model, hence the FE model calibrated via GA is more representative of the real physical structure;
- When considering an orthotropic material behaviour, the computational costs of the GA-based approach are reduced as compared to apparently more manageable sensitivity analyses, being unnecessary to create a new metamodel and to assess again the most influential parameters.

The second part shows an example of an iterative calibration by “trial and error” of the NM18. The example is made knowing the target values of the calibration and shows the difficulty to manage manually the elevated number of parameters, necessary for the calibration, even considering different percentages of Sobol's sensitivity indexes.

### A.1. Genetic algorithm workflow

#### a) Initialization:

Once the parameter ranges and initial values are defined, a population is randomly generated, and all individuals are initialized for the adjustment. The size of the population is given by the value of the parameter NB\_PARENTS and is imposed by the user in the command file. This value is dependent on several factors such as the uncertainty of the solution. The greater the uncertainty, the larger the population. The stabilized value for the study was set to 10.

### b) Functional Evaluation:

In the first stage only one evaluation is made because the populations are identical, then in the re-calibration loop, as many evaluations of the functional are made during this one iteration as the number of children defined by the parameter NB\_FILLS, which is in turn defined by the user. The larger the parameter that defines the renewal of the population, the more CPU time is required for the step by the algorithm. For the present case, 6 parameters, corresponding to half the size of the population, were defined.

### c) Stopping Criteria:

Once the population of  $n$  parents is defined along with the individuals, the value of the criteria set to stop the calibration process is automatically checked and the best individual of the renewed population is returned as the solution. The check is performed over two variables:

- The best value of the functional calculation;
- The number of iterations already performed by the algorithm.

The former implies that the algorithm stops when the residual tolerance of two consecutive steps reaches the value defined by the user, which in the current case was set equal to  $1e^{-4}$ ; the latter means that the algorithm stops when the maximum number of iterations specified by the user is attained. In the present application, an increasing number of iterations was set for the algorithm, starting with 100 and then moving to 200, 500 and finally 2000.

### d) Selection – Crossover – Mutation:

The best individual parent is drawn from the population according to a Tournament selection method, [73]. In order to combine the genetic information of two parents and generate new offspring, a uniform crossover operator is employed, [72], [136]–[139], meaning that information is taken by both parents with equal probability. The mutation operator also follows a uniform scheme, in which the values of selected genes are replaced by uniform random values falling within the user-defined upper and lower bounds, [73], [140]. All the operations are controlled by the value of the parameter ECART\_TYPE (standard deviation) defined as:

$$\sigma = \sqrt{\frac{\sum_{i=1}^N (x_i - \mu)^2}{N}} \quad \text{Eq. 34}$$

where  $x_i$  is the  $i^{th}$  value from the population,  $\mu$  is the population mean, and the denominator  $N$  stands for the population size. For the present study, the value of the parameter ECART\_TYPE was defined as 0.5.

**e) Replacement:**

Once the  $m$  children are generated, the global population of the iteration stage results equal to  $n + m$  (i.e. NB\_PARENTS + NB\_FILLS). In the current implementation, this value was set as 15. The operator that controls the replacement realizes a hierarchy of the individuals according to the values associated by the calculus and replaces the population with the best parents found among the global population.

**A.2 Metamodel**

In order to reduce the computational strain and effectively calculate the Sobol Indices, surrogate models were constructed. The procedure took place considering as input vectors the material physical parameters of the isotropic and orthotropic models. The design of experiments utilized was based on a probabilistic approach where all the parameter ranges were defined by normal distributions and the data was then selected for the design of experiments by a Monte – Carlo algorithm. The whole process was carried out in the Openturns environment, [141]. The output, that was thoroughly calculated considering not only the eigenvalues of the physical system, but also the MAC values between the experimental and numerical models, was used to create the metamodel with a Kriging approach, (Chapter 3).

**A.2.1 Parameters definition**

Normal probability distribution was the base for defining Young’s moduli (E) [MPa], Poisson coefficient ( $\nu$ ) [-], and mass density ( $\gamma$ ) [kN/m<sup>3</sup>] in the metamodel. At first, it was decided to consider the whole ranges of parameters allowed by the Italian technical regulations, having distribution values of the Young’s moduli from 800 MPa to 5000 MPa for masonry, and from 17000 MPa to 38000 MPa for concrete.

*Table A. 1: Initial parameters normal probabilistic distribution*

	<b>Mean</b>	<b>Standard Deviation</b>	<b>Min - Max</b>
Masonry E [MPa]	3000	600	800 - 5000
Concrete E [MPa]	28000	2800	17000 - 30000
Masonry $\nu$ [-]	0.25	0.05	0.05 - 0.45
Concrete $\nu$ [-]	0.25	0.05	0.05 - 0.45
Masonry $\gamma$ [kN/m <sup>3</sup> ]	18	1	13 - 22
Concrete $\gamma$ [kN/m <sup>3</sup> ]	25	1	21 - 26

## A.2.2 Validation

The validation of the metamodel, namely its capability to explain the observed outcome, was done by selecting a three-way approach and assuming as acceptable statistic an  $R^2$  index greater than or equal to 0.9 for each resulting prediction. For the first check, validation solutions were provided as follows: 1) analytically; 2) dividing the dataset into an 80% – 20% scheme, using the 80% percentage as training (820 samples) and the 20% (204 samples) as validation of the trained model; 3) using a K-Fold procedure.

### A.2.2.1 Analytical validation results

The results of the analytical validation, for both material approaches, are shown below (Figure A.1÷A.4).

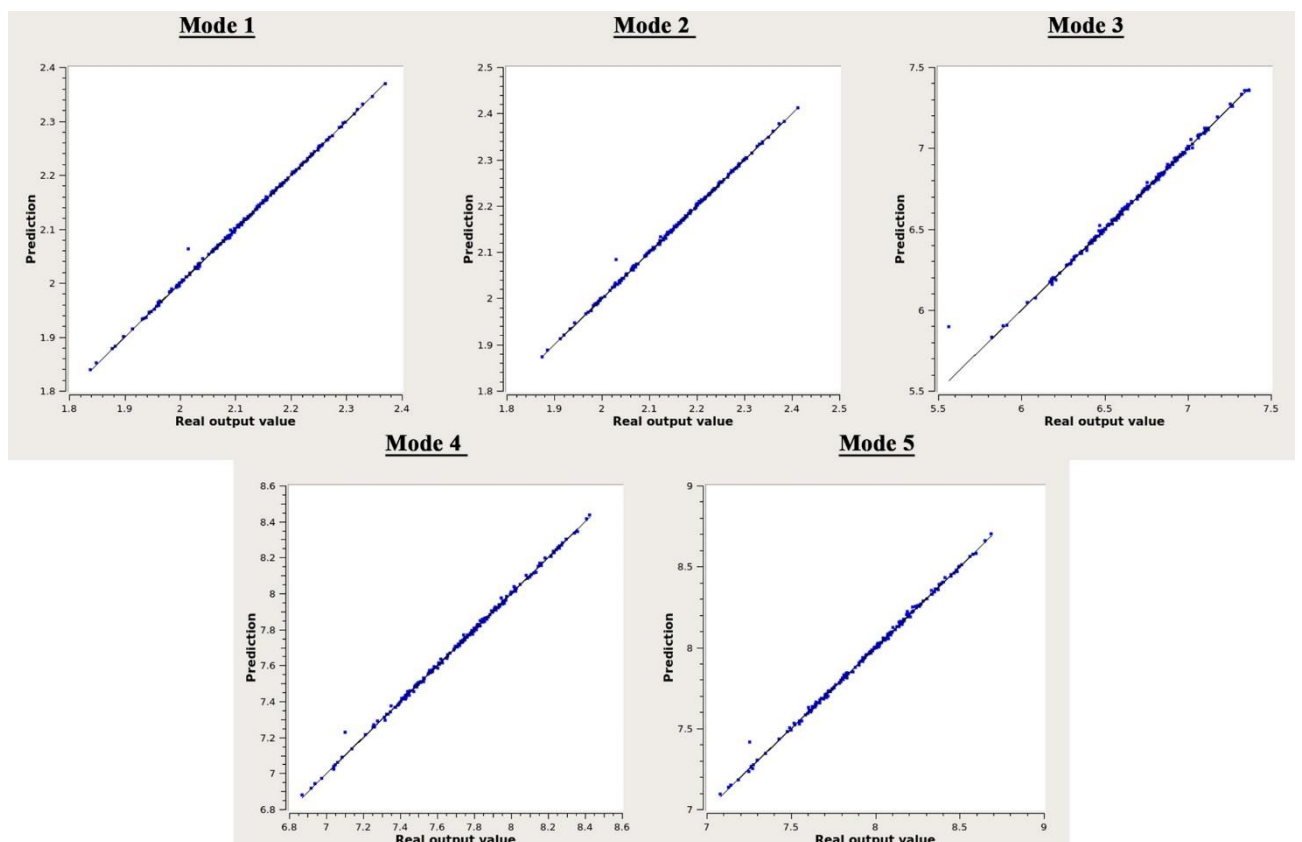


Figure A. 1: Analytical model validation for isotropic model: curve fitting of frequencies test samples.



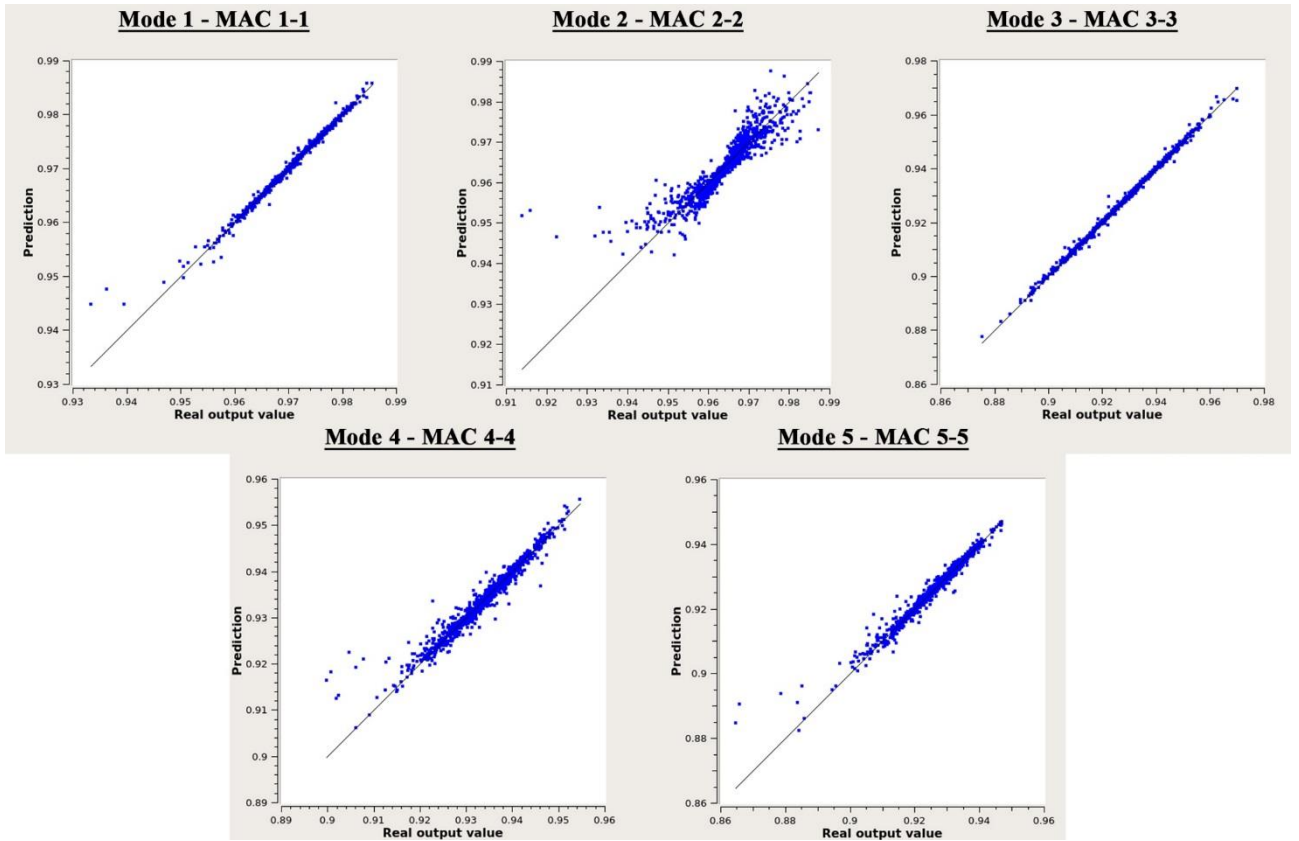


Figure A. 2: Analytical model validation for isotropic model: curve fitting of mode shapes test samples.

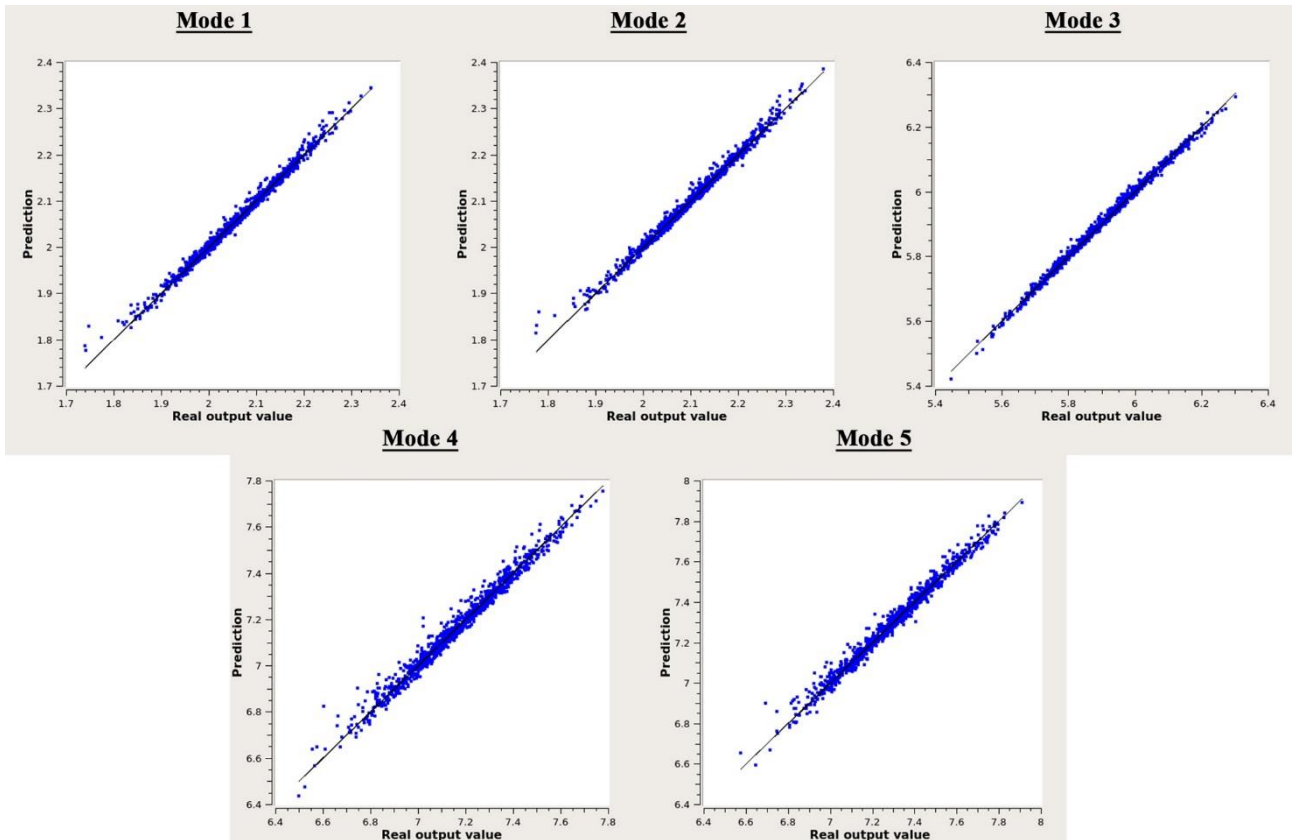


Figure A. 3: Analytical model validation for Orthotropic model: curve fitting of frequencies test samples.

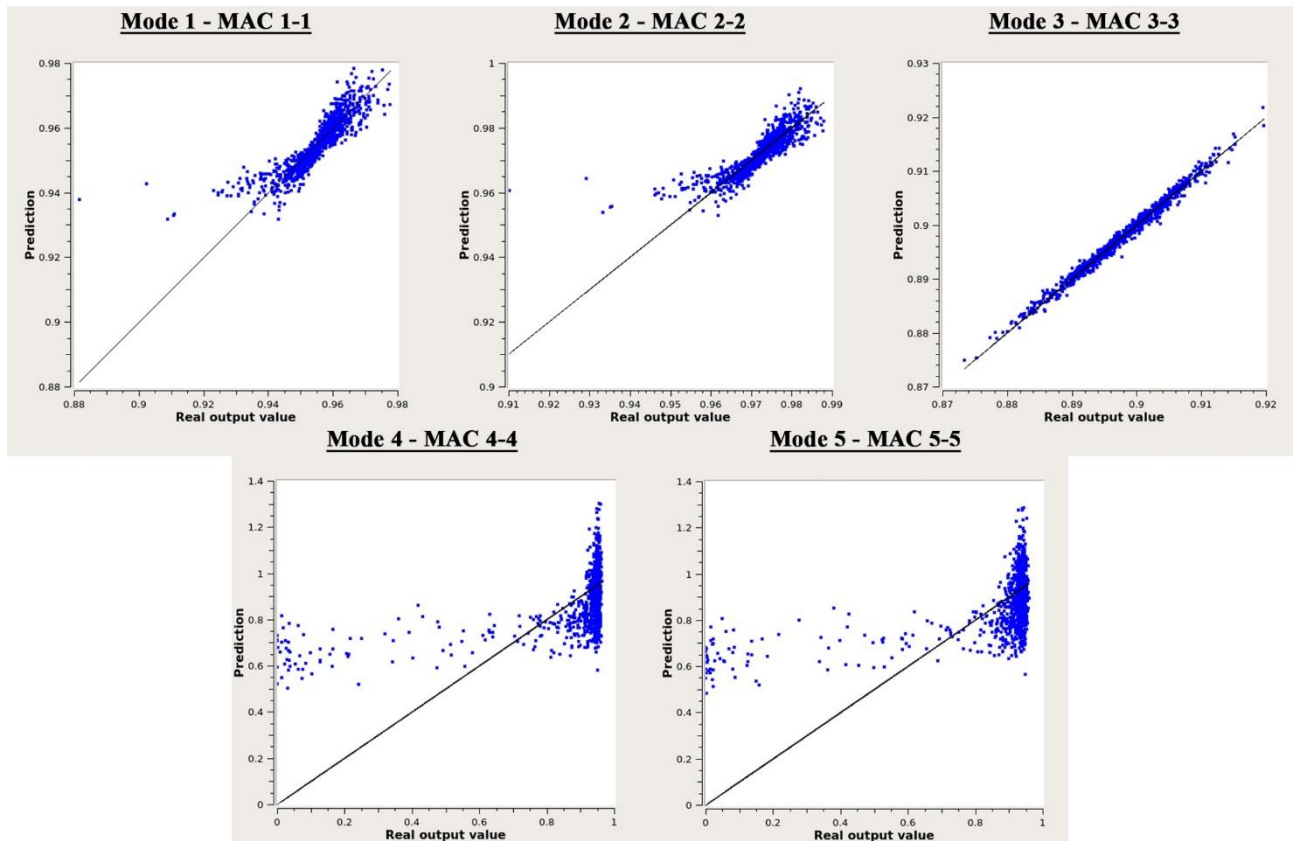


Figure A. 4: Analytical model validation for Orthotropic model: curve fitting of mode shapes test samples.

In Table A.2 and Table A.3 it is possible to observe the values of the coefficient of determination for both frequencies and MAC coefficients. It is noticed how  $R^2$  is practically near to 1 when predicting frequency values either with an isotropic or an orthotropic approach, while it sensibly decreases for the higher order modes when evaluating the mode shapes using an orthotropic model.

Table A. 2: Analytical validation of frequencies

Mode	Number of points	Percentage training/validation	Isotropic model		Orthotropic model	
			Residual	$R^2$	Residual	$R^2$
1	1024	80 - 20	0.000075	0.999	0.000289	0.990
2	1024	80 - 20	0.000084	0.999	0.000301	0.989
3	1024	80 - 20	0.000464	0.997	0.000298	0.995
4	1024	80 - 20	0.000323	0.999	0.000967	0.978
5	1024	80 - 20	0.000365	0.999	0.000897	0.982

Table A. 3: Analytical validation of mode shapes

MAC	Number of points	Percentage training/validation	Isotropic model		Orthotropic model	
			Residual	R <sup>2</sup>	Residual	R <sup>2</sup>
1_1	1024	80 - 20	0.00022	0.985	0.000140	0.752
2_2	1024	80 - 20	0.000109	0.814	0.000119	0.723
3_3	1024	80 - 20	0.000024	0.997	0.000024	0.987
4_4	1024	80 - 20	0.000057	0.945	0.005210	0.251
5_5	1024	80 - 20	0.000057	0.963	0.005294	0.246

### A.2.2.2 Test – Train split validation results

The second validation scheme was done on the model where the predictor was trained with 80% of the data and the residual 20% was used for the validation test, whose results are presented in the following Figures A.5-A.8.

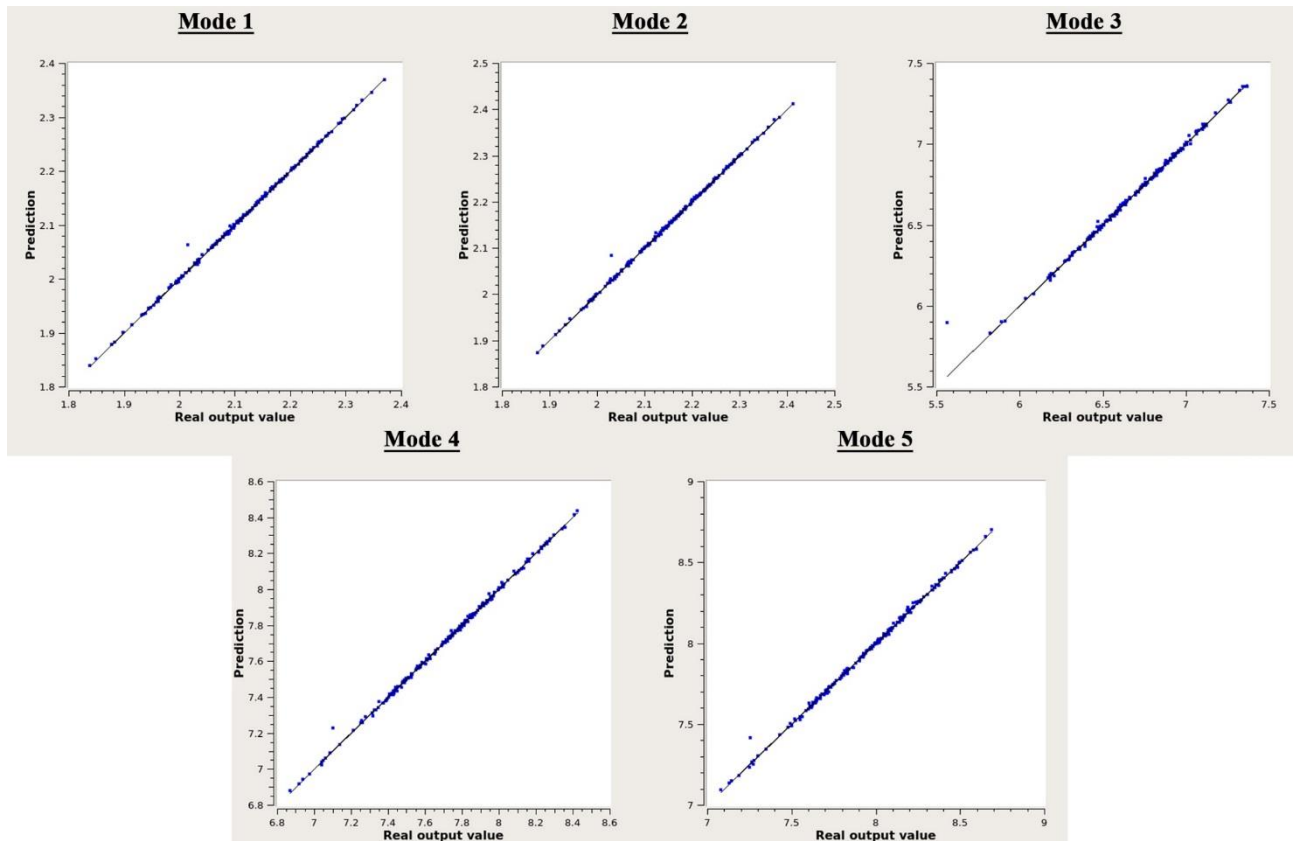


Figure A. 5: Train/Test split validation for Isotropic model: curve fitting of frequencies test samples.

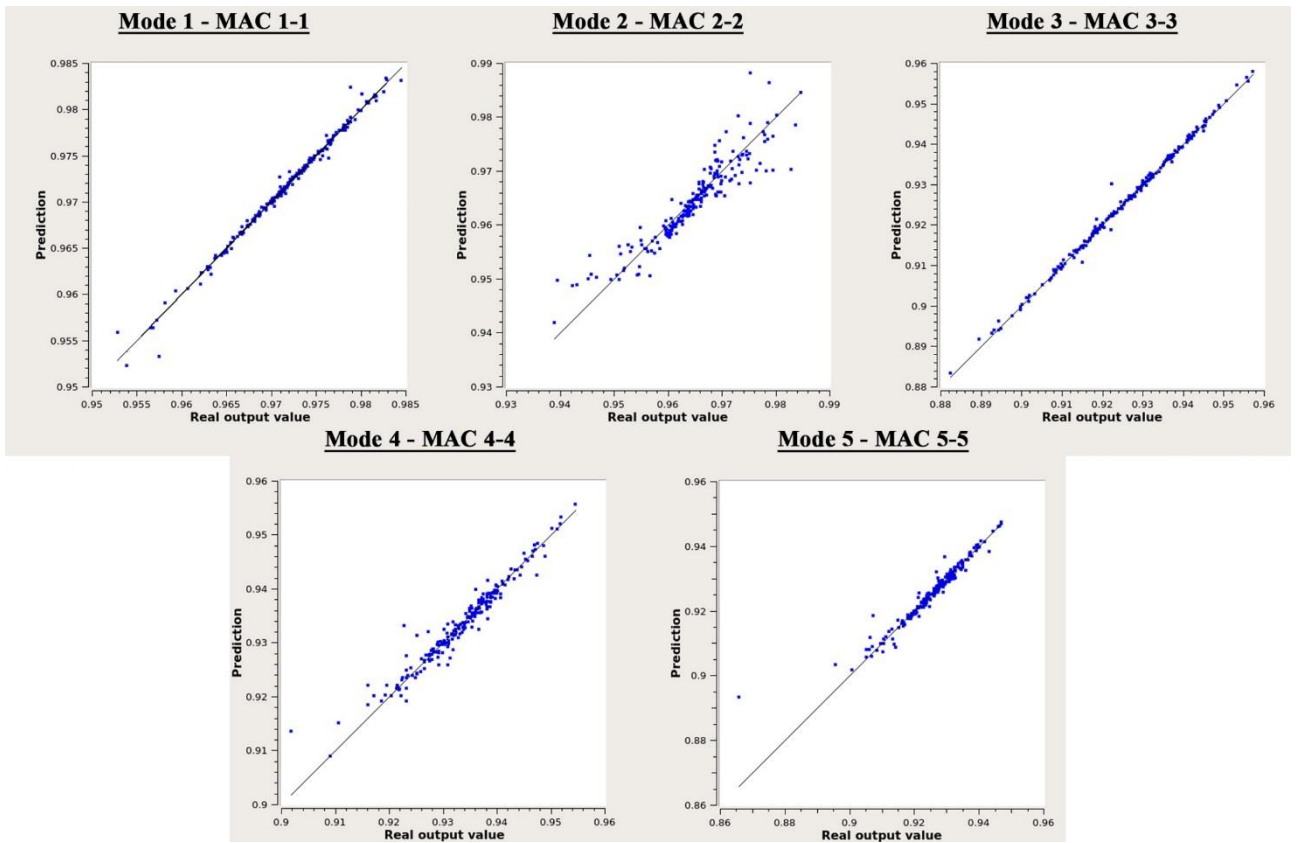


Figure A. 6: Train/Test validation for Orthotropic model: curve fitting of mode shapes test samples.

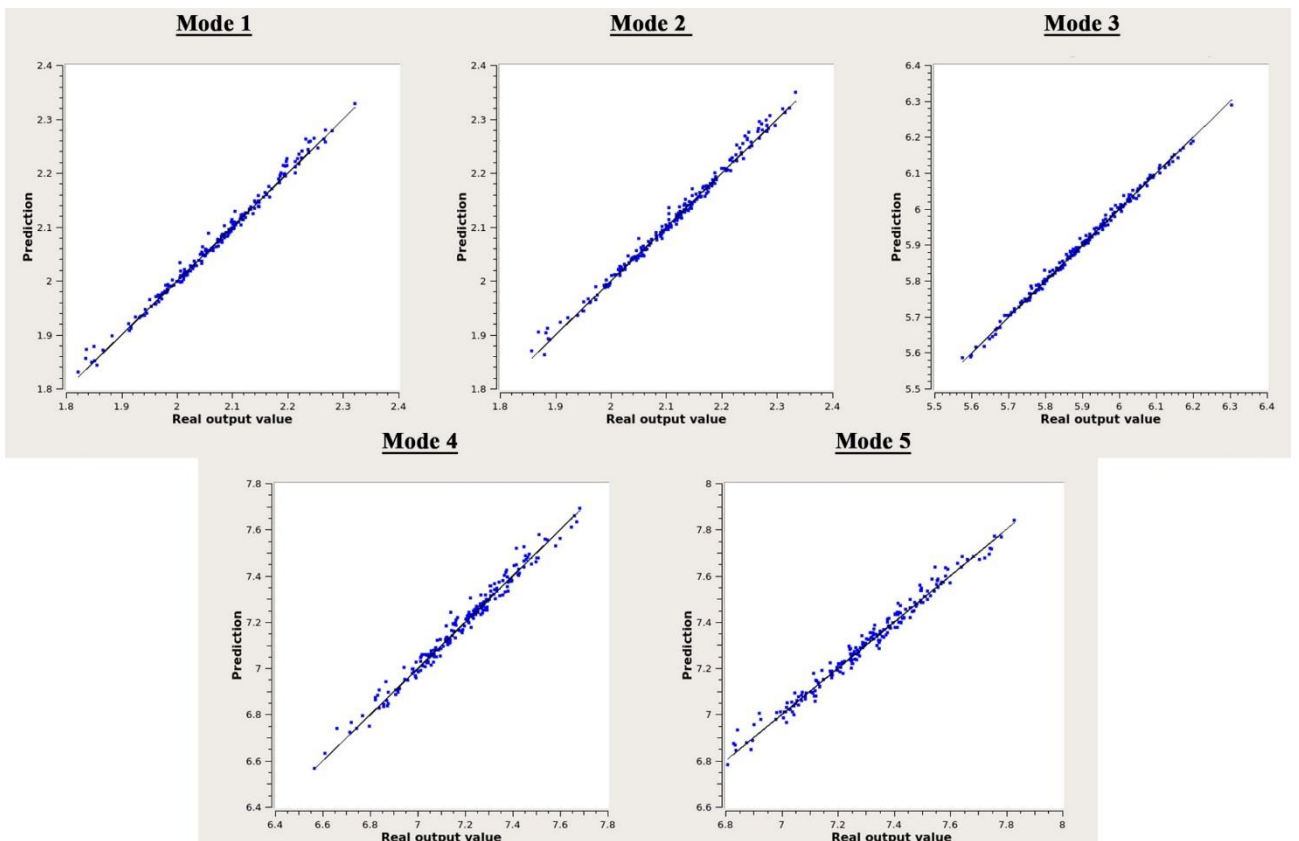


Figure A. 7: Train/Test validation for Orthotropic model: curve fitting of frequencies test samples.

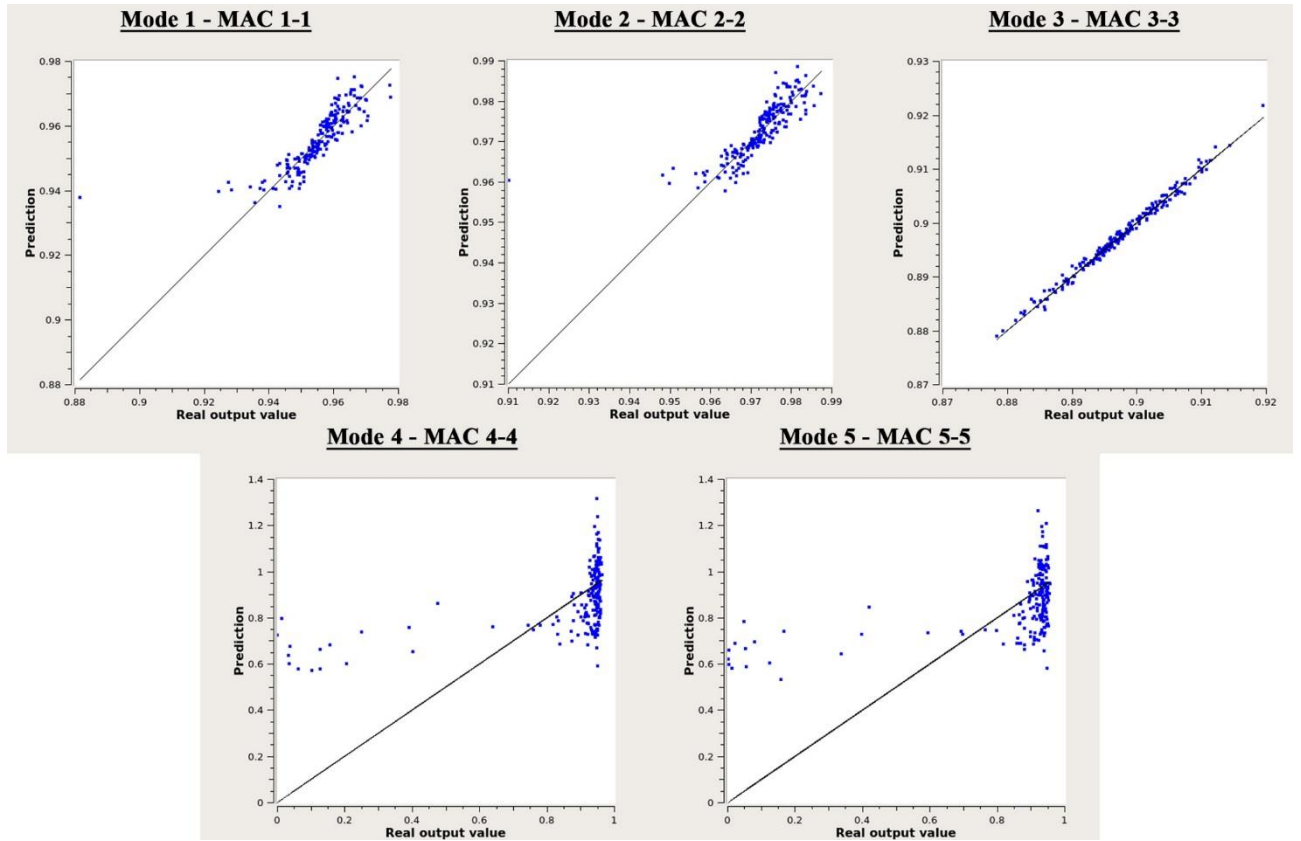


Figure A. 8: Train/Test split validation for Orthotropic model: curve fitting of mode shapes test samples.

Table A. 4: Train/Test split validation of frequencies.

Mode	Number of points	Percentage	Isotropic model		Orthotropic model	
			Residual	R <sup>2</sup>	Residual	R <sup>2</sup>
1	204	20	0.000266	0.999	0.000639	0.991
2	204	20	0.000301	0.998	0.000668	0.991
3	204	20	0.001779	0.993	0.000606	0.996
4	204	20	0.000863	0.998	0.002086	0.980
5	204	20	0.001026	0.998	0.001967	0.982

Table A. 5: Train/Test validation of mode shapes.

MAC	Number of points	Percentage	Isotropic model		Orthotropic model	
			Residual	R <sup>2</sup>	Residual	R <sup>2</sup>
1_1	204	20	0.000042	0.988	0.000395	0.668
2_2	204	20	0.000213	0.854	0.000337	0.625
3_3	204	20	0.000063	0.996	0.000054	0.988
4_4	204	20	0.000133	0.944	0.012807	0.234
5_5	204	20	0.000182	0.929	0.013189	0.233

### A.2.2.3 K-fold validation results

Lastly, the K-Fold method was employed using 10 numbers of folds.

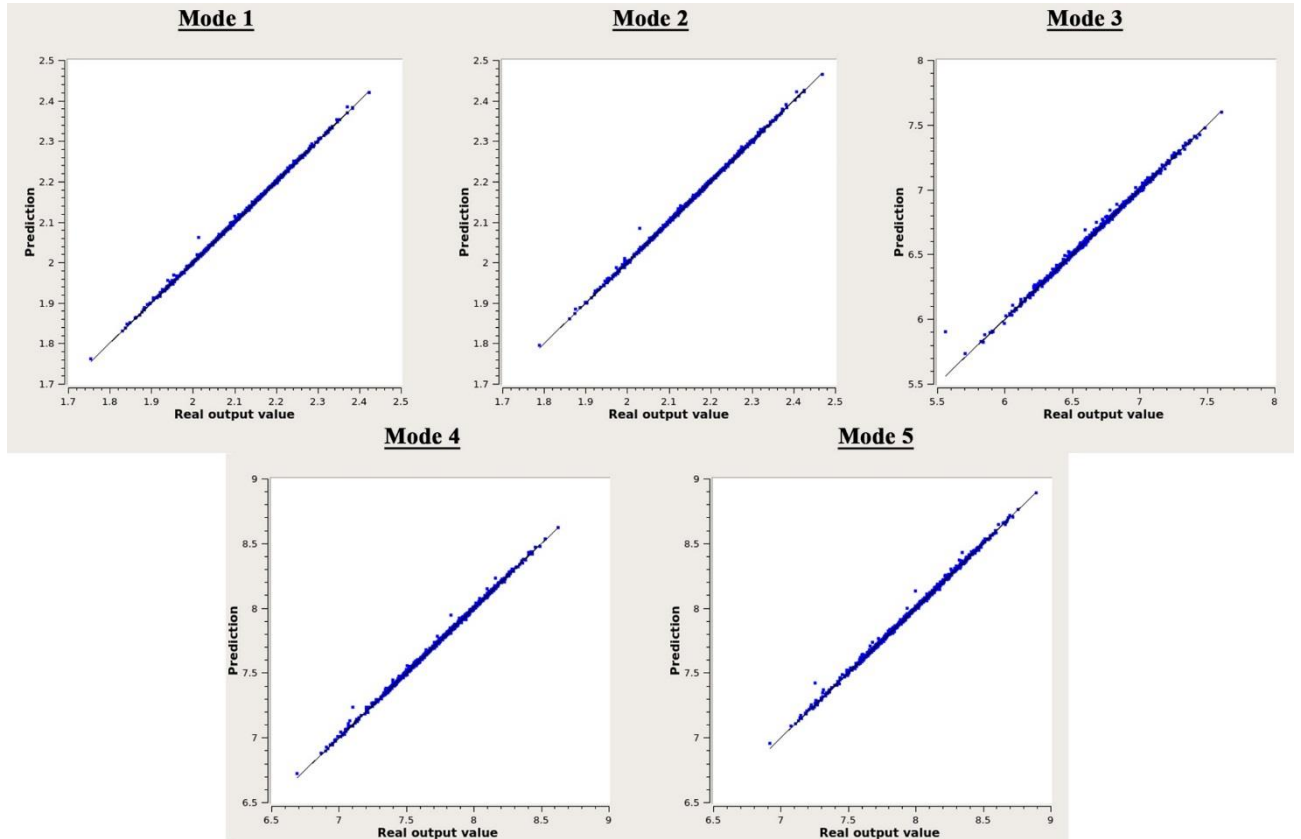


Figure A. 9: K-fold validation for Isotropic model: curve fitting of frequencies test samples.

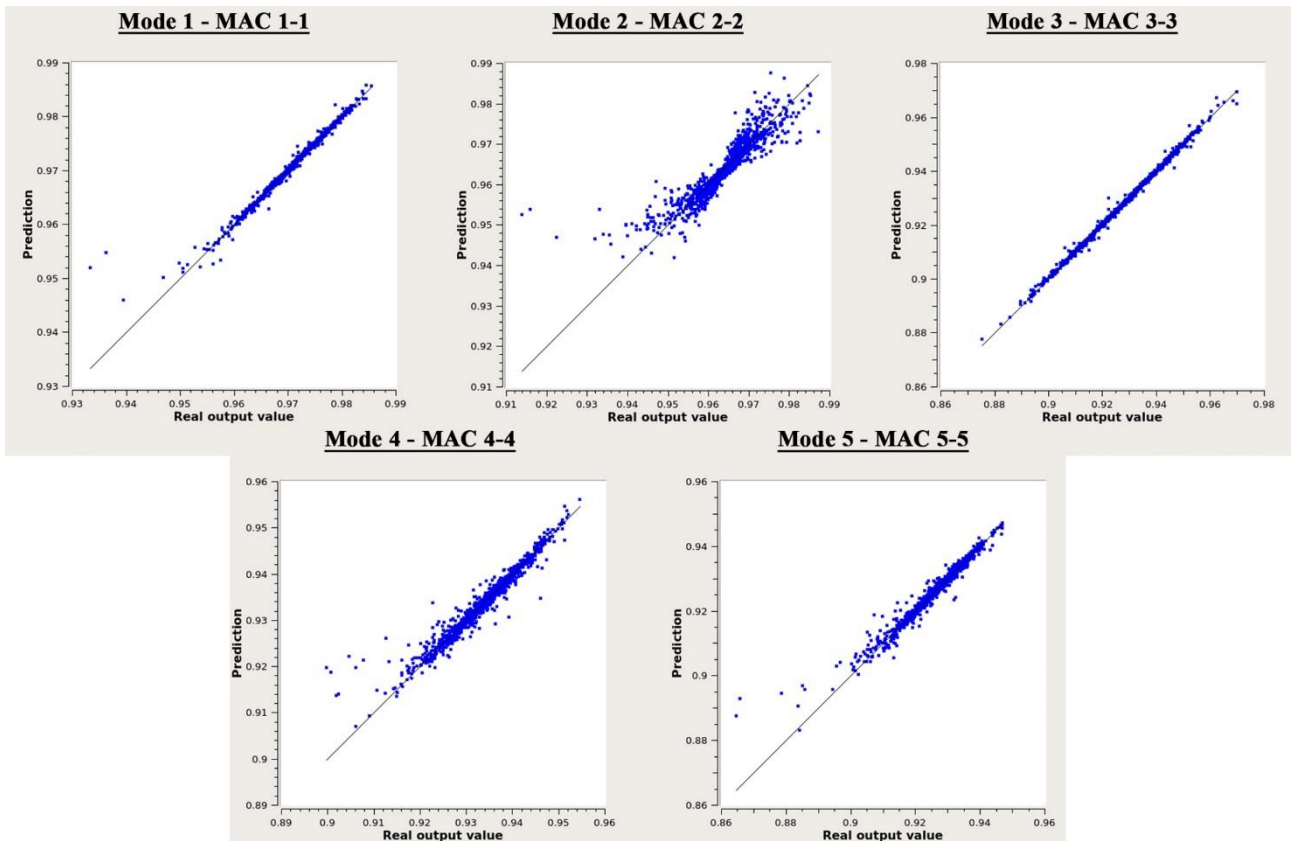


Figure A. 10: K-fold validation for Isotropic model: curve fitting of mode shapes test samples.

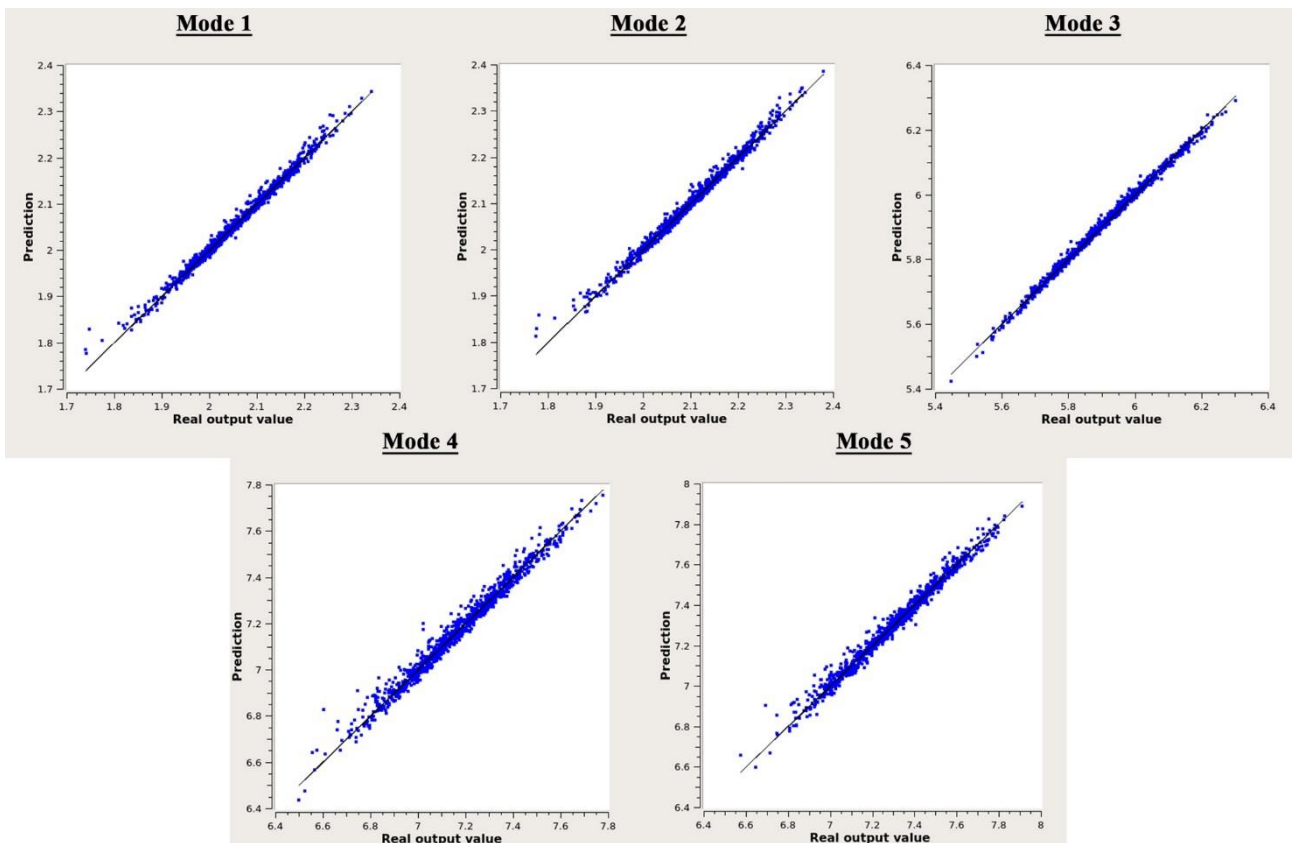


Figure A. 11: K-fold validation for Orthotropic model: curve fitting of frequencies test samples.

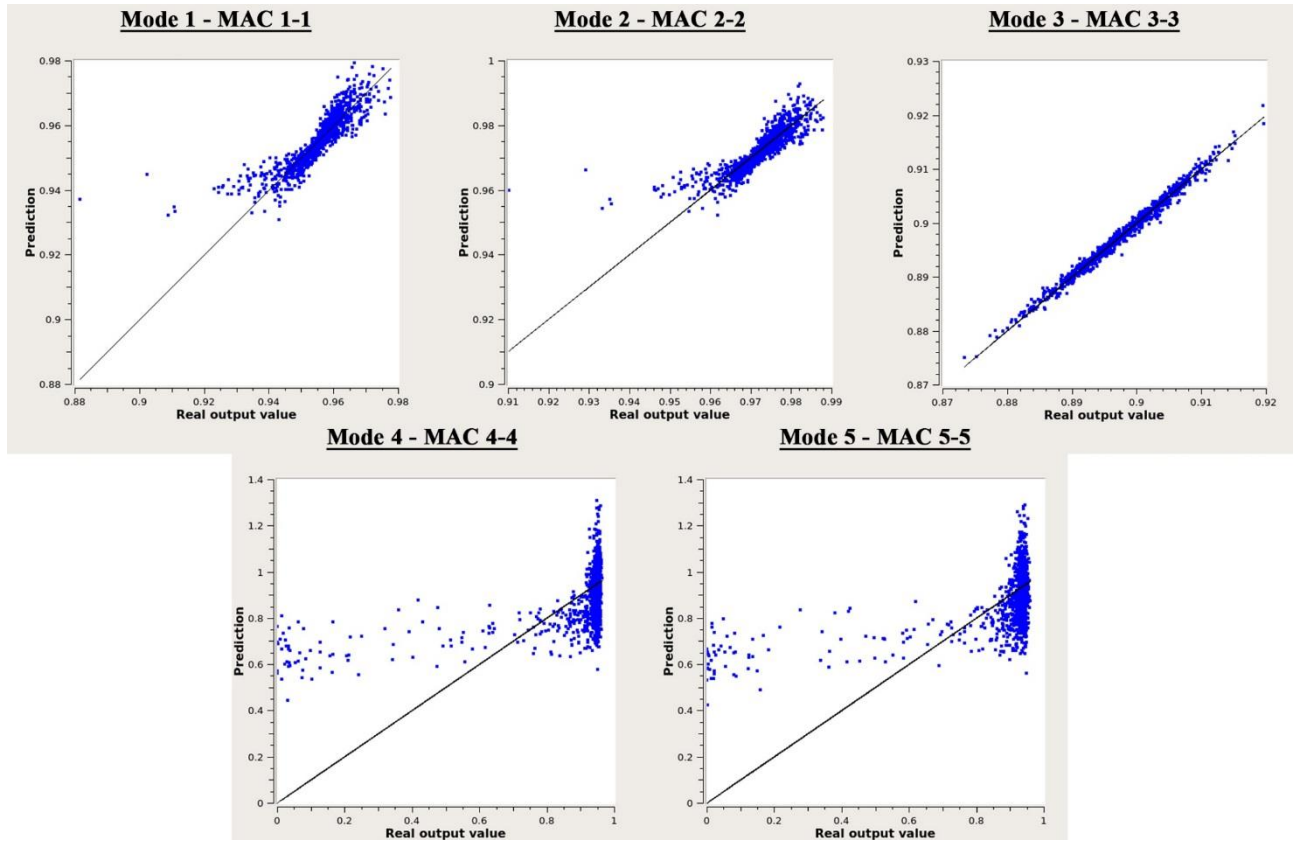


Figure A. 12: K-fold validation for Orthotropic model: curve fitting of mode shapes test samples.

Table A. 6: K-fold validation of frequencies.

Mode	Number of points	Number of folds	Isotropic Approach		Orthotropic Approach	
			Residual	R <sup>2</sup>	Residual	R <sup>2</sup>
1	1024	10	0.000226	0.999	0.000918	0.989
2	1024	10	0.000255	0.999	0.000956	0.989
3	1024	10	0.001338	0.997	0.000950	0.995
4	1024	10	0.001030	0.999	0.003051	0.977
5	1024	10	0.001142	0.998	0.002865	0.981

Table A. 7: K-fold validation of mode shapes.

MAC	Number of points	Number of folds	Isotropic Approach		Orthotropic Approach	
			Residual	R <sup>2</sup>	Residual	R <sup>2</sup>
1_1	1024	10	0.000072	0.979	0.000438	0.747
2_2	1024	10	0.000334	0.821	0.000372	0.720
3_3	1024	10	0.000079	0.997	0.000077	0.987
4_4	1024	10	0.000190	0.939	0.016444	0.231
5_5	1024	10	0.000187	0.958	0.016704	0.225



### A.3. Sensitivity analyses for isotropic material approach

Sensitivity analyses based on the Sobol Index (SI) calculation were conducted in order to evaluate the influence of isotropic material parameters in the outcome of the model updating process for NM19, starting from the model of 2018 (NM18) already calibrated through the GA procedure.

SI was calculated as:

$$SI_{ik} = \left| \frac{X_k}{Y_i} \cdot \frac{\Delta Y_i}{\Delta X_k} \right| \cdot 100 \quad (\text{A.3.1})$$

where:

- $X_k$  is the  $k$ -th uncertain parameter;
- $Y_i$  is the  $i$ -th predicted parameter;
- $\Delta$  the variation produced in the relevant parameter.

SIs were calculated both in relation to the output variation produced by changing every single parameter by 100% (indicated as “First Order Index”) and in relation to the output variation produced in correlation with other updating parameters changes (“Total Order Index”), as shown in Figure A. 13 and Figure A. 14. Moreover, to better track the influence of the number of updating parameters in the calibration process outcome, simulations were run considering different SI thresholds (1%, 5% and 10%). It is found that the highest changes in the modal frequencies produced by a first order index are mainly associated to the materials Young’s modulus of basement inner walls and central body as far as the first two vibration modes are concerned, whereas higher order bending modes result sensitive to both the variations of Poisson’s coefficient and mass density in the different parts. Moving to a total order index, the range of parameters influencing the natural frequencies of the different modes reduces to the Young’s modulus of the materials composing the basement and the central body of the tower. Yet, this reduction comes at a very high computational cost which strongly undermines the efficiency of the updating process and that could be easily bypassed resorting to the proposed GA-based approach.

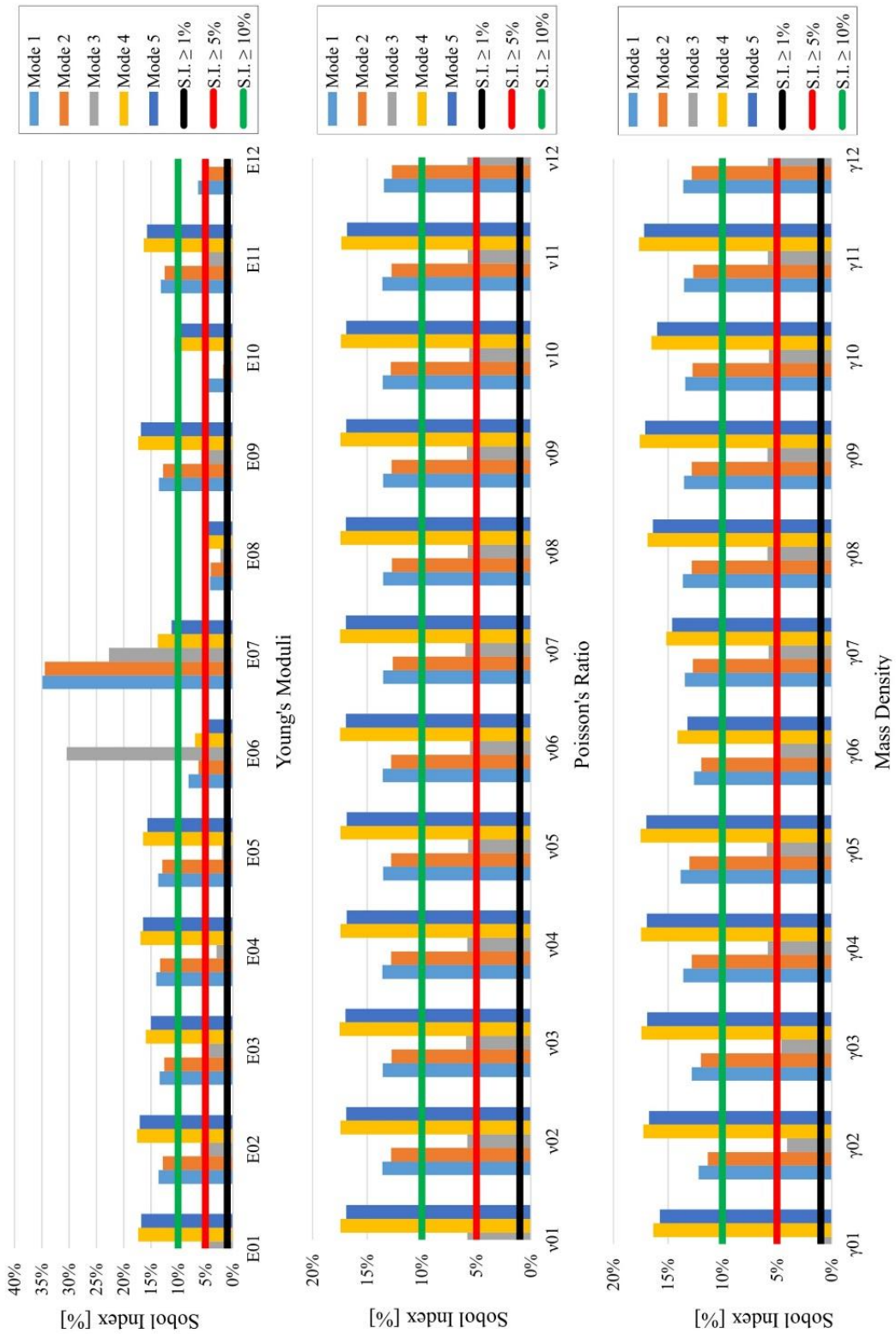


Figure A. 13: Sobol sensitivity analysis over first order indices for Kriging method. Thresholds of Sobol Indices (SI) respectively highlighted in black ( $SI = \pm 1\%$ ), red ( $SI = \pm 5\%$ ) and green ( $SI = \pm 10\%$ )

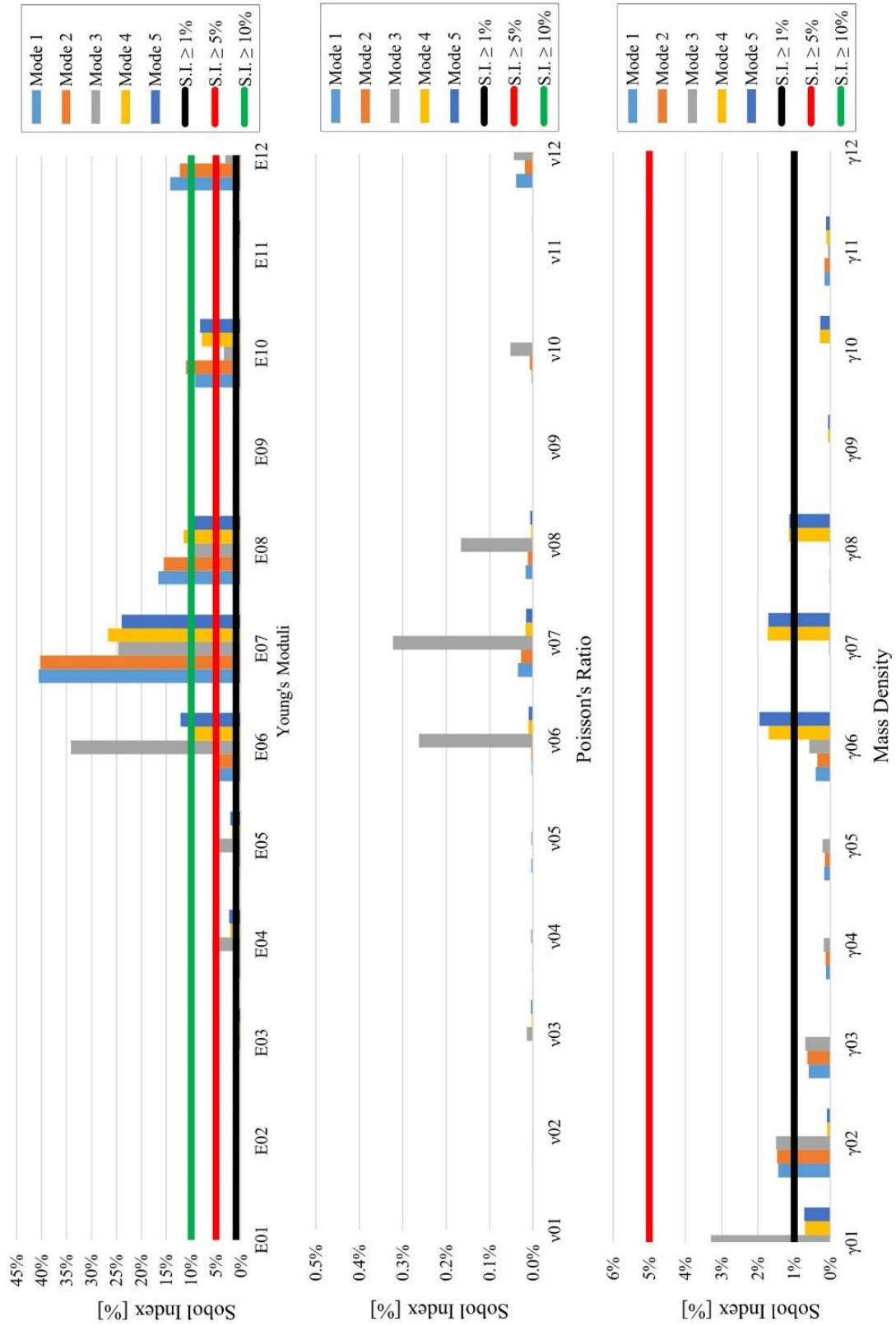


Figure A. 14: Sobol sensitivity analysis over total order indices for Kriging method. Thresholds of Sobol Indices (SI) respectively highlighted in black (SI= ± 1%), red (SI= ± 5%) and green (SI= ± 10%)

In light of the results obtained considering Total Order Sobol sensitivity analysis the following parameters were considered for calibration of NM19 with orthotropic material approach (Table A. 8):

*Table A. 8: Material parameters considered for calibration of NM19 after Sobol sensitivity analysis, using isotropic approach.*

	<b>Isotropic material parameters</b>	<b>Total</b>
<b>S.I. <math>\geq 1\%</math></b>	$E_{03} - E_{04} - E_{05} - E_{06} - E_{07} - E_{08} - E_{10} - E_{12}$ $\gamma_{01} - \gamma_{02} - \gamma_{06} - \gamma_{07} - \gamma_{08}$	13
<b>S.I. <math>\geq 5\%</math></b>	$E_{04} - E_{06} - E_{07} - E_{08} - E_{10} - E_{12}$	6
<b>S.I. <math>\geq 10\%</math></b>	$E_{06} - E_{07} - E_{08} - E_{10} - E_{12}$	5

Afterwards, the results from the calibration process of NM19, updated from the baseline numerical model of 2018, were compared first against the ones obtained from the optimized NM18, and then against those achieved with NM19\_0, i.e. a model built from scratch and calibrated directly via GA using the experimental results of 2019 and considering all the parameters as updating variables (Figure A. 15). Except for a few cases, the variation of NM19 materials Young's moduli with respect to NM18 and NM19\_0 counterparts shows a better agreement with the first model, proving that updating with new information a refined baseline model previously calibrated with reference data not only is faster and less demanding from a computational point of view, but also less prone to statistical variations from random error sources.

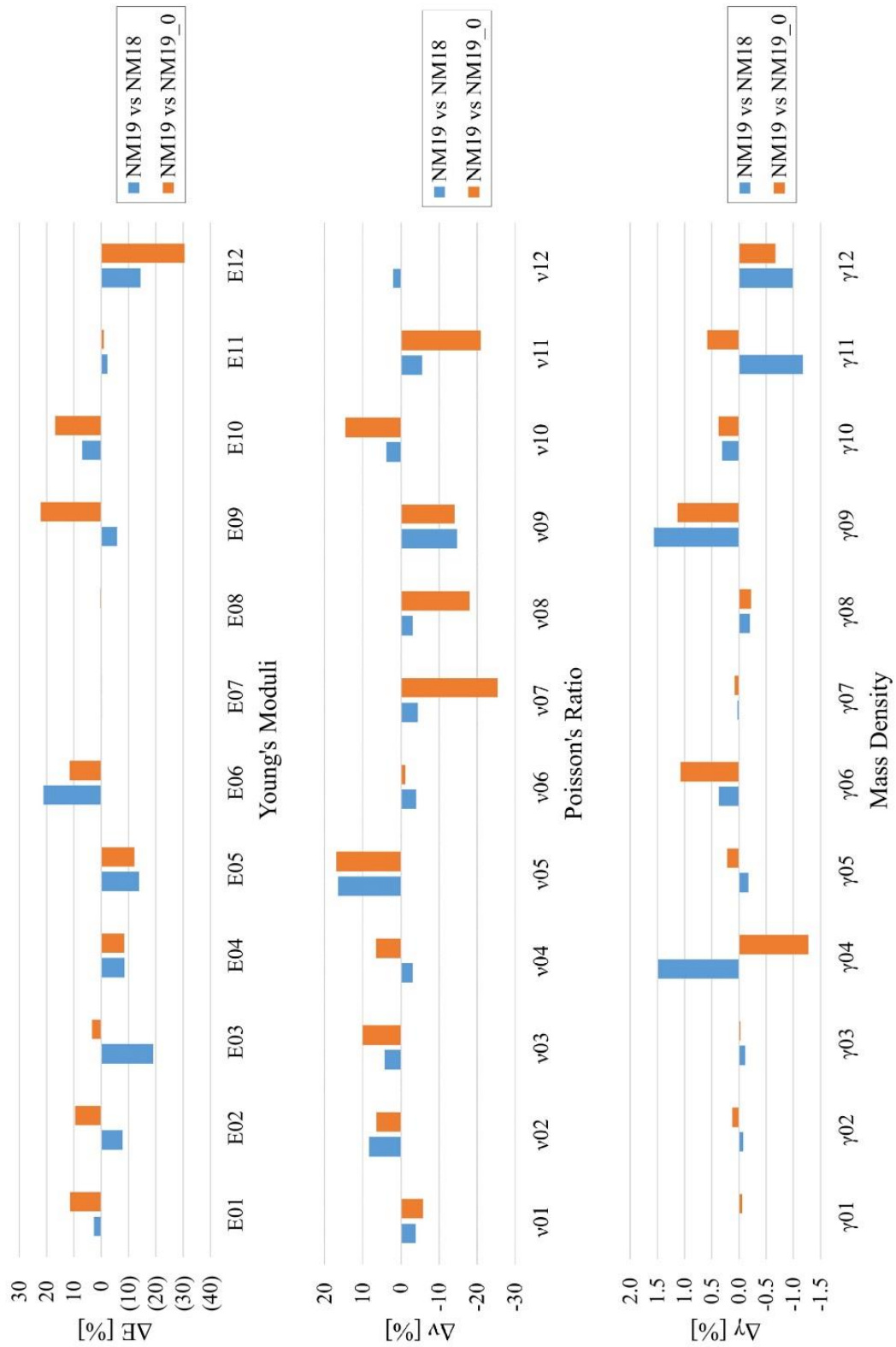


Figure A. 15: Variation of NM19 material parameters in comparison to NM18 (in blue) and NM19\_0 (in orange) considering all parameters in the calibration process.



Figure A. 16: Variation of NM19 material parameters with respect to NM18 considering a reduced number of variables based on different thresholds of SI.

Figure A. 16 compares the percentage variation of the Young's moduli, Poisson's coefficients and mass density of NM19 materials with respect to those of NM18 considering a number of parameters reduced on the basis of the sensitivity analyses previously described and for different thresholds of SI.

The comparison shows levels of variation similar or marginally better than those obtained by considering all the material parameters in the calibration. Nevertheless, the improvement is very little to justify the excessive computation time of a global sensitivity analysis. Furthermore, looking at the frequency relative errors, it is observed that the natural frequencies of the first five modes featured by the updated model of the tower (NM19) show very low variations ( $\Delta f < 0.8\%$ ) regardless of the number of parameters considered in the calibration process (Table A. 9).

Table A. 9: Variation of calibrated frequencies of NM19 in relation to the number of parameters subdued to updating process.

Mode	All Parameters					S.I. = 1%		S.I. = 5%		S.I. = 10%	
	$f_{NM18}$ [Hz]	$f_{NM19_0}$ [Hz]	$f_{NM19}$ [Hz]	$ \Delta f_{NM18} $ [%]	$ \Delta f_{NM19_0} $ [%]	$f_{NM19}$ [Hz]	$ \Delta f_{NM18} $ [%]	$f_{NM19}$ [Hz]	$ \Delta f_{NM18} $ [%]	$f_{NM19}$ [Hz]	$ \Delta f_{NM18} $ [%]
$\varphi_1$	2.070	2.078	2.079	0.43	0.05	2.076	0.29	2.062	0.39	2.064	0.29
$\varphi_2$	2.111	2.121	2.123	0.57	0.09	2.121	0.47	2.109	0.09	2.110	0.05
$\varphi_3$	6.245	6.279	6.277	0.51	0.03	6.283	0.60	6.342	1.53	6.338	1.47
$\varphi_4$	6.693	6.693	6.645	0.72	0.72	6.647	0.69	6.671	0.33	6.674	0.28
$\varphi_5$	6.839	6.843	6.789	0.74	0.80	6.793	0.68	6.824	0.22	6.826	0.19

#### A.4. Sensitivity analyses for orthotropic material approach

Sensitivity analyses for orthotropic material approach were carried out with the same methodology applied for the isotropic model. The first order influence of the different material parameters on the global behaviour of the orthotropic model NM19, built again using NM18 as starting model, is shown in Figure A. 17. The results for the total order index are reported in Figure A. 18.

It is immediately observable how in the orthotropic model, even considering different thresholds of the SI, other parameters, such as mass density, give non negligible contributions to the model updating in comparison to the isotropic model, for which the most burdensome parameters resulted to be the Young's moduli. Overall, it is found again that the highest changes in the modal frequencies produced by a first order index are essentially associated to the materials Young's modulus of basement inner walls and central body as far as the first two vibration modes are concerned, whereas the torsion mode is particularly sensitive also to the variations of shear modulus, Poisson's coefficient and mass density of the different parts. Considering a total order index, the range of parameters influencing the natural frequencies of the different modes sensibly reduces, but as previously referred, such a reduction comes at a very high computational cost which is not required by the proposed GA-based model updating procedure.

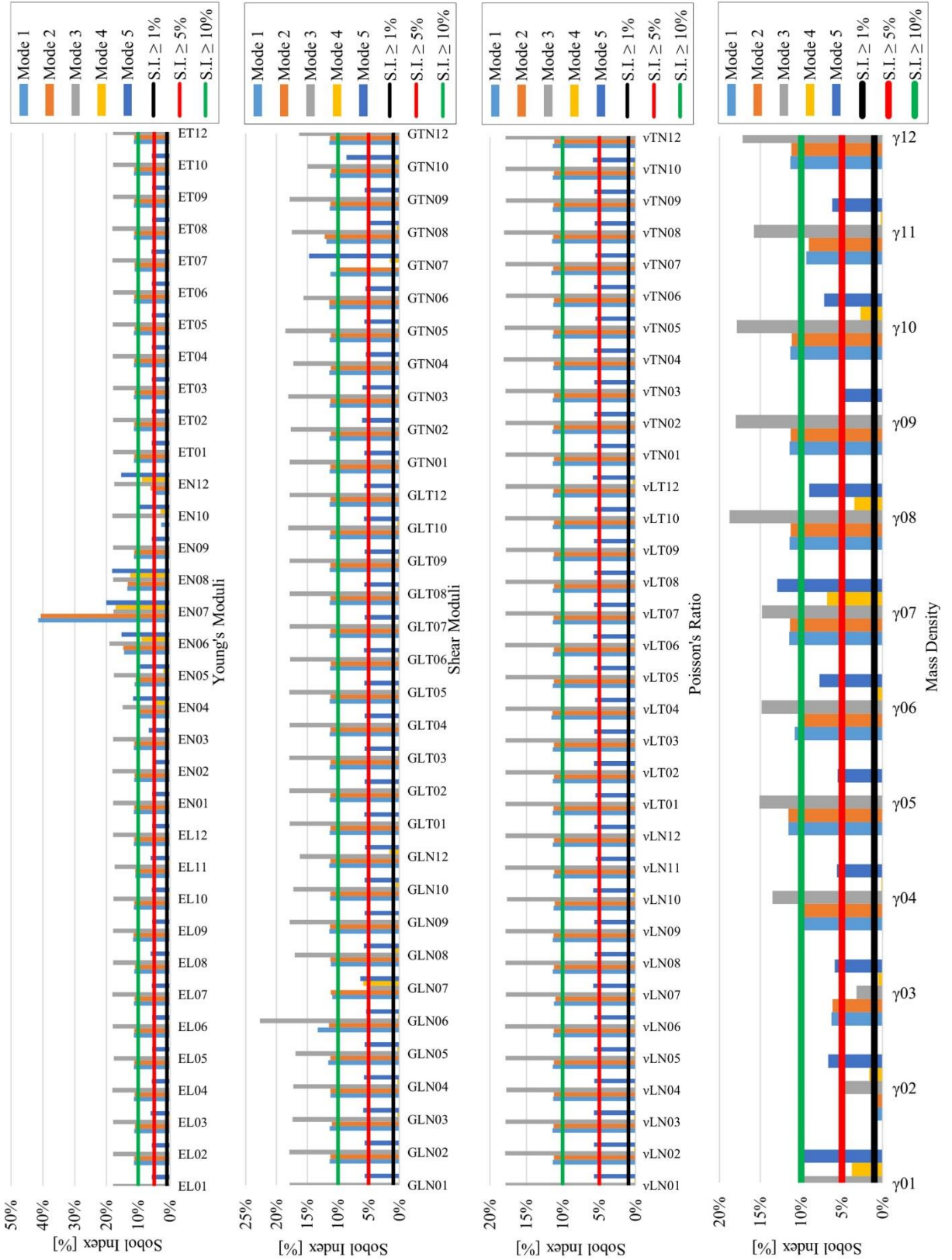


Figure A. 17: Sobol sensitivity analysis over first order indices for Kriging method. Thresholds of Sobol Indices (SI) respectively highlighted in black (SI=  $\pm$  1%), red (SI=  $\pm$  5%) and green (SI=  $\pm$  10%)



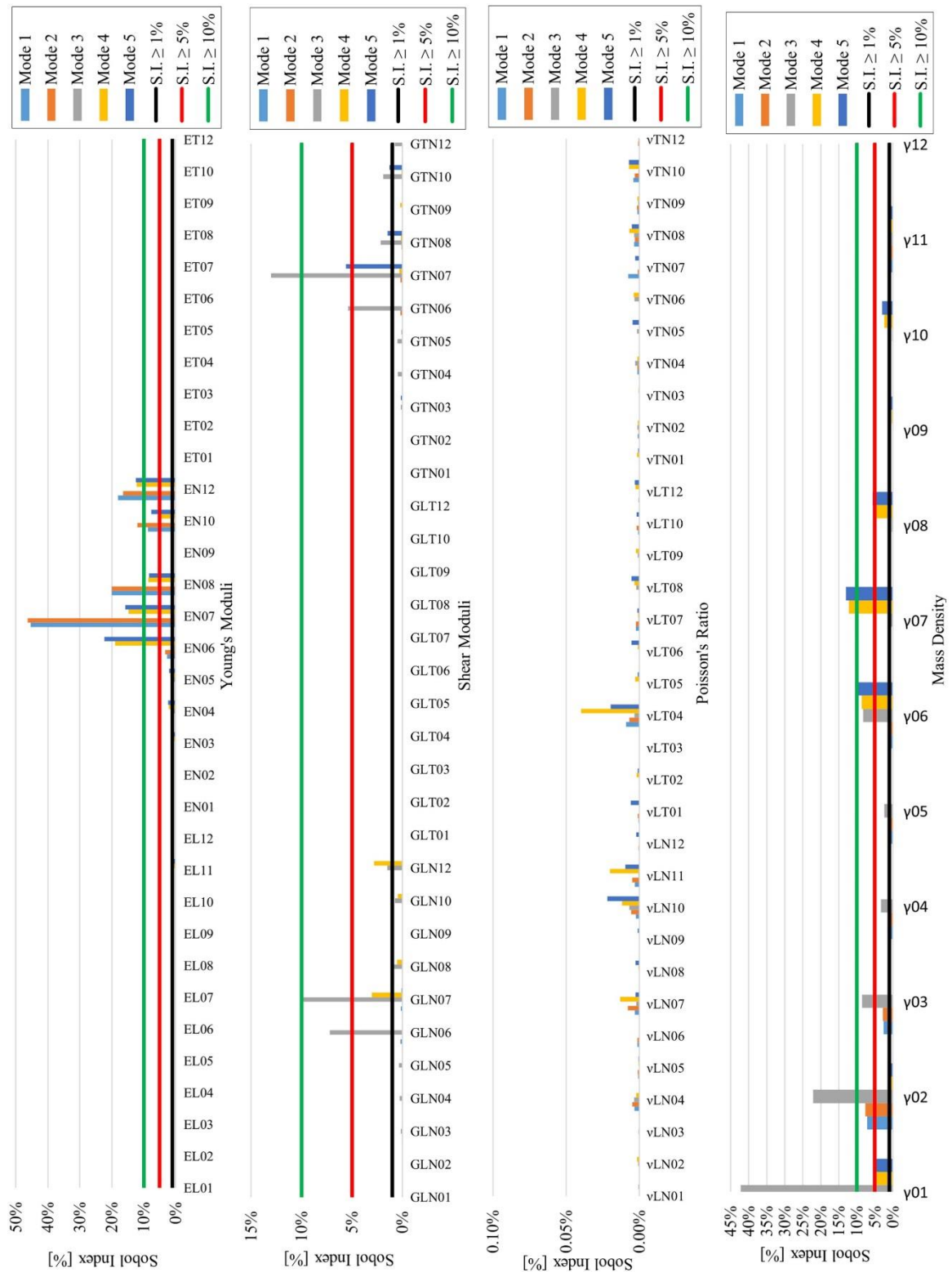


Figure A. 18: Sobol sensitivity analysis over total order indices for Kriging method. Thresholds of Sobol Indices (SI) respectively highlighted in black (SI= ± 1%), red (SI= ± 5%) and green (SI= ± 10%)

In light of the results obtained considering Total Order Sobol sensitivity analysis the following parameters were considered for calibration of NM19 with orthotropic material approach (Table A. 10):

Table A. 10: Material parameters considered for calibration of NM19 after Sobol sensitivity analysis, using orthotropic approach.

	<b>Orthotropic material parameters</b>	<b>Total</b>
<b>S.I. <math>\geq 1\%</math></b>	$E_{N04} - E_{N05} - E_{N06} - E_{N07} - E_{N08} - E_{N10} - E_{N12}$ $G_{LN06} - G_{LN07} - G_{LN08} - G_{LN12} - G_{TN06} - G_{TN07} - G_{TN08} - G_{TN10} - G_{TN12}$ $\gamma_{01} - \gamma_{02} - \gamma_{03} - \gamma_{04} - \gamma_{05} - \gamma_{06} - \gamma_{07} - \gamma_{08} - \gamma_{10} - \gamma_{11} - \gamma_{12}$	27
<b>S.I. <math>\geq 5\%</math></b>	$E_{N06} - E_{N07} - E_{N08} - E_{N10} - E_{N12}$ $G_{LN06} - G_{LN07} - G_{TN06} - G_{TN07}$ $\gamma_{01} - \gamma_{02} - \gamma_{06} - \gamma_{07} - \gamma_{08}$	14
<b>S.I. <math>\geq 10\%</math></b>	$E_{N06} - E_{N07} - E_{N08} - E_{N10} - E_{N12}$ $G_{LN07} - G_{TN07}$ $\gamma_{01} - \gamma_{02} - \gamma_{07}$	10

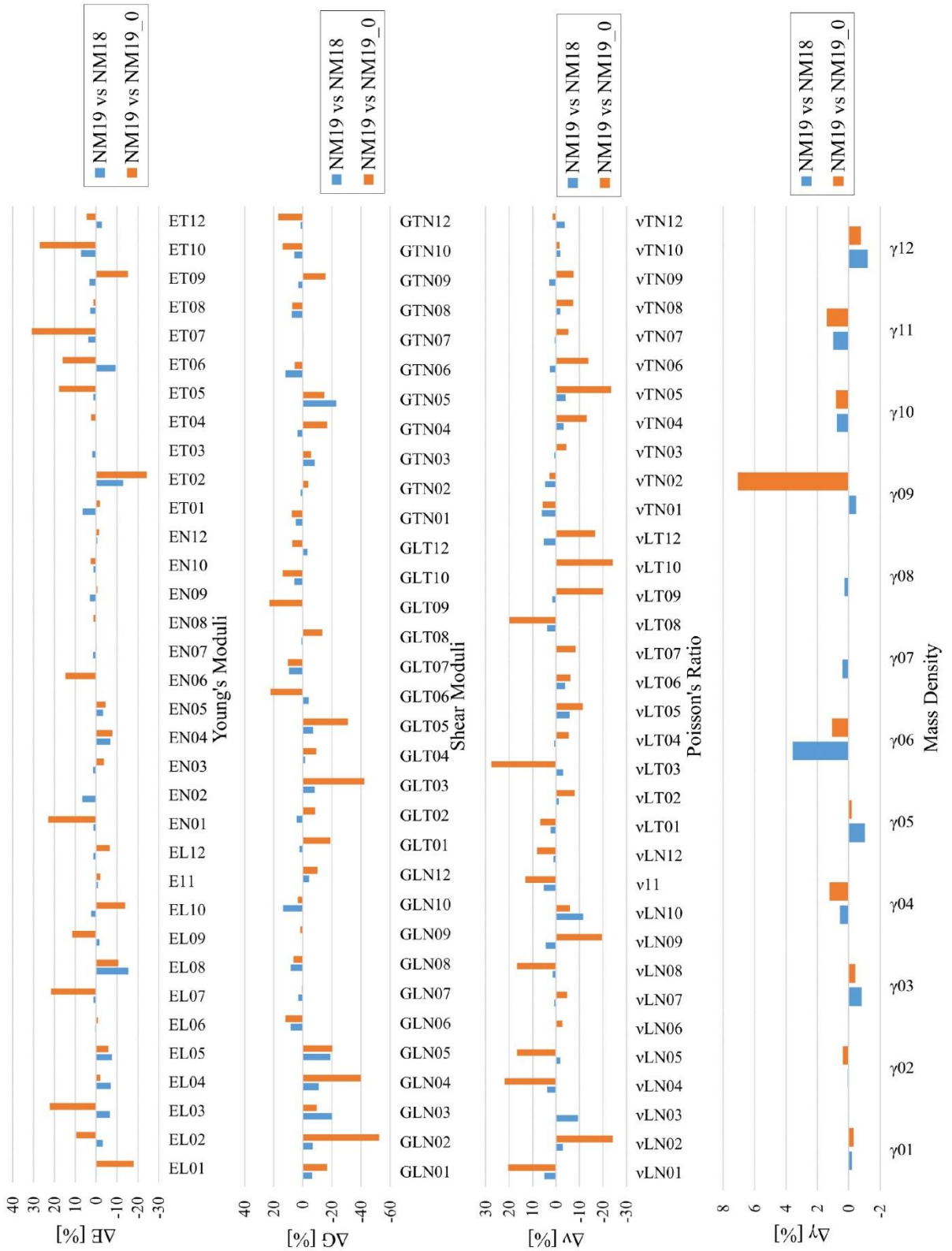


Figure A. 19: Variation of NM19 material parameters in comparison to NM18 (in blue) and NM19\_0 (in orange), considering all parameters in the calibration process.

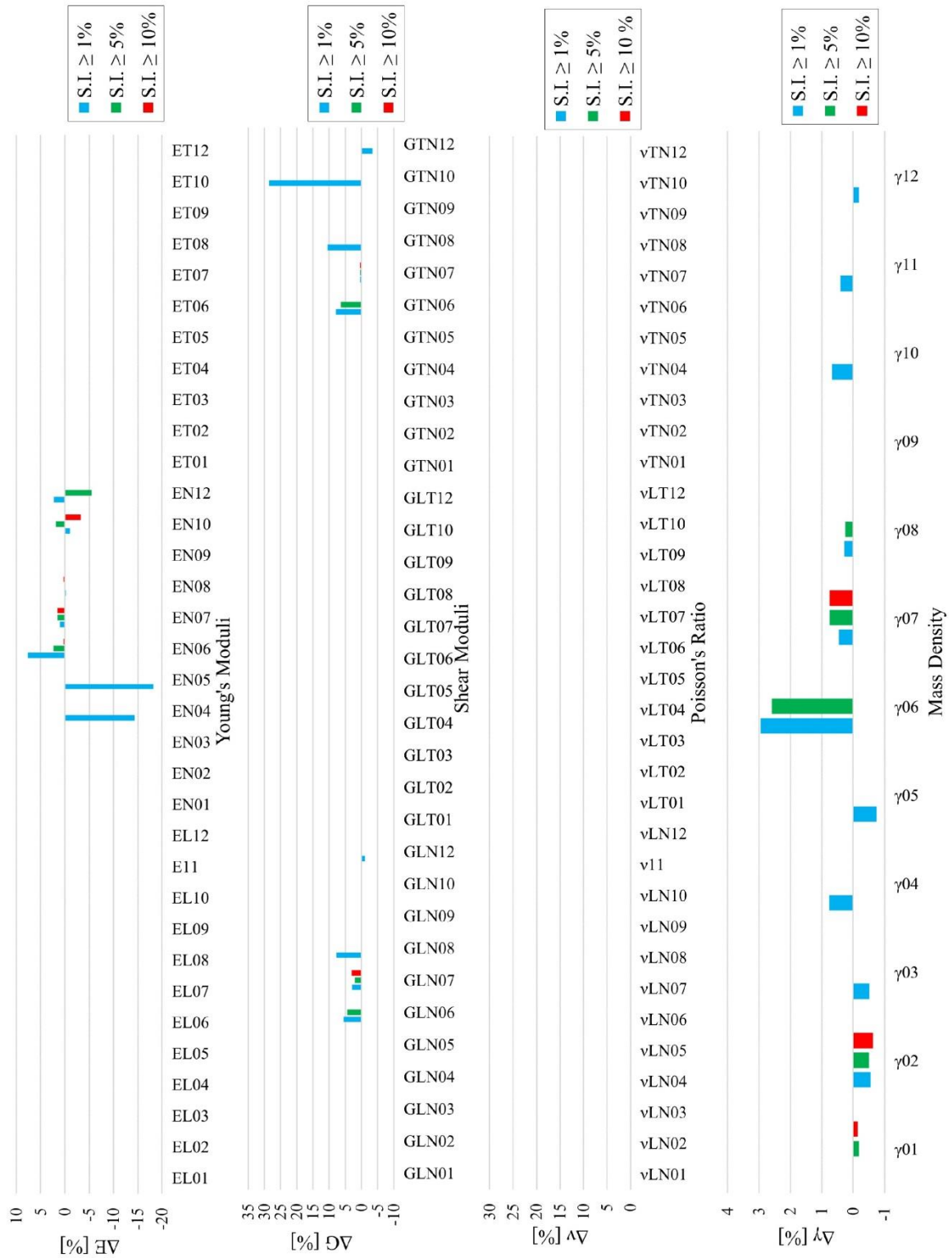


Figure A. 20: Variation of NM19 material parameters with respect to NM18 considering a reduced number of variables based on different thresholds of SI.

Comparing the final values of the material parameters of the updated model of 2019 (NM19) with those obtained from models NM18 and NM19\_0, both calibrated directly against experimental data, it is observed a better agreement between NM19 and NM18

(Figure A. 19). This allows to draw the same conclusions emerged for the isotropic counterparts, namely that updating with new information a refined baseline model previously calibrated not only is faster and less demanding from a computational viewpoint as compared to the construction and full updating of another metamodel from scratch, but also less prone to statistical variations from random error sources. Still, if weighing up the total percentage variation of the parameters with respect to the relevant isotropic models, the differences become larger due to the greater number of parameters involved in the updating process of the orthotropic models.

Lastly, the comparison between NM18 and NM19, both calibrated with a reduced number of parameters chosen on the basis of the sensitivity analyses previously described, shows a very marginal level of variation among the final materials variables, confirming the goodness of the sensitivity-based calibration process (Figure A. 20). Nevertheless, the very high computational cost required by the global sensitivity analysis with respect to the optimization procedure herein proposed cannot be overlooked. Moreover, analogously to the isotropic case, the frequency relative errors of the first five modes of the tower are always very low regardless of the number of updating parameters considered in the optimization (Table A. 11), thus no substantial improvement is found by reducing the unknown variables beforehand.

Table A. 11: Variation of calibrated frequencies of NM19 in relation to the number of parameters subdued to updating process.

Mode	All Parameters					S.I. = 1%		S.I. = 5%		S.I. = 10%	
	$f_{NM18}$ [Hz]	$f_{NM19\_0}$ [Hz]	$f_{NM19}$ [Hz]	$ \Delta f_{NM18} $ [%]	$ \Delta f_{NM19\_0} $ [%]	$f_{NM19}$ [Hz]	$ \Delta f_{NM18} $ [%]	$f_{NM19}$ [Hz]	$ \Delta f_{NM18} $ [%]	$f_{NM19}$ [Hz]	$ \Delta f_{NM18} $ [%]
$\varphi_1$	2.084	2.093	2.091	0.33	0.10	2.095	0.53	2.092	0.38	2.093	0.43
$\varphi_2$	2.137	2.134	2.143	0.28	0.42	2.143	0.28	2.141	0.19	2.139	0.09
$\varphi_3$	6.284	6.288	6.229	0.88	0.95	6.278	0.10	6.280	0.06	6.265	0.30
$\varphi_4$	6.516	6.532	6.510	0.09	0.34	6.488	0.43	6.495	0.32	6.508	0.12
$\varphi_5$	6.907	6.852	6.930	0.33	1.13	6.878	0.42	6.903	0.06	6.913	0.09

## A.5. Convergence criteria

This section summarizes the comparison among the convergence rates of the different optimization processes, namely the GA-based updating versus the Sobol method. The latter was carried out using the parameters reported in Table A. 8 and Table A. 10.

These rates are analyzed for both isotropic and orthotropic material approaches, considering the convergences of the models calibrated from zero (NM18 and NM19\_0) – i.e. directly targeting the corresponding EM results (see Figure A. 21, Figure A. 22, Figure A. 24, Figure A. 25) – and the convergence of the optimization process performed to update model NM18 with 2019 experimental information (indicated as EM19), see Figure A. 23 and Figure A. 26.

In order to ensure the stability of the global optimal solution, the processes have been repeated by increasing progressively the number of iterations. In the first run of the optimization procedure this number was set equal to 100, in the second run equal to 200, 500 for the third run and 2000 for the last calibration. Noticeable differences can be seen among the convergence rates of the various optimization procedures.

It must be noted that, in the plots, the number of iterations visible along the horizontal axis corresponds to the product between the total number of iterations previously listed and the generated sub-iterations. This happens because, as it was indicated in Section A.1, the number of sub-iterations that are calculated during one iteration are as many as the NB\_FILLS. Having this parameter defined as 6, the number of iterations multiplied by the number of sub-iterations gives the total number of operations reported in the figures of the convergence rates.

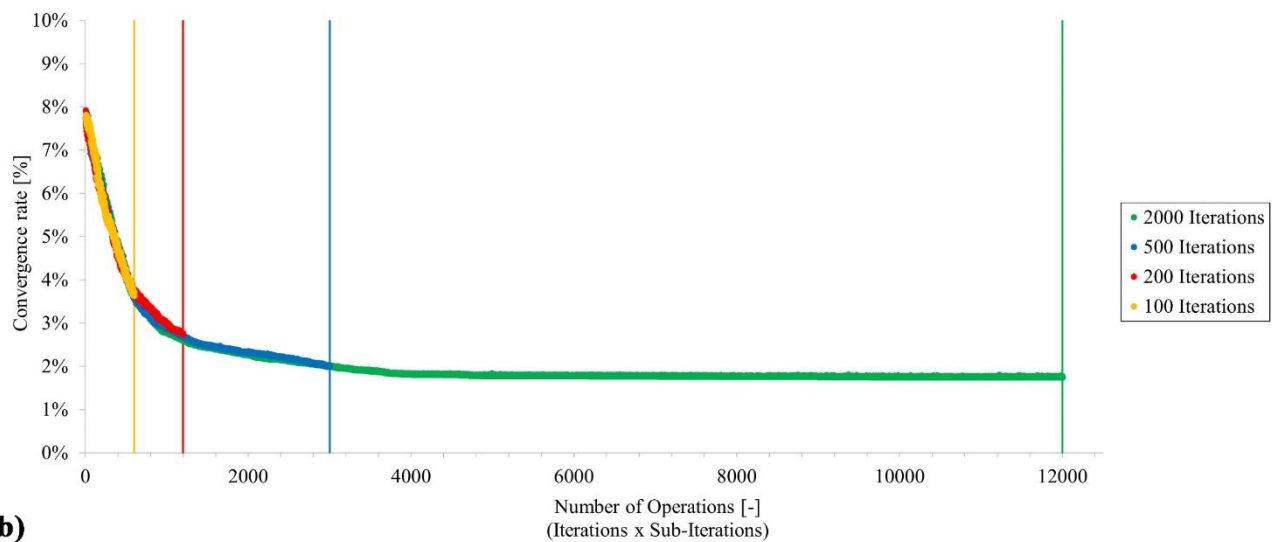
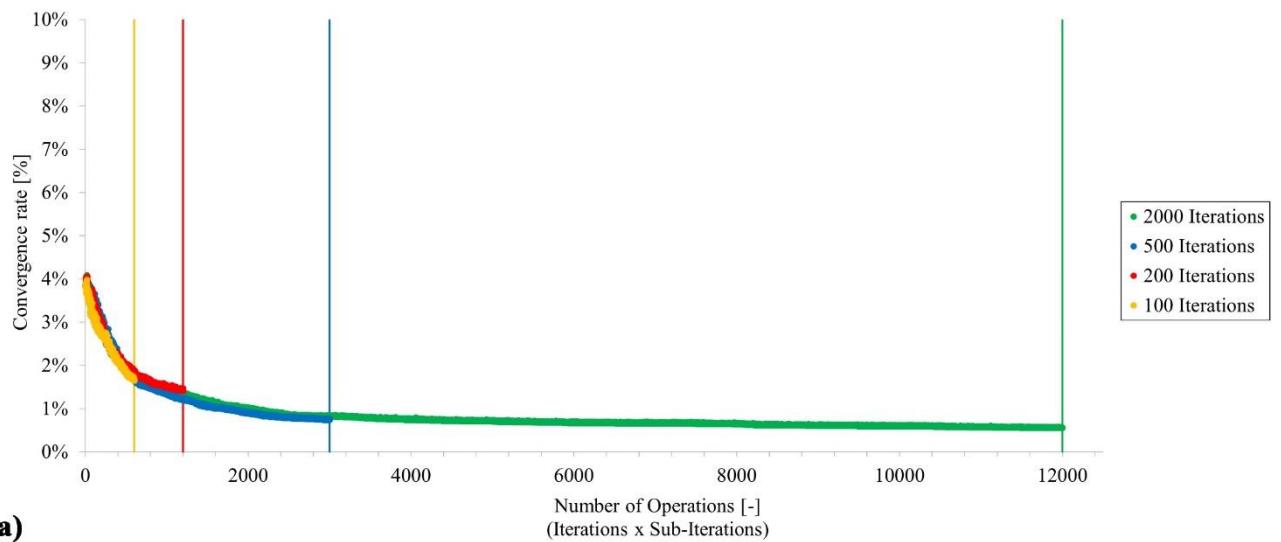


Figure A. 21: Influence of number of iterations on the convergence rate of NM2018 with isotropic material approach: calibration considering (a) all material parameters and (b) reduced number of parameters (based on thresholds fixed for  $S$ ).

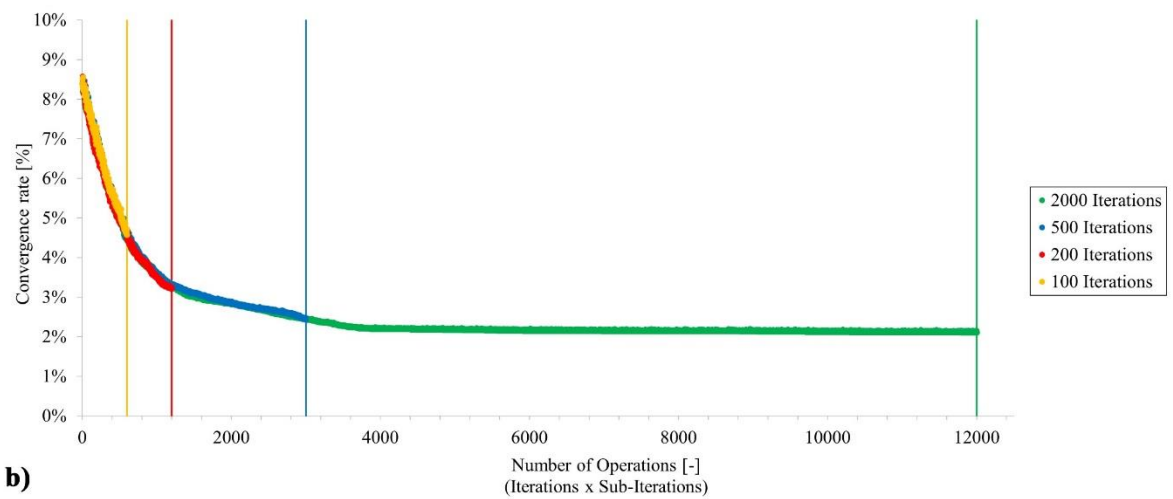
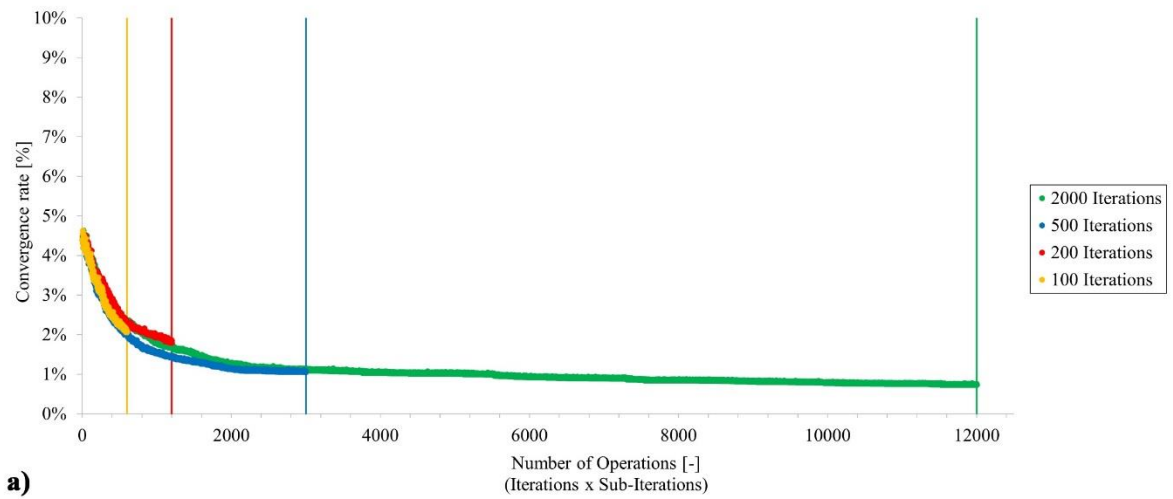


Figure A. 22: Influence of number of iterations on the convergence rate of NM2019\_0 with isotropic material approach: calibration considering (a) all material parameters and (b) reduced number of parameters (based on thresholds fixed for  $S_I$ ).

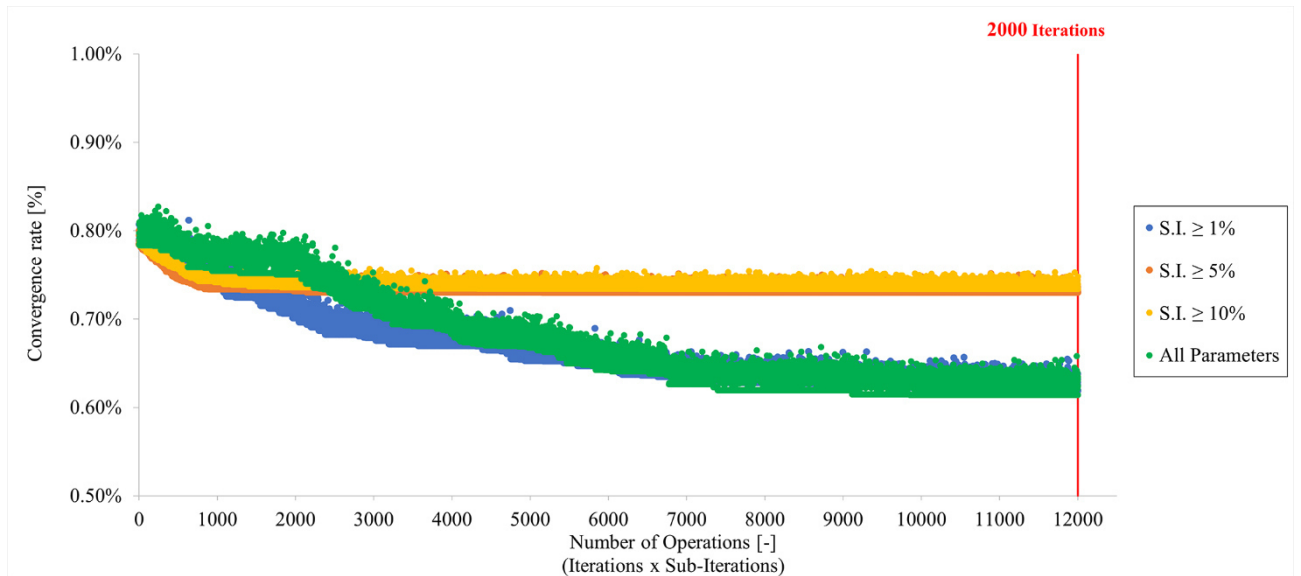


Figure A. 23: Comparison of convergence rate variations in the updating process of NM2019 isotropic model starting from NM2018 and using 2000 iterations: GA-based approach (green) versus Sobol method for different thresholds (blue, orange and yellow).



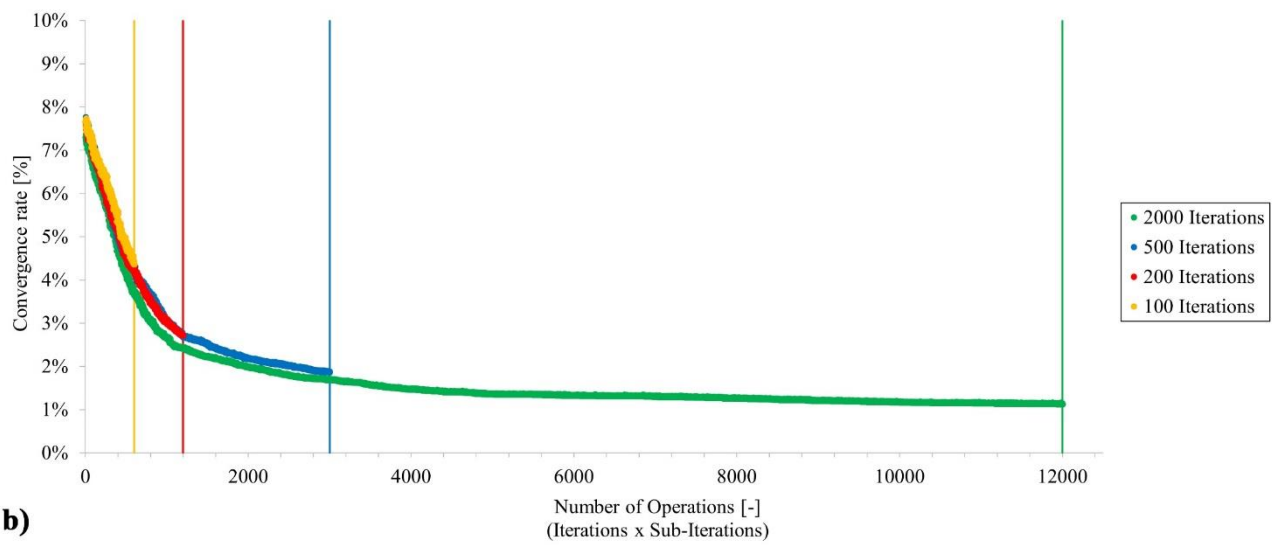
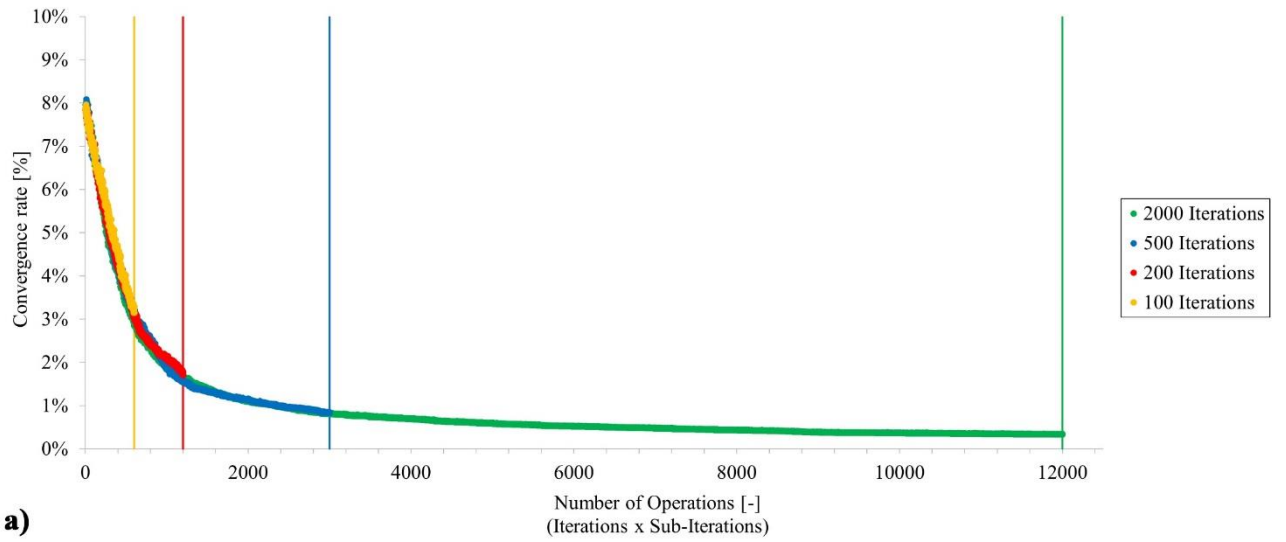


Figure A. 24: Influence of number of iterations on the convergence rate of NM2018 with orthotropic material approach: calibration considering (a) all material parameters and (b) reduced number of parameters (based on thresholds fixed for SI).

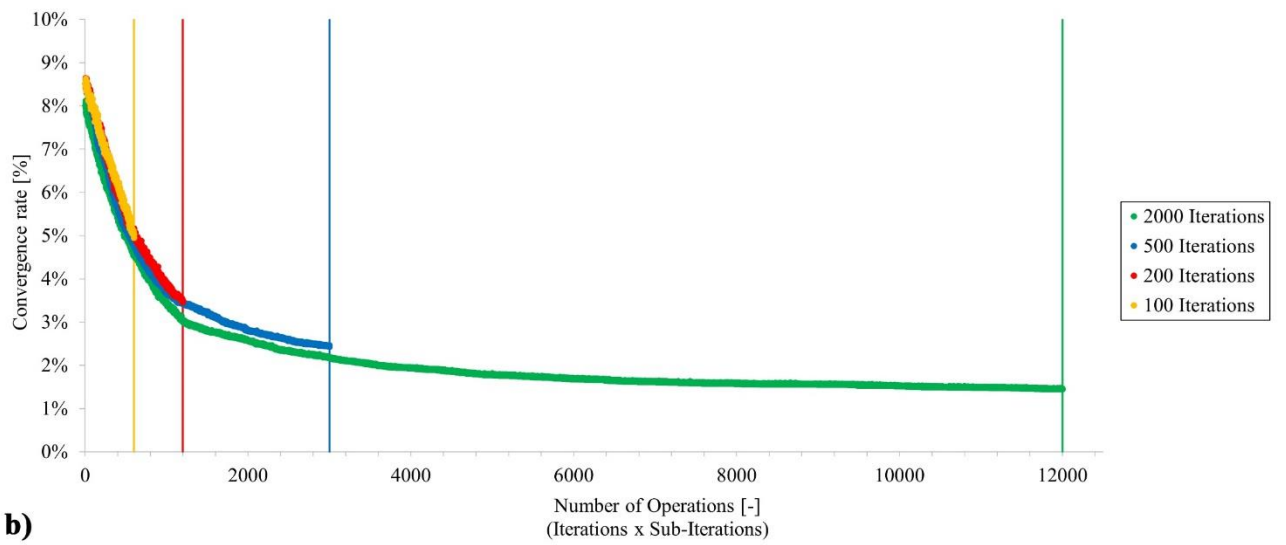
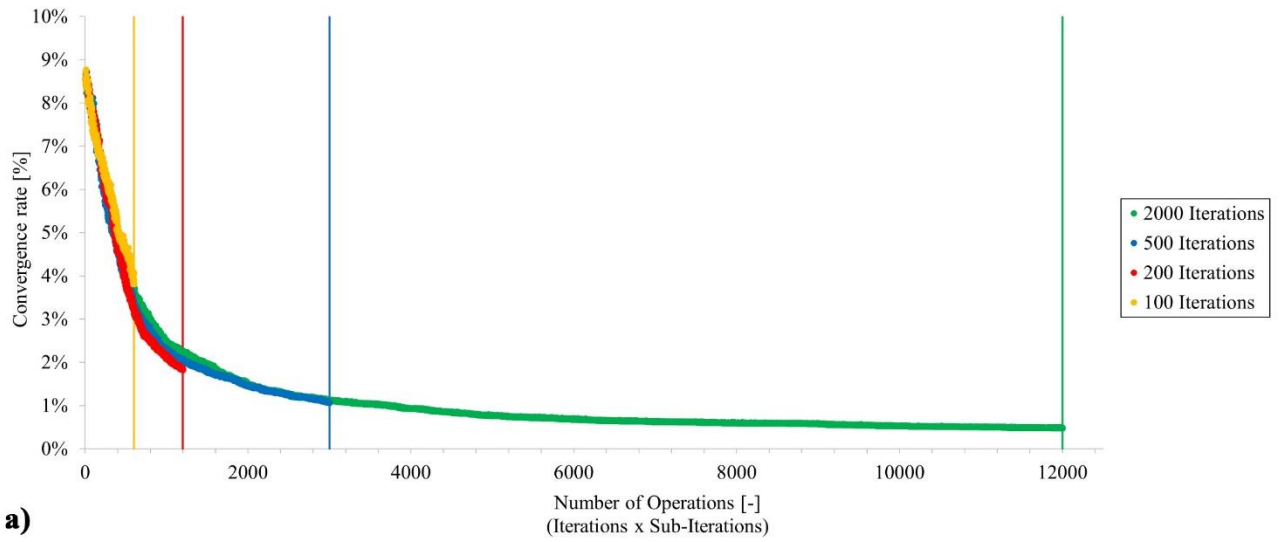


Figure A. 25: Influence of number of iterations on the convergence rate of NM2019\_0 with orthotropic material approach: calibration considering (a) all material parameters and (b) educed number of parameters (based on thresholds fixed for SI).

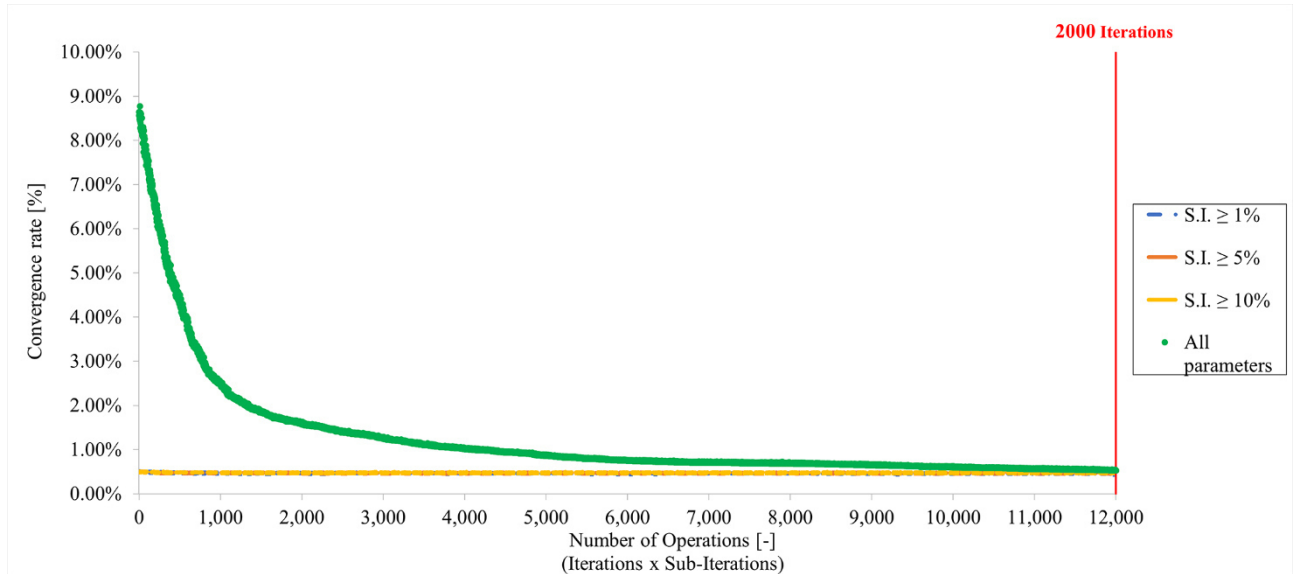


Figure A. 26: Comparison of convergence rate variations in the updating process of NM2019 orthotropic model starting from NM2018 and using 2000 iterations: GA-based approach (green) versus Sobol method for different thresholds (blue, orange and yellow).

Table A. 12, Table A. 13, Table A. 14, Table A. 15 summarize the frequency relative errors estimated for the five vibration modes of the tower as the number of iterations of the optimization process increases. As expected, the lowest errors are found with the highest number of iterations (2000), whose run is much more feasible, robust and remarkably less time-consuming using the proposed GA-based optimization approach.

Table A. 12: Variation of frequencies of calibrated NM2018 with isotropic approach in relation to different number of iterations.

Mode	100 Iterations			200 Iterations		500 Iterations		2000 Iterations	
	$f_{EM18}$ [Hz]	$f_{NM18}$ [Hz]	$ \Delta f_{EM18-NM18} $ [%]	$f_{NM18}$ [Hz]	$ \Delta f_{EM18-NM18} $ [%]	$f_{NM18}$ [Hz]	$ \Delta f_{EM18-NM18} $ [%]	$f_{NM18}$ [Hz]	$ \Delta f_{EM18-NM18} $ [%]
$\varphi_1$	2.082	1.987	4.56	2.014	3.27	2.062	0.96	2.070	0.58
$\varphi_2$	2.156	2.021	6.26	2.049	4.96	2.098	2.69	2.111	2.09
$\varphi_3$	6.293	6.326	0.52	6.379	1.37	6.281	0.19	6.280	0.21
$\varphi_4$	6.442	6.818	5.84	6.842	6.21	6.751	4.80	6.700	4.00
$\varphi_5$	6.941	7.000	0.85	7.022	1.17	6.901	0.58	6.850	1.31

Table A. 13: Variation of frequencies of calibrated NM2019\_0 with isotropic approach in relation to different number of iterations.

Mode	100 Iterations			200 Iterations		500 Iterations		2000 Iterations	
	$f_{EM19}$	$f_{NM19_0}$	$ \Delta f_{EM19-NM19_0} $	$f_{NM19_0}$	$ \Delta f_{EM19-NM19_0} $	$f_{NM19_0}$	$ \Delta f_{EM19-NM19_0} $	$f_{NM19_0}$	$ \Delta f_{EM19-NM19_0} $
	[Hz]	[Hz]	[%]	[Hz]	[%]	[Hz]	[%]	[Hz]	[%]
$\varphi_1$	2.092	1.989	4.92	2.011	3.87	2.057	1.67	2.078	0.67
$\varphi_2$	2.165	2.024	6.51	2.046	5.50	2.091	3.42	2.121	2.03
$\varphi_3$	6.302	6.352	0.79	6.345	0.68	6.287	0.24	6.279	0.36
$\varphi_4$	6.449	6.797	5.40	6.838	6.03	6.755	4.74	6.693	3.78
$\varphi_5$	6.872	6.976	1.51	7.021	2.17	6.908	0.52	6.843	0.42

Table A. 14: Variation of frequencies of calibrated NM2018 with orthotropic approach in relation to different number of iterations

Mode	100 Iterations			200 Iterations		500 Iterations		2000 Iterations	
	$f_{EM18}$	$f_{NM18}$	$ \Delta f_{EM18-NM18} $	$f_{NM18}$	$ \Delta f_{EM18-NM18} $	$f_{NM18}$	$ \Delta f_{EM18-NM18} $	$f_{NM18}$	$ \Delta f_{EM18-NM18} $
	[Hz]	[Hz]	[%]	[Hz]	[%]	[Hz]	[%]	[Hz]	[%]
$\varphi_1$	2.082	2.079	0.14	2.070	0.58	2.074	0.38	2.084	0.10
$\varphi_2$	2.156	2.123	1.53	2.115	1.90	2.119	1.72	2.137	0.88
$\varphi_3$	6.293	6.277	0.25	6.283	0.16	6.276	0.27	6.284	0.14
$\varphi_4$	6.442	6.645	3.15	6.645	3.15	6.647	3.18	6.516	1.15
$\varphi_5$	6.941	6.789	2.19	6.790	2.18	6.794	2.12	6.907	0.49

Table A. 15: Variation of frequencies of calibrated NM2019\_0 with orthotropic approach in relation to different number of iterations.

Mode	100 Iterations			200 Iterations		500 Iterations		2000 Iterations	
	$f_{EM19}$	$f_{NM19_0}$	$ \Delta f_{EM19-NM19_0} $	$f_{NM19_0}$	$ \Delta f_{EM19-NM19_0} $	$f_{NM19_0}$	$ \Delta f_{EM19-NM19_0} $	$f_{NM19_0}$	$ \Delta f_{EM19-NM19_0} $
	[Hz]	[Hz]	[%]	[Hz]	[%]	[Hz]	[%]	[Hz]	[%]
$\varphi_1$	2.092	2.079	0.62	2.070	1.05	2.074	0.86	2.093	0.05
$\varphi_2$	2.165	2.123	1.94	2.115	2.31	2.119	2.12	2.134	1.43
$\varphi_3$	6.302	6.277	0.40	6.283	0.30	6.276	0.41	6.288	0.22
$\varphi_4$	6.449	6.645	3.04	6.645	3.04	6.647	3.07	6.532	1.29
$\varphi_5$	6.872	6.789	1.21	6.790	1.19	6.794	1.14	6.852	0.29

## A.6 Example of an iterative “Trial and Error” calibration for the NM18

This example as was stated in the introduction of the Appendix serves the purpose of highlighting the difficulty that exists in managing elevated number of parameters without of the nature-inspired genetic algorithm even when the target values are known. The example considers initially all the parameters, then 1% and 10% of the parameters sensitive to the output, results taken from Sobols sensitivity analysis with the Kriging approach metamodel. The discretization remains the twelve-group discretization previously shown in Figure 22.

### A.6.1 Iterative approach without consideration of Sobol’s Indexes

Table A. 16: Frequency values and relative error against the identified experimental values of the EM2018 for the iterative approach with all the parameters, not considering Sobols indexes.

Mode	$f_{EM18}$ [Hz]	It 1 [Hz]	$[f_{EM18} - It1]$ [%]	It 2 [Hz]	$[f_{EM18} - It2]$ [%]	It 3 [Hz]	$[f_{EM18} - It3]$ [%]	It 4 [Hz]	$[f_{EM18} - It4]$ [%]	It 5 [Hz]	$[f_{EM18} - It5]$ [%]
$\phi 1$	2.082	0.978	53.03	2.127	2.16	1.741	16.38	1.731	16.86	1.867	10.33
$\phi 2$	2.156	0.993	53.94	2.166	0.46	1.771	17.86	1.757	18.51	1.902	11.78
$\phi 3$	6.293	3.205	49.07	6.962	10.63	5.595	11.09	5.204	17.30	5.506	12.51
$\phi 4$	6.442	3.688	42.75	7.825	21.47	6.382	0.93	6.141	4.67	6.439	0.05
$\phi 5$	6.941	3.777	45.58	8.055	16.05	6.561	5.47	6.731	3.03	6.572	5.32

Table A. 17: Parameter values not considering Sobols indexes. The Poissons ration and mass density where not perturbed during the analysis to see how much effect the Youngs modulus has on the results.

Updating parameter	E [MPa]					v [-]	$\gamma$ [kN/m <sup>3</sup> ]
	It1	It2	It3	It4	It5	It1*	It1*
$X_{01M}$	600	3000	2000	2000	2000	0.2	18
$X_{02M}$	600	3000	2000	2000	2000	0.2	18
$X_{03M}$	600	3000	1500	1000	1000	0.2	18
$X_{04M}$	600	3000	1500	1000	1000	0.2	18
$X_{05M}$	600	3000	2000	1000	1000	0.2	18
$X_{06M}$	600	3000	2000	2000	2500	0.2	18
$X_{07M}$	600	3000	2000	2100	3000	0.2	18
$X_{08F}$	600	3000	2000	2100	2100	0.2	18
$X_{09M}$	600	3000	2000	2000	2000	0.2	18
$X_{10M}$	600	3000	2000	2000	3000	0.2	18
$X_{11C}$	28000	28000	28000	28000	28000	0.3	24
$X_{12F}$	600	3000	2000	2000	1500	0.2	18

## A.6.2 Iterative approach considering 1% of Sobol's Indexes

Table A. 18: Frequency values and relative error against the identified experimental values of the EM2018 for the iterative approach considering 1% of Sobols indexes.

Mode	$f_{EM18}$	It 1	$[\frac{f_{EM18} - It1}{It1}]$	It 2	$[\frac{f_{EM18} - It2}{It2}]$	It 3	$[\frac{f_{EM18} - It3}{It3}]$	It 4	$[\frac{f_{EM18} - It4}{It4}]$	It 5	$[\frac{f_{EM18} - It5}{It5}]$
	[Hz]	[Hz]	[%]	[Hz]	[%]	[Hz]	[%]	[Hz]	[%]	[Hz]	[%]
$\phi 1$	2.082	0.976	53.12	2.164	3.940	1.612	22.57	1.954	6.15	1.986	4.61
$\phi 2$	2.156	1.101	48.93	2.203	2.180	1.642	23.84	1.99	7.70	2.019	6.35
$\phi 3$	6.293	3.285	47.80	7.066	12.28	4.754	24.46	5.733	8.90	5.719	9.12
$\phi 4$	6.442	3.79	41.17	7.956	23.50	5.698	11.55	6.544	1.58	6.54	1.52
$\phi 5$	6.941	3.885	44.03	8.184	17.91	5.814	16.24	6.673	3.86	6.66	4.05

Table A. 19: Parameter values considering 1% of Sobols indexes. The highlighted values in red show the parameter values that remained fixed during each simulation. The highlighted values in yellow show the parameters that could be changed in each simulation.

Updating parameter	E [MPa]					$\nu$ [-]	$\gamma$ [kN/m <sup>3</sup> ]				
	It1	It2	It3	It4	It5		It1*	It1	It2	It3	It4
$X_{01M}$	2000	2000	2000	2000	2000	0.2	17	17	17	16	15
$X_{02M}$	2000	2000	2000	2000	2000	0.2	17	17	17	16	15
$X_{03M}$	600	3000	1000	1000	1000	0.2	18	18	18	18	18
$X_{04M}$	600	3000	1000	1000	1000	0.2	18	18	18	18	18
$X_{05M}$	600	3000	1000	1000	1000	0.2	18	18	18	18	18
$X_{06M}$	600	3000	1000	1000	2000	0.2	17	17	17	18.5	19
$X_{07M}$	600	3000	2500	3000	3200	0.2	17	17	17	18.5	19
$X_{08F}$	600	3000	1000	3000	3000	0.2	17	17	17	19	19
$X_{09M}$	2000	2000	2000	2000	2000	0.2	18	18	18	18	18
$X_{10M}$	600	3000	2500	3000	3000	0.2	18	18	18	18	18
$X_{11C}$	28000	28000	28000	28000	28000	0.3	24	24	24	24	24
$X_{12F}$	600	3000	1500	1600	1700	0.2	18	18	18	18	18

## A.6.3 Iterative approach considering 10% of Sobol's Indexes

Table A. 20:: Frequency values and relative error against the identified experimental values of the EM2018 for the iterative approach considering 10% of Sobols indexes.

Mode	$f_{EM18}$	It 1	$[\frac{f_{EM18} - It1}{It1}]$	It 2	$[\frac{f_{EM18} - It2}{It2}]$	It 3	$[\frac{f_{EM18} - It3}{It3}]$	It 4	$[\frac{f_{EM18} - It4}{It4}]$	It 5	$[\frac{f_{EM18} - It5}{It5}]$
	[Hz]	[Hz]	[%]	[Hz]	[%]	[Hz]	[%]	[Hz]	[%]	[Hz]	[%]
$\phi 1$	2.082	0.967	53.55	2.1	0.86	1.935	7.06	1.988	4.51	2.021	2.93
$\phi 2$	2.156	1.015	52.92	2.136	0.93	1.969	8.67	2.021	6.26	2.055	4.68
$\phi 3$	6.293	3.491	44.53	6.57	4.40	6.185	1.72	6.335	0.67	6.396	1.64
$\phi 4$	6.442	3.900	39.46	7.545	17.12	7.051	9.45	7.233	12.28	7.316	13.57
$\phi 5$	6.941	4.031	41.92	7.738	11.48	7.242	4.34	7.428	7.02	7.509	8.18

Table A. 21: Parameter values considering 10% of Sobols indexes. The highlighted values in red show the parameter values that remained fixed during each simulation. The highlighted values in yellow show the parameters that could be changed in each simulation.

Updating parameter	E [MPa]					v[-]	$\gamma$ [kN/m <sup>3</sup> ]
	It1	It2	It3	It4	It5		
X <sub>01M</sub>	2000	2000	2000	2000	2000	0.2	18
X <sub>02M</sub>	2000	2000	2000	2000	2000	0.2	18
X <sub>03M</sub>	2000	2000	2000	2000	2000	0.2	18
X <sub>04M</sub>	2000	2000	2000	2000	2000	0.2	18
X <sub>05M</sub>	2000	2000	2000	2000	2000	0.2	18
X <sub>06M</sub>	600	3000	2500	2800	2800	0.2	18
X <sub>07M</sub>	600	3000	2500	2500	2700	0.2	18
X <sub>08F</sub>	600	3000	2500	2800	2800	0.2	18
X <sub>09M</sub>	2000	2000	2000	2000	2000	0.2	18
X <sub>10M</sub>	600	3000	2500	2500	2700	0.2	18
X <sub>11C</sub>	28000	28000	28000	28000	28000	0.3	24
X <sub>12F</sub>	600	3000	2500	2500	2800	0.2	18

The first example, shown in A.6.1, considered a non-sensitivity approach with all the parameters of the isotropic behavioral model present for the calibration. For the example five steps of calibration were performed and the results show that perturbing the Young's modulus between the extremes changes significantly the frequency values as can be seen in Table A. 16. The first iteration performed considered the lower bounds range of the elastic modulus taken from the Italian Technical Standards for construction. The properties regarding the discretization of the cement floors along with the Poisson's modulus and mass density remained unchanged. The second iteration considered the upper bound of the ranges taken from the Italian Standards. The perturbation of the frequency results indicates a closer correlation with the upper bounds instead of the lower bounds with the 3<sup>rd</sup>, 4<sup>th</sup> and 5<sup>th</sup> frequency values remaining over the error of 10%. The third iteration closed the gap between the values of the 3<sup>rd</sup> and 4<sup>th</sup> frequency but lost the correlation between the first three. In the fourth and fifth iterations, the correlation becomes clearer with the last reducing the error in a homogeneous way for the entirety of the results. The example in conclusion didn't perturbate the concrete, Poisson's ratio and mass densities. Without the updating of all the parameters it was not possible to achieve a reduced error even knowing the target values resulting from the automatic calibration with the genetic algorithm.

The second attempt shown in A.6.2 considered a reduced number of parameters. The number of parameters to apply was taken from Sobol's sensitivity analysis and applied 1% of the parameters sensitive to the output results. The concentration of sensitivity indicates that the upper masonry part of the model is most sensitive to the output

results. In particular the properties regarding Youngs modulus and mass densities. Poissons ratio and concrete seem to produce low values of sensitivity, considering 1% of the sensitivity indexes. The same scheme was followed for the iterations, the first iteration considered the lower bounds and the second iteration the upper bounds of the Italian Technical Standards for construction and maintained all the non-sensitive properties at 2000 Mpa for Youngs Modulus, 0.2/0.3 for Poissons ratio regarding the masonry and concrete and 18/25 Kg/m<sup>3</sup> for the mass density of the masonry and concrete. The error values descent on each iteration from 40% in the first iteration to 20% in the second iteration. In those iterations, due to the reduced number of parameters it was possible to mildly adjust also the mass density properties which the analysis indicated as sensible properties for the simulations. During the 3<sup>rd</sup>,4<sup>th</sup> and 5<sup>th</sup> iterations the error decreases to the point where results better than the previous approach with values lower than 10%. This example showed that considerations of all the possible parameters must be made because updating not only the sensitive Youngs Modulus but also the mass density properties of the model produces higher accuracy in the results.

The last examples data is shown in A.6.3 where 10% of the parameters sensitive to the output results were considered. In respect to the two previous examples, this considers a very reduced number of sensitive properties which do not take in consideration the mass density and poisons ratio. The properties in correlation to the twelve-part discretization show the middle part of the structure to be the most sensitive (Figure 22). Each iteration shows declination of the error between the experimental and numerical results. It is important to notice that even when these reduced properties are close to the target values (reported in Table 10), they miss the accuracy that can be produced with the automatic updating and result in higher error values.

These examples show the difficulty to approach a model update manually even when sensitive indexes are applied. The accuracy of the material properties values for the isotropic behavioral model can be missed due to the elevated number of parameters (36 for the approach in A.6.1, 13 for the approach in A.6.2 and 5 for the approach in A.6.3) and the interactions they have with each other. The same procedure was not applied for the orthotropic behavioral model where the maximum number of parameters is 113 because a manual approach is not applicable due to the sensitive interaction each component of the behavioral model has on the results and can indicates a heavily time-consuming operation.

The “trial and error” approach shows its limitations in terms of accuracy and value management, drawbacks which can be overcome with the application of automated methods which consider large number of parameters. The accuracy is important also due to the Non-Destructive nature of the technique which allows to make further considerations for linear or non-linear simulations when necessary, with a stable base-model. The discretization of the model and the precision of the values concerning the internal morphology can be a great asset to the scope of damage identification, localization and quantification while searching automatically for the global optimum of the problem.



## References

- [1] E. Bassoli, L. Vincenzi, M. Bovo, and C. Mazzotti, "Dynamic identification of an ancient masonry bell tower using a MEMS-based acquisition system," *2015 IEEE Work. Environ. Energy, Struct. Monit. Syst. EESMS 2015 - Proc.*, no. July, pp. 226–231, 2015.
- [2] F. J. Pallarés, M. Betti, G. Bartoli, and L. Pallarés, "Structural health monitoring (SHM) and Nondestructive testing (NDT) of slender masonry structures: A practical review," *Constr. Build. Mater.*, vol. 297, 2021.
- [3] P. B. Lourenco, P. Amado Mendes, L. F. Ramos, A. Barontini, and M. G. Masciotta, "An Overview on Structural Health Monitoring: From the Current State-of-the-Art to New Bio-inspired Sensing Paradigms," *Int. J. Bio-Inspired Comput.*, vol. 1, no. 1, p. 1, 2018.
- [4] J. J. Moughty and J. R. Casas, "A state of the art review of modal-based damage detection in bridges: Development, challenges, and solutions," *Appl. Sci.*, vol. 7, no. 5, 2017.
- [5] O. Avci, O. Abdeljaber, S. Kiranyaz, M. Hussein, M. Gabbouj, and D. J. Inman, "A Review of Vibration-Based Damage Detection in Civil Structures: From Traditional Methods to Machine Learning and Deep Learning Applications," *Mech. Syst. Signal Process.*, vol. 147, no. January, p. 107077, 2020.
- [6] D. A. Tibaduiza Burgos, R. C. Gomez Vargas, C. Pedraza, D. Agis, and F. Pozo, *Damage identification in structural health monitoring: A brief review from its implementation to the use of data-driven applications*, vol. 20, no. 3. 2020.
- [7] T. R. Fasel, S. W. Gregg, T. J. Johnson, C. Farrar, and H. Sohn, "Experimental modal analysis and damage detection in a simulated three story building," *Proc. SPIE - Int. Soc. Opt. Eng.*, vol. 4753 I, 2002.
- [8] K. Worden, C. R. Farrar, G. Manson, and G. Park, "The fundamental axioms of structural health monitoring," *Proc. R. Soc. A Math. Phys. Eng. Sci.*, vol. 463, no. 2082, pp. 1639–1664, 2007.
- [9] F. Graziotti, G. Magenes, and A. Penna, "Experimental campaign on double-leaf stone masonry specimens at the University of Pavia," *Exp. Res. Seism. Behav. Mason. spandrels an Int. Perspect.*, no. July, pp. 5–46, 2016.
- [10] F. Micelli and A. Cascardi, "Structural assessment and seismic analysis of a 14th century masonry tower," *Eng. Fail. Anal.*, vol. 107, no. October, p. 104198, 2020.
- [11] A. Cabboi, C. Gentile, and A. Saisi, "From continuous vibration monitoring to FEM-based damage assessment: Application on a stone-masonry tower," *Constr. Build. Mater.*, vol. 156, pp. 252–265, 2017.
- [12] A. Saisi, C. Gentile, and A. Ruccolo, "Static and dynamic monitoring of a Cultural Heritage bell-tower in Monza, Italy," *Procedia Eng.*, vol. 199, pp. 3356–3361, 2017.
- [13] F. Clementi, A. Ferrante, E. Giordano, F. Dubois, and S. Lenci, "Damage assessment of ancient masonry churches stroked by the Central Italy earthquakes of 2016 by the non-smooth contact dynamics method," *Bull. Earthq. Eng.*, vol. 18, no. 2, pp. 455–486, Jan. 2020.
- [14] L. F. Ramos, G. De Roeck, P. B. Lourenço, and A. Campos-Costa, "Damage identification on arched masonry structures using ambient and random impact vibrations," *Eng. Struct.*, vol. 32, no. 1, pp. 146–162, 2010.

- [15] F. Clementi, S. Lenci, and T. Sadowski, "Fracture characteristics of unfired earth," *Int. J. Fract.*, vol. 149, no. 2, pp. 193–198, 2008.
- [16] G. Brando *et al.*, "Structural Survey and Empirical Seismic Vulnerability Assessment of Dwellings in the Historical Centre of Cusco, Peru," *Int. J. Archit. Herit.*, vol. 00, no. 00, pp. 1–29, 2019.
- [17] M. Azimi, A. D. Eslamlou, and G. Pekcan, *Data-driven structural health monitoring and damage detection through deep learning: State-of-the-art review*, vol. 20, no. 10. 2020.
- [18] D. Bui-Ngoc, T. Bui-Tien, H. Nguyen-Tran, M. Abdel Wahab, and G. De Roeck, "Structural health monitoring using handcrafted features and convolution neural network," *Lect. Notes Civ. Eng.*, vol. 110, no. January, pp. 103–112, 2021.
- [19] A. Kita, N. Cavalagli, M. Giovanna, P. B. Lourenço, and F. Ubertini, "Rapid post-earthquake damage localization and quantification in masonry structures through multidimensional non-linear seismic IDA," *Eng. Struct.*, vol. 219, no. April, p. 110841, 2020.
- [20] I. Trizio, A. Marra, F. Savini, and G. Fabbrocino, "SURVEY METHODOLOGIES AND 3D MODELLING FOR CONSERVATION OF HISTORICAL MASONRY BRIDGES," vol. VIII, no. September, pp. 163–170, 2021.
- [21] P. G. Asteris *et al.*, "Masonry compressive strength prediction using artificial neural networks," *Commun. Comput. Inf. Sci.*, vol. 962, pp. 200–224, 2019.
- [22] A. Gouda Mohamed and M. Marzouk, "Building condition assessment using artificial neural network and structural equations," *Expert Syst. Appl.*, vol. 186, no. May, p. 115743, 2021.
- [23] C. Gentile, M. Guidobaldi, and A. Saisi, "One-year dynamic monitoring of a historic tower: damage detection under changing environment," *Meccanica*, vol. 51, no. 11, pp. 2873–2889, Nov. 2016.
- [24] E. García-Macías and F. Ubertini, "Automated operational modal analysis and ambient noise deconvolution interferometry for the full structural identification of historic towers: A case study of the Sciri Tower in Perugia, Italy," *Eng. Struct.*, vol. 215, no. May, p. 110615, 2020.
- [25] C. NEVES, *Structural Health Monitoring of Bridges: Data-based damage detection method using Machine Learning*, no. October. 2020.
- [26] M. O'Shea and J. Murphy, "Design of a BIM integrated structural health monitoring system for a historic offshore lighthouse," *Buildings*, vol. 10, no. 7, 2020.
- [27] Y. Ying *et al.*, "Toward data-driven structural health monitoring: Application of machine learning and signal processing to damage detection," *J. Comput. Civ. Eng.*, vol. 27, no. 6, pp. 667–680, 2013.
- [28] A. Entezami, H. Sarmadi, and S. Mariani, "An Unsupervised Learning Approach for Early Damage Detection by Time Series Analysis and Deep Neural Network to Deal with Output-Only (Big) Data," *Eng. Proc.*, vol. 2, no. 1, p. 17, 2020.
- [29] S. Das, P. Saha, and S. K. Patro, "Vibration-based damage detection techniques used for health monitoring of structures: a review," *J. Civ. Struct. Heal. Monit.*, vol. 6, no. 3, pp. 477–507, 2016.
- [30] F. Benedettini and C. Gentile, "Operational modal testing and FE model tuning of a cable-stayed bridge," *Eng. Struct.*, vol. 33, no. 6, pp. 2063–2073, 2011.

- [31] E. García-macías and F. Ubertini, “MOVA / MOSS : Two integrated software solutions for comprehensive Structural Health Monitoring of structures,” vol. 143, pp. 1–26, 2020.
- [32] G. Capellari, E. Chatzi, S. Mariani, and S. E. Azam, “Optimal design of sensor networks for damage detection,” *Procedia Eng.*, vol. 199, pp. 1864–1869, 2017.
- [33] S. Cantero-Chinchilla, J. L. Beck, M. Chiachío, J. Chiachío, D. Chronopoulos, and A. Jones, “Optimal sensor and actuator placement for structural health monitoring via an efficient convex cost-benefit optimization,” *Mech. Syst. Signal Process.*, vol. 144, p. 106901, 2020.
- [34] T. Ercan and C. Papadimitriou, “Optimal sensor placement for reliable virtual sensing using modal expansion and information theory,” *Sensors*, vol. 21, no. 10, 2021.
- [35] G. Standoli, E. Giordano, G. Milani, and F. Clementi, “Model Updating of Historical Belfries Based on Oma Identification Techniques,” *Int. J. Archit. Herit.*, vol. 00, no. 00, pp. 1–25, 2020.
- [36] A. Pierdicca, F. Clementi, A. Fortunati, and S. Lenci, “Tracking modal parameters evolution of a school building during retrofitting works,” *Bull. Earthq. Eng.*, vol. 17, no. 2, pp. 1029–1052, 2019.
- [37] N. Cavalagli, C. Pepi, M. Gioffré, V. Gusella, and F. Ubertini, “Surrogate models for earthquake-induced damage detection and localization in historic structures using long-term dynamic monitoring data: Application to a masonry dome,” *COMPdyn Proc.*, vol. 1, pp. 1329–1343, 2019.
- [38] W. H. Hu, C. Moutinho, E. Caetano, F. Magalhes, and L. Cunha, “Continuous dynamic monitoring of a lively footbridge for serviceability assessment and damage detection,” *Mech. Syst. Signal Process.*, vol. 33, pp. 38–55, 2012.
- [39] R. R. Chowdhury, M. A. Adnan, and R. K. Gupta, “Real time principal component analysis,” *Proc. - Int. Conf. Data Eng.*, vol. 2019-April, no. April, pp. 1678–1681, 2019.
- [40] G. Bartoli, M. Betti, L. Facchini, A. M. Marra, and S. Monchetti, “Bayesian model updating of historic masonry towers through dynamic experimental data,” *Procedia Eng.*, vol. 199, pp. 1258–1263, 2017.
- [41] X. Wang, Q. Gao, and Y. Liu, “Damage detection of bridges under environmental temperature changes using a hybrid method,” *Sensors (Switzerland)*, vol. 20, no. 14, pp. 1–20, 2020.
- [42] J. M. W. Brownjohn *et al.*, “Bayesian operational modal analysis of offshore rock lighthouses: Close modes, alignment, symmetry and uncertainty,” *Mech. Syst. Signal Process.*, vol. 133, p. 106306, 2019.
- [43] T. G. Ritto and F. A. Rochinha, “Digital twin, physics-based model, and machine learning applied to damage detection in structures,” *Mech. Syst. Signal Process.*, vol. 155, p. 107614, 2021.
- [44] G. Angjeliu, D. Coronelli, and G. Cardani, “Development of the simulation model for Digital Twin applications in historical masonry buildings: The integration between numerical and experimental reality,” *Comput. Struct.*, vol. 238, no. October, p. 106282, 2020.
- [45] A. Carbonari, L. Messi, B. Naticchia, M. Vaccarini, and M. Pirani, “Development of a BIM-based holonic system for real-time monitoring of building operational efficiency,” *Front. Eng. Manag.*, vol. 7, no. 1, pp. 89–103, 2020.
- [46] T. Zordan, B. Briseghella, and T. Liu, “Finite element model updating of a tied-arch bridge

- using Douglas-Reid method and Rosenbrock optimization algorithm,” *J. Traffic Transp. Eng. (English Ed.)*, vol. 1, no. 4, pp. 280–292, 2014.
- [47] N. F. Alkayem, M. Cao, and M. Ragulskis, “Damage diagnosis in 3D structures using a novel hybrid multiobjective optimization and FE model updating framework,” *Complexity*, vol. 2018, 2018.
- [48] E. García-Macías, L. Ierimonti, I. Venanzi, and F. Ubertini, “An Innovative Methodology for Online Surrogate-Based Model Updating of Historic Buildings Using Monitoring Data,” *Int. J. Archit. Herit.*, no. September, 2019.
- [49] V. N. Moreira, J. C. Matos, and D. V. Oliveira, “Probabilistic-based assessment of a masonry arch bridge considering inferential procedures,” *Eng. Struct.*, vol. 134, pp. 61–73, 2017.
- [50] M. Mishra, A. S. Bhatia, and D. Maity, “A comparative study of regression, neural network and neuro-fuzzy inference system for determining the compressive strength of brick–mortar masonry by fusing nondestructive testing data,” *Eng. Comput.*, vol. 37, no. 1, pp. 77–91, 2021.
- [51] M. G. Masciotta, L. F. Ramos, P. B. Lourenço, and M. Vasta, “Structural monitoring and damage identification on a masonry chimney by a spectral-based identification technique,” in *Proceedings of the International Conference on Structural Dynamic , EUROODYN Volume 2014-January, 2014*, 2014, pp. 211–218.
- [52] M. Baruch and I. Y. B. Itzhackj, “Ortogonalization of Measured Modes,” vol. 16, no. 4, pp. 346–351.
- [53] A. Berman, “Mass Matrix Correction Using an Incomplete Set of Measured Modes,” no. October, pp. 1147–1148, 1979.
- [54] A. Berman and E. J. Nagy, “Improvement of a Large Analytical Model Using Test Data,” vol. 21, no. 8, pp. 1168–1173.
- [55] S. Guo and N. G. Hemingway, “AN ORTHOGONALITY SENSITIVITY METHOD FOR ANALYTICAL DYNAMIC MODEL CORRECTION USING MODAL TEST DATA,” vol. 187, pp. 771–780, 1995.
- [56] J. R. Allemang and L. D. Brown, “A Correlation Coefficient for Modal Vector Analysis,” 1982.
- [57] R. Pascual, J. C. Golinval, and M. Razeto, “Frequency domain correlation technique for model correlation and updating,” *Proc. Int. Modal Anal. Conf. - IMAC*, vol. 1, no. August 2014, pp. 587–592, 1997.
- [58] X.-S. S. Yang and M. Karamanoglu, *Nature-Inspired Metaheuristic Algorithms Second Edition*, vol. 4, no. C. 2013.
- [59] “Guidelines for Structural Health Monitoring UNI/TR 11634.” .
- [60] X. Yang, *Nature-Inspired Optimization Algorithms*, no. March. 2014.
- [61] O. A. González-estrada *et al.*, “Structural health monitoring using the Firefly optimization algorithm and finite elements To cite this version : HAL Id : hal-01538689 Structural health monitoring using the Firefly optimization algorithm and finite elements Supervisión de salud estructural,” 2020.
- [62] T. H. Yi, H. N. Li, and M. Gu, “Sensor placement optimisation for Dalian international trade mansion focusing on application demands,” *Int. J. Sens. Networks*, vol. 15, no. 3, pp. 157–162, 2014.

- [63] G. F. Gomes and J. V. P. Pereira, "Sensor placement optimization and damage identification in a fuselage structure using inverse modal problem and firefly algorithm," *Evol. Intell.*, vol. 13, no. 4, pp. 571–591, 2020.
- [64] J. Kennedy and R. Eberhart, "Particle swarm optimization," pp. 1942–1948, 1995.
- [65] J. Pal and S. Banerjee, "A combined modal strain energy and particle swarm optimization for health monitoring of structures," *J. Civ. Struct. Heal. Monit.*, vol. 5, no. 4, pp. 353–363, 2015.
- [66] I. Boulkaibet, T. Marwala, M. I. Friswell, H. H. Khodaparast, and S. Adhikari, "Fuzzy finite element model updating using metaheuristic optimization algorithms Electrical and Electronic Engineering Department , University of Johannesburg , PO Box 524 , Auckland Park 2006 , South Africa College of Engineering , Swansea University Bay ," 2006.
- [67] Y. Zhao, J. Du, H. Bao, and Q. Xu, "Optimal sensor placement based on eigenvalues analysis for sensing deformation of wing frame using iFEM," *Sensors (Switzerland)*, vol. 18, no. 8, 2018.
- [68] A. M. Turing, "Computing Machinery and Intelligence," pp. 433–460, 1950.
- [69] N. A. Baricelli, "Numerical testing of evolution theories."
- [70] J. H. Holland, *Adaptation in Natural and Artificial Systems*. MIT Press, 55, Hayward St., Cambridge, MA, United States.
- [71] T. Bartz-Beielstein, J. Branke, J. Mehnen, and O. Mersmann, "Evolutionary Algorithms," *Wiley Interdiscip. Rev. Data Min. Knowl. Discov.*, vol. 4, no. 3, pp. 178–195, 2014.
- [72] S. Picek, M. Golub, and D. Jakobovic, "Evaluation of crossover operator performance in genetic algorithms with binary representation," *Lect. Notes Comput. Sci. (including Subser. Lect. Notes Artif. Intell. Lect. Notes Bioinformatics)*, vol. 6840 LNBI, pp. 223–230, 2011.
- [73] A. Hassanat, K. Almohammadi, E. Alkafaween, E. Abunawas, A. Hammouri, and V. B. S. Prasath, "Choosing mutation and crossover ratios for genetic algorithms-a review with a new dynamic approach," *Inf.*, vol. 10, no. 12, 2019.
- [74] H. Maaranen, K. Miettinen, and A. Penttinen, *On initial populations of a genetic algorithm for continuous optimization problems*, vol. 37, no. 3. 2007.
- [75] W. A. Khan, N. N. Hamadneh, S. L. Tilahun, and J. M. T. Ngotchouye, "A Review and Comparative Study of Firefly Algorithm and its Modified Versions," *Optim. Algorithms - Methods Appl.*, 2016.
- [76] D. Palupi Rini, S. Mariyam Shamsuddin, and S. Sophiyati Yuhaniz, "Particle Swarm Optimization: Technique, System and Challenges," *Int. J. Comput. Appl.*, vol. 14, no. 1, pp. 19–27, 2011.
- [77] M. Stolpe and K. Sandal, "Structural optimization with several discrete design variables per part by outer approximation," pp. 2061–2073, 2018.
- [78] H. Ahmadian, G. M. L. Gladwell, and F. Ismail, "Parameter selection strategies in finite element model updating," *J. Vib. Acoust. Trans. ASME*, vol. 119, no. 1, pp. 37–45, 1997.
- [79] Z. Yuan, P. Liang, T. Silva, K. Yu, and J. E. Mottershead, "Parameter selection for model updating with global sensitivity analysis," *Mech. Syst. Signal Process.*, vol. 115, pp. 483–496, Jan. 2019.
- [80] N. Abu Husain, H. Haddad Khodaparast, and H. Ouyang, "Parameter selection and

- stochastic model updating using perturbation methods with parameter weighting matrix assignment,” *Mech. Syst. Signal Process.*, vol. 32, pp. 135–152, 2012.
- [81] C. Zang, S. C. Ma, and M. I. Friswell, “Structural model updating with an improved parameter selection method,” *Int. Conf. Noise Vib. Eng. 2012, ISMA 2012, Incl. USD 2012 Int. Conf. Uncertain. Struct. Dyn.*, vol. 3, no. September 2012, pp. 2227–2236, 2012.
- [82] A. . Millar, “Subset Selection in Regression,” 1990.
- [83] E. Lejeune, “Geometric Stability Classification: Datasets, Metamodels, and Adversarial Attacks,” *Comput. Des.*, vol. 131, p. 102948, Feb. 2021.
- [84] A. I. J. Forrester and A. J. Keane, “Recent advances in surrogate-based optimization,” *Prog. Aerosp. Sci.*, vol. 45, no. 1–3, pp. 50–79, Jan. 2009.
- [85] N. V. Queipo, R. T. Haftka, W. Shyy, T. Goel, R. Vaidyanathan, and P. Kevin Tucker, “Surrogate-based analysis and optimization,” *Prog. Aerosp. Sci.*, vol. 41, no. 1, pp. 1–28, 2005.
- [86] G. Matheron, “Principles of geostatistics,” *Econ. Geol.*, vol. 58, no. 8, pp. 1246–1266, Dec. 1963.
- [87] J. P. C. Kleijnen and W. van Beers, “Statistical Tests for Cross-Validation of Kriging Models,” *SSRN Electron. J.*, no. January, 2019.
- [88] B. G. Marcot and A. M. Hanea, “What is an optimal value of k in k-fold cross-validation in discrete Bayesian network analysis?,” *Comput. Stat.*, vol. 36, no. 3, pp. 2009–2031, 2021.
- [89] M. Kuhn and K. Johnson, *Applied Predictive Modeling*. 2013.
- [90] W. Hoeffding, “A Class of Statistics with Asymptotically Normal Distribution,” *Ann. Math. Stat.*, vol. 19, no. 3, pp. 293–325, 1948.
- [91] B. Efron and C. Stein, “The Jackknife estimate of variance,” *Ann. Stat.*, 1991.
- [92] I. I. Sobol, “Sensitivity Estimates for Non linear Mathematical Models,” 1993.
- [93] T. Homma and A. Saltelli, “Importance measures in global sensitivity analysis of nonlinear models,” *Reliab. Eng. Syst. Saf.*, vol. 52, no. 1, pp. 1–17, 1996.
- [94] G. . Barchiesi, *Ostra in Cartolina*. Banca di Credito Cooperativo, 1994.
- [95] *Guida storica artistica e turistica di Ostra*. Ostra, 2015.
- [96] F. Clementi, A. Pierdicca, A. Formisano, F. Catinari, and S. Lenci, “Numerical model upgrading of a historical masonry building damaged during the 2016 Italian earthquakes: the case study of the Podestà palace in Montelupone (Italy),” *J. Civ. Struct. Heal. Monit.*, vol. 7, no. 5, pp. 703–717, Nov. 2017.
- [97] C. G. A.Saisi, P.Borlenghi, “FE Modelling for Seismic Assessment of an Ancient Tower From Ambient Vibration,” in *International Operational Modal Analysis Conference*, 2019.
- [98] I. Venanzi, A. Kita, N. Cavalagli, L. Ierimonti, and F. Ubertini, “Continuous OMA for Damage Detection and Localization in the Sciri tower in Perugia, Italy.” .
- [99] D. Pellegrini *et al.*, “Modal analysis of historical masonry structures: Linear perturbation and software benchmarking,” *Constr. Build. Mater.*, vol. 189, no. March 2019, pp. 1232–1250, 2018.
- [100] F. Ubertini, G. Comanducci, N. Cavalagli, A. Laura Pisello, A. Luigi Materazzi, and F. Cotana,

- “Environmental effects on natural frequencies of the San Pietro bell tower in Perugia, Italy, and their removal for structural performance assessment,” *Mech. Syst. Signal Process.*, vol. 82, pp. 307–322, Jan. 2017.
- [101] E. Giordano, F. Clementi, A. Barontini, M. Giovanna, E. Chatzi, and F. Luís, “Damage detection and optimal sensor placement in health monitoring of ‘ Collegiata di Santa Maria ’ in Visso ( Central Italy ) Damage detection and optimal sensor placement in health monitoring of ‘ Collegiata di Santa Maria ’ in Visso ( Central Italy ),” pp. 44–53, 2019.
- [102] M. G. Masciotta and L. F. Ramos, “Dynamic identification of historic masonry structures,” *Long-term Perform. Durab. Mason. Struct. Degrad. Mech. Heal. Monit. Serv. Life Des.*, no. January, pp. 241–264, 2018.
- [103] W. Torres, J. L. Almazán, C. Sandoval, and R. Boroschek, “Operational modal analysis and FE model updating of the Metropolitan Cathedral of Santiago, Chile,” *Eng. Struct.*, vol. 143, pp. 169–188, 2017.
- [104] G. Standoli, E. Giordano, G. Milani, and F. Clementi, “Model Updating of Historical Belfries Based on Oms Identification Techniques,” *Int. J. Archit. Herit.*, vol. 00, no. 00, pp. 1–25, 2020.
- [105] N. Cavalagli, G. Comanducci, C. Gentile, M. Guidobaldi, A. Saisi, and F. Ubertini, “Detecting earthquake-induced damage in historic masonry towers using continuously monitored dynamic response-only data,” *Procedia Eng.*, vol. 199, pp. 3416–3421, 2017.
- [106] Svibs, “Artemis Modal Manual,” p. 305, 2019.
- [107] F. Ubertini, C. Gentile, and A. L. Materazzi, “Automated modal identification in operational conditions and its application to bridges,” *Eng. Struct.*, vol. 46, pp. 264–278, 2013.
- [108] B. Peeters and G. De Roeck, “Reference-based stochastic subspace identification for output-only modal analysis,” *Mech. Syst. Signal Process.*, 1999.
- [109] A. Bajrić and J. Høgsberg, “Identification of damping and complex modes in structural vibrations,” *J. Sound Vib.*, 2018.
- [110] R. Brincker, L. Zhang, and P. Andersen, “Modal identification from ambient responses using frequency domain decomposition,” *Smart Mater. Struct.*, 2001.
- [111] B. Sevim, A. Bayraktar, A. C. Altunişik, S. Adanur, and M. Akköse, “Modal parameter identification of a prototype arch dam using enhanced frequency domain decomposition and stochastic subspace identification techniques,” *J. Test. Eval.*, vol. 38, no. 5, 2010.
- [112] M. Pastor, M. Binda, and T. Harčarik, “Modal assurance criterion,” *Procedia Eng.*, vol. 48, pp. 543–548, 2012.
- [113] L. F. Ramos, L. Marques, P. B. Lourenc, G. De Roeck, A. Campos-costa, and J. Roque, “Monitoring historical masonry structures with operational modal analysis : Two case studies,” vol. 24, pp. 1291–1305, 2010.
- [114] L. F. Ramos, L. Marques, P. B. Lourenço, G. De Roeck, A. Campos-Costa, and J. Roque, “Monitoring historical masonry structures with operational modal analysis: Two case studies,” *Mech. Syst. Signal Process.*, vol. 24, no. 5, pp. 1291–1305, Jul. 2010.
- [115] Ministero delle Infrastrutture e dei Trasporti, “D.M 17 gennaio 2018 ‘Aggiornamento delle Norme tecniche per le Costruzioni,’” *Suppl. Ordin. alla “Gazzetta Uff. n. 42 del 20 febbraio 2018- Ser. Gen.*, pp. 1–198, 2018.

- [116] M. Girardi, C. Padovani, D. Pellegrini, and L. Robol, "A finite element model updating method based on global optimization," *Mech. Syst. Signal Process.*, vol. 152, no. December, 2021.
- [117] R. S. Olivito and S. Porzio, "A new multi-control-point pushover methodology for the seismic assessment of historic masonry buildings," *J. Build. Eng.*, vol. 26, no. May, p. 100926, 2019.
- [118] S. Bagchi, T. B. Roy, and A. Bagchi, "Multiple damage localization of gravity dam: Strain energy based approach using random data," *Proceedings, Annu. Conf. - Can. Soc. Civ. Eng.*, vol. 2019-June, no. Cantieni 2009, 2019.
- [119] A. Garcia-Gonzalez, A. Gonzalez-Herrera, and A. Garcia-Cerezo, "Damage localization based on modal parameters using the finite element method and neural networks," *Civil-Comp Proc.*, vol. 93, no. January, 2010.
- [120] F. Bianconi, G. P. Salachoris, F. Clementi, and S. Lenci, "A Genetic Algorithm Procedure for the Automatic Updating of FEM Based on Ambient Vibration Tests," 2020.
- [121] T. Bartz-Beielstein, J. Branke, J. Mehnen, and O. Mersmann, "Evolutionary Algorithms," *Wiley Interdiscip. Rev. Data Min. Knowl. Discov.*, vol. 4, no. 3, pp. 178–195, 2014.
- [122] S. Kokot and Z. Zembaty, "Damage reconstruction of 3D frames using genetic algorithms with Levenberg--Marquardt local search," *Soil Dyn. Earthq. Eng.*, vol. 29, no. 2, pp. 311–323, 2009.
- [123] M. . Betti, G. . Bartoli, R. . Corazzi, and V. . Kovacevic, "Strumenti Open Source per l'ingegneria strutturale. Modellazione meccanica non lineare di edifici in muratura," *Boll. Ing.*, vol. 60, no. 12, pp. 3–15, 2013.
- [124] Ministero delle Infrastrutture e dei Trasporti, "D.M 17 gennaio 2018 'Aggiornamento delle Norme tecniche per le Costruzioni,'" *Suppl. Ordin. alla "Gazzetta Uff. n. 42 del 20 febbraio 2018- Ser. Gen.*, pp. 1–198, 2018.
- [125] Á. Bautista-De Castro, L. J. Sánchez-Aparicio, P. Carrasco-García, L. F. Ramos, and D. González-Aguilera, "A multidisciplinary approach to calibrating advanced numerical simulations of masonry arch bridges," *Mech. Syst. Signal Process.*, vol. 129, pp. 337–365, 2019.
- [126] A. Aloisio, L. Di Battista, R. Alaggio, E. Antonacci, and M. Fragiaco, "Assessment of structural interventions using Bayesian updating and subspace-based fault detection methods: the case study of S. Maria di Collemaggio basilica, L'Aquila, Italy," *Struct. Infrastruct. Eng.*, no. February, pp. 1–15, 2020.
- [127] T. Barth, "A brief overview of uncertainty quantification and error estimation in numerical simulation," ... *Syst. Dir. NASA Ames Res. Cent. ...*, pp. 1–19, 2005.
- [128] V. C. Kovačević, S. Monchetti, M. Betti, and C. Borri, "METAMODELS IN COMPUTATIONAL MECHANICS FOR BAYESIAN FEM UPDATING OF ANCIENT HIGH-RISE MASONRY STRUCTURES," no. September, pp. 15–19, 2019.
- [129] G. Zini, M. Betti, and G. Bartoli, "A quality-based automated procedure for operational modal analysis," *Mech. Syst. Signal Process.*, vol. 164, no. December 2020, p. 108173, 2022.
- [130] Q. Sun and D. Dias, "Global sensitivity analysis of probabilistic tunnel seismic deformations using sparse polynomial chaos expansions," *Soil Dyn. Earthq. Eng.*, vol. 141, p. 106470,



Feb. 2021.

- [131] S. R. Arwade, M. Moradi, and A. Louhghalam, "Variance decomposition and global sensitivity for structural systems," *Eng. Struct.*, vol. 32, no. 1, pp. 1–10, Jan. 2010.
- [132] E. García-Macías, L. Ierimonti, I. Venanzi, and F. Ubertini, "Comparison of surrogate models for handling uncertainties in shm of historic buildings," *Lect. Notes Mech. Eng.*, no. September, pp. 1645–1657, 2020.
- [133] M. G. Masciotta and L. F. Ramos, "Dynamic identification of historic masonry structures," in *Long-term Performance and Durability of Masonry Structures*, Woodhead., P. B. Ghiassi, Bahman; Lourenco, Ed. Publishing Series in Civil and Structural Engineering, Woodhead Publishing (2019), 2019, pp. 241–264.
- [134] F. Pianosi, F. Sarrazin, and T. Wagener, "A Matlab toolbox for Global Sensitivity Analysis," *Environ. Model. Softw.*, vol. 70, pp. 80–85, Aug. 2015.
- [135] M. Betti, G. Bartoli, L. Papini, and K. I. Engineering, "Uncertainties in civil engineering : a FE-model based process for research and application," no. June, 2020.
- [136] K. Vekaria and C. Clack, "Selective crossover in genetic algorithms: An empirical study," 1998, pp. 438–447.
- [137] U. A.J. and S. P.D., "Crossover Operators in Genetic Algorithms: a Review," *ICTACT J. Soft Comput.*, vol. 06, no. 01, pp. 1083–1092, 2015.
- [138] G. Syswerda, "Simulated Crossover in Genetic Algorithms," 1993, pp. 239–255.
- [139] X.-B. Hu and E. Di Paolo, "An efficient genetic algorithm with uniform crossover for air traffic control," *Comput. Oper. Res.*, vol. 36, no. 1, pp. 245–259, Jan. 2009.
- [140] O. Abdoun, J. Abouchabaka, and C. Tajani, "Analyzing the Performance of Mutation Operators to Solve the Travelling Salesman Problem," 2012.
- [141] M. Baudin, A. Dutfoy, B. Looss, and A. L. Popelin, "OpenTURNS: An industrial software for uncertainty quantification in simulation," *Handb. Uncertain. Quantif.*, pp. 2001–2038, 2017.